Physicochemical lithography of functional nanolayers

Lee George Harris

DOCUMENT SUPPLY CENTRE

Boston Spa, Wetherby, West Yorkshire LS23 7BQ

BRITISH LIBRARY DOCTORAL THESIS AGREEMENT FORM

The British Thesis Service is designed to promote awareness of and improve access to the results of publicly funded British Doctoral Research.
Theses in the scheme are publicised through various current awareness media including printed subject bulletins and on-line databases.

On demand access is provided for individual researchers and libraries from a single, central collection of more than 120,000 doctoral theses.

Access Agreement

Through my *university/~~college~~/~~department~~, I agree to supply the British Library Document Supply Centre, with a copy of my thesis.

I agree that my thesis may be copied on demand for loan or sale by the British Library, or its agents, to requesting libraries (who may add the copy to their collection for loan or consultation) or individuals. I understand that any copies of my thesis will contain the following statement:

This copy has been supplied on the understanding that it is copyright material and that no quotation from the thesis may be published without proper acknowledgement.

I confirm that the thesis and abstracts are my original work, that further copying will not infringe any rights of others, and that I have the right to make these authorisations. Other publication rights may be granted as I choose.

The British Library agrees to pay me a royalty of ten percent on any sales of the second and subsequent copies of my thesis per year. The royalty will be paid annually in April. *In order to be eligible for such royalties, I agree that my obligation is to notify the British Library of any change of address.*

Author's signature _____ Date 18-APRIL-2007

** please delete as applicable.*

STANDARDS

The physical presentation of your thesis should be in accordance with the following specifications:

The copy must be legible. The size of character used in the main text, including displayed matter and notes, should be not less than 2.0mm for capitals and 1.5mm for x-height (height of lower case x)

• **BRITISH DOCTORAL THESIS AGREEMENT FORM**

Please type or print in black ink

Personal Data

1 Surname HARRIS

Forenames LEE GEORGE

2 Present mailing address 31 GRANGE STREET

DELVES LANE, CONSETT

Co. DURHAM

DH8 7AG

Future mailing address 31 GRANGE STREET

DELVES LANE, CONSETT

Co. DURHAM

DH8 7AG

Effective date for future address _____

Doctoral Degree Data

3 Full name of University conferring degree, and college or division if appropriate

UNIVERSITY OF DURHAM

Department OF CHEMISTRY

4 Name of co-sponsoring body(ies) (if any)

NONE

5 Abbreviations for degree awarded

Ph.d

6 Date degree awarded APRIL 2007

7 Title of thesis PHYSICOCHEMICAL LITHOGRAPHY OF FUNCTIONAL NANOCOATINGS

8 List up to five additional descriptive keywords or short phrases not in your thesis title to help subject access.

a BIOSENSORS

b PULSED PLASMA POLYMERIZATION

c SURFACE MODIFICATION

d

e

9 Subject category for your thesis. Enter a code from the Subject Category list overleaf and write in the category selected. You may enter two additional categories and/or codes on the extra lines provided.

070 CHEMISTRY

06A BIOCHEMISTRY

201 PLASMA PHYSICS; GAS DISCHARGES

10 Language of text (if not English)

IMPORTANT:
You must sign the Access Agreement on page 1 of this leaflet and enclose it with this form and your thesis

University of Durham

FACULTY OF SCIENCE

DEGREE OF
DOCTOR OF PHILOSOPHY IN CHEMISTRY
(F1A001)

The following candidate has satisfied the Examiners, subject to conferment at Congregation. Please note that the University Regulations state that a candidate must be free of debt before the degree can be conferred.

CANDIDATE

LEE GEORGE HARRIS
(USTINOV COLLEGE)

TITLE OF THESIS

Physicochemical Lithography of Functional Nanolayers

Hedley

Signed on behalf of the Graduate School Commitee

Graduate School
Mountjoy Research Centre
Block 2
Stockton Road
Durham
DH1 3UP

20 April 2007

000417943

PHYSICOCHEMICAL LITHOGRAPHY OF FUNCTIONAL NANOLAYERS

Lee George Harris

Ph.D Thesis

Department of Chemistry

Durham University

December 2006

ABSTRACT

To further understand the biological interactions that govern our daily lives it is essential to develop new techniques for the robust tethering of immobilized bio-molecules to substrates for applications such as bio-mimicry, diagnostics, and durability as well as further self assembly. Current technologies devised for this purpose include the functionalization and lithography of Langmuir-Blodgett films, self-assembled monolayers and spin-coated layers. Whilst these methods provide suitable surfaces, they suffer from being substrate dependent and inappropriate for complex 3D-geometries, thus prohibiting their application to a wide range of materials. Pulsed plasma polymerised films can overcome this hurdle and are utilised in this thesis to present amine, epoxide, thiol and protein resistant interfaces.

For instance, genomic arrays have been created via di-sulfide bridge formation between DNA and thiol groups. Whilst proteomic arrays have been fabricated either via electrostatic immobilization of proteins to charged regions surrounded by a protein resistant background, or alternately, covalent attachment to epoxide surface groups. Similarly, glycomic arrays have been produced by the covalent attachment of D-maltose and β-D-galacto-methanethiosulfonate to amine and thiol surface groups respectively. Furthermore, it has been shown that sequential plasmachemical nanolayering can provide a passivated upper layer and a reactive underlayer which can be subsequently exposed via mechanical removal of the top layer, to yield reactive pixels on the micron and nano-scale.

Finally, the substrate independent nature of plasma polymers has been utilised for the coating of compact disc surfaces with reactive nanolayers. Subsequent protein immobilization has been accomplished via inkjet printing and has shown promise for potential use as in point-of-care diagnostics.

CONTENTS

CHAPTER 2 MOLECULAR SCRATCHCARDS FOR PROTEOMICS AND GENOMICS

CHAPTER 3 GLYCOSYLATION OF FUNCTIONAL NANOCOATINGS

CHAPTER 4 DIGITAL MOLECULAR INFORMATION LAYERS FOR SENSORS AND DIAGNOSTICS

PHYSICOCHEMICAL LITHOGRAPHY OF FUNCTIONAL NANOLAYERS

Lee George Harris

Ph.D Thesis

Department of Chemistry

Durham University

December 2006

For My Friends and Family

STATEMENT OF COPYRIGHT

DECLARATION

The work described in this thesis was carried out in the Department of Chemistry at Durham University between October 2003 and December 2006. It is the original work of the author except where otherwise acknowledged, and has not been previously submitted for a degree in this or any other university.

LIST OF PUBLICATIONS AND PRESENTATIONS

Work in this thesis has either been presented, published or will be submitted as follows:

"A Method for Creating a Chemically Patterned Surface", L. G. Harris, J.P.S. Badyal, WO2006117527, 2006.

"A Method for Creating a Amine Functionalized Surface", L. G. Harris, J. P. S. Badyal, GB Pat. Appl. No. 0621224.5, 2006

"Molecular Scratchcards for Proteomics and Genomics", L. G. Harris; W. C. E. Schofield.; J. P. S. Badyal, Chemistry of Materials, 2007, 19, 1546

"Glycosylation of Functional Nanocoatings", L. G. Harris; J. P. S. Badyal.; B.Davis, in preparation.

"Protein Immobilization to Protein Resistant Surfaces", L .G. Harris; J. P. S. Badyal, in preparation.

Plasma Functionalization of Compact Discs for Molecular Diagnostics, Guest Speaker, Department of Computing Science, Durham University, 2005.

Compact Discs for Molecular Diagnostics, Poster Presentation, Institute of Photonics, Durham University, 2005.

ACKNOWLEDGEMENTS

I would like to thank Professor J. P. S. Badyal for his assistance, encouragement and financial support throughout my Ph.D. I also wish to thank Dr. Luke Ward and Dr. Wayne Schofield for bearing my rants, ravings and temper. I would like to express my thanks to Kelvin and Barry in the electrical workshop, Jim and Neil in the mechanical workshop and Peter and Malcolm in the glassblowing workshop, whose expertise and input has been invaluable.

I would also like to thank my friends and family, who have had provided advice and welcome distractions over the last three years, and finally, Traci, who has supported myself, financially and emotionally, over the last three years and who still loves me for it, despite her best efforts.

ABSTRACT

To further understand the biological interactions that govern our daily lives it is essential to develop new techniques for the robust tethering of immobilized bio-molecules to substrates for applications such as bio-mimicry, diagnostics, and durability as well as further self assembly. Current technologies devised for this purpose include the functionalization and lithography of Langmuir-Blodgett films, self-assembled monolayers and spin-coated layers. Whilst these methods provide suitable surfaces, they suffer from being substrate dependent and inappropriate for complex 3D-geometries, thus prohibiting their application to a wide range of materials. Pulsed plasma polymerised films can overcome this hurdle and are utilised in this thesis to present amine, epoxide, thiol and protein resistant interfaces.

For instance, genomic arrays have been created via di-sulfide bridge formation between DNA and thiol groups. Whilst proteomic arrays have been fabricated either via electrostatic immobilization of proteins to charged regions surrounded by a protein resistant background, or alternately, covalent attachment to epoxide surface groups. Similarly, glycomic arrays have been produced by the covalent attachment of D-maltose and β-D-galacto-methanethiosulfonate to amine and thiol surface groups respectively. Furthermore, it has been shown that sequential plasmachemical nanolayering can provide a passivated upper layer and a reactive underlayer which can be subsequently exposed via mechanical removal of the top layer, to yield reactive pixels on the micron and nano-scale.

Finally, the substrate independent nature of plasma polymers has been utilised for the coating of compact disc surfaces with reactive nanolayers. Subsequent protein immobilization has been accomplished via inkjet printing and has shown promise for potential use as in point-of-care diagnostics.

"The work of science has nothing to do with consensus. Consensus is the business of politics. The greatest scientists in history are great precisely because they broke with the consensus."

Anon

CONTENTS

CHAPTER 2 MOLECULAR SCRATCHCARDS FOR PROTEOMICS AND GENOMICS

CHAPTER 3 GLYCOSYLATION OF FUNCTIONAL NANOCOATINGS

CHAPTER 4 DIGITAL MOLECULAR INFORMATION LAYERS FOR SENSORS AND DIAGNOSTICS

CHAPTER 1

PLASMA MODIFICATION OF SURFACES AND THEIR ANALYSIS

1.1 Plasma Modification of Surfaces

1.1.1 Introduction

The term plasma was introduced by Irving Langmuir to describe regions of zero net space charge within a gas.[1] It may be further characterized as a fully or partially ionized, quasi-neutral gas, consisting of charged ions, electrons, electromagnetic radiation, metastables and neutrals which display a collective behaviour.[2] Now considered as the fourth state of matter, approximately 95% of the universe is thought to compromise of plasma.

1.1.2 Plasma Forms

Plasma can be subdivided, by electron energy, into two categories. The first category (equilibrium plasma) contains all of the reactive species (electrons, ions, and neutrals) in thermal equilibrium[3] with examples including stars,[4] lightning[5] and fusion plasmas.[6] The second category (non-equilibrium plasma) is characterized by the absence of a thermal equilibrium between the species, with the electron temperature (10^4 – 10^5 K) greater than that of the surrounding ions and neutrals (~ 300 K).[7] These cold plasmas enable energetic reactions to proceed whilst the gas temperature does not rise significantly above that of the ambient environment, allowing for the treatment of heat sensitive materials,[2,8] thin film formation[9] and etching.[10]

1.1.3 Plasma Discharge

Due to the effects of naturally occurring ionization sources gases always contain some free electrons that may be accelerated by the application of an electric field. It is possible for the accelerated electrons to undergo elastic and inelastic collisions, leading to the ionization and excitation of any species present, with a cascade of secondary electrons produced at a breakdown voltage (V_b), via these collisions.[11]

The secondary electron emission is sufficient to maintain the discharge at a steady state as a result of the initial ionization producing reactive species that induce further excitation and ionization in a variety of differing mechanisms, Table 1.1.[12]

Process	Example
Ionization	$e^- + A \rightarrow 2e^- + A^+$
Excitation	$e^- + A \rightarrow e^- + A^*$
Relaxation	$A^* \rightarrow A + hv$
Dissociation	$e^- + AB \rightarrow e^- + A\bullet + B\bullet$
Penning Ionization	$A^* + B \rightarrow A + B^+ + e^-$
Metastable - Metastable	$A^* + A^* \rightarrow A + A^+ + e^-$
Electron - Metastable	$e^- + A^* \rightarrow A^+ + 2e^-$

Table 1.1 Plasma discharge processes: *A* and *B* represent ions, *A** excited ions, and e^- electrons.

If an electric field is placed inside the plasma the electrons will move to reduce the effect of this field, resulting in the formation of a potential difference between itself and the surrounding gas.[2,9] This distance over which this charge separation occurs is known as the Debye length λ_D, Equation 1.1. For the plasma to remain quasi-neutral the volume of the discharge must be greater than λ_D.

$$\lambda_D = \left(\frac{\varepsilon_o k T_e}{n_e e^2} \right)^{\frac{1}{2}} \qquad \textbf{Equation 1.1}$$

ε_o = Permittivity of free space.

k = Boltzman constant.

T_e = Electron temperature.

n_e = Electron density.

e = Electron charge.

1.1.4 Plasma Polymerization

Plasma polymerization forms nanometer thin films, from the vapour phase, onto a substrate, modifying the properties of the surface without effecting those of the bulk,[13,14,15,16,17,18,19,20] however the properties of these plasma polymers may vary from those of conventional polymers. This is a result of the plasma polymerization processes differing from the molecular processes of conventional polymerization. The plasma process offers several advantages over conventional techniques such as substrate independence and the ability to provide pin hole free, nanometer thin films on complex geometries with low amounts of precursor required and low waste generation.[7,14] Technological applications include adhesion,[21] biocompatibility,[22,23] biosensing,[24,25,26] electrical conduction,[27,28] durability,[29] genomics,[30] nitrogen fixation,[31] super repellency,[32,33] photovoltaic cells[34] and protein resistance.[35]

It is possible for polymerization in the gas phase to proceed via a variety of processes, including plasma induced polymerization, where precursor polymerization occurs through a double bond, Figure 1.1 A. Alternatively non-reactive and reactive products can be formed from the precursor, Figure 1.1 B and E, with film formation proceeding via these reactive intermediates[2] in a process known as plasma polymerization, which does not require a double bond Figure 1.1 C, D, and F.

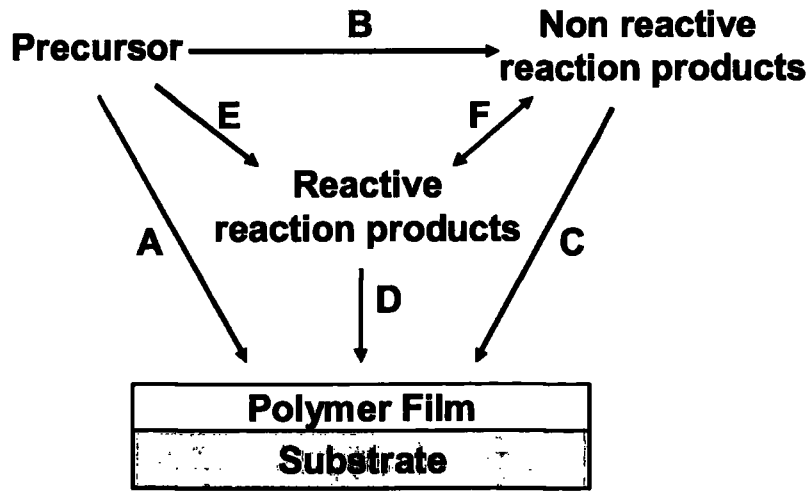

Figure 1.1 Processes of plasma polymerization.

The plasma polymerization processes include initiation, propagation, termination and reinitiation. Initiation concerns the generation of reactive species, propagation involves the interaction of these reactive species with each other and the surface (leading to the formation of a polymeric chain), with termination taking place in the gas phase and on the surface. Furthermore, terminated steps do not permanently cease the processes as the products can undergo reinitiation and further propagation reactions in the reactive plasma medium. This can be further described by a rapid step growth polymerization (RSGP) mechanism, Figure 1.2. RSGP proceeds via two equally contributing parallel cycles. Cycle I involves the repeated activation of the reaction products from monofunctional activated species, with cycle II occurring though difunctional speices.[9]

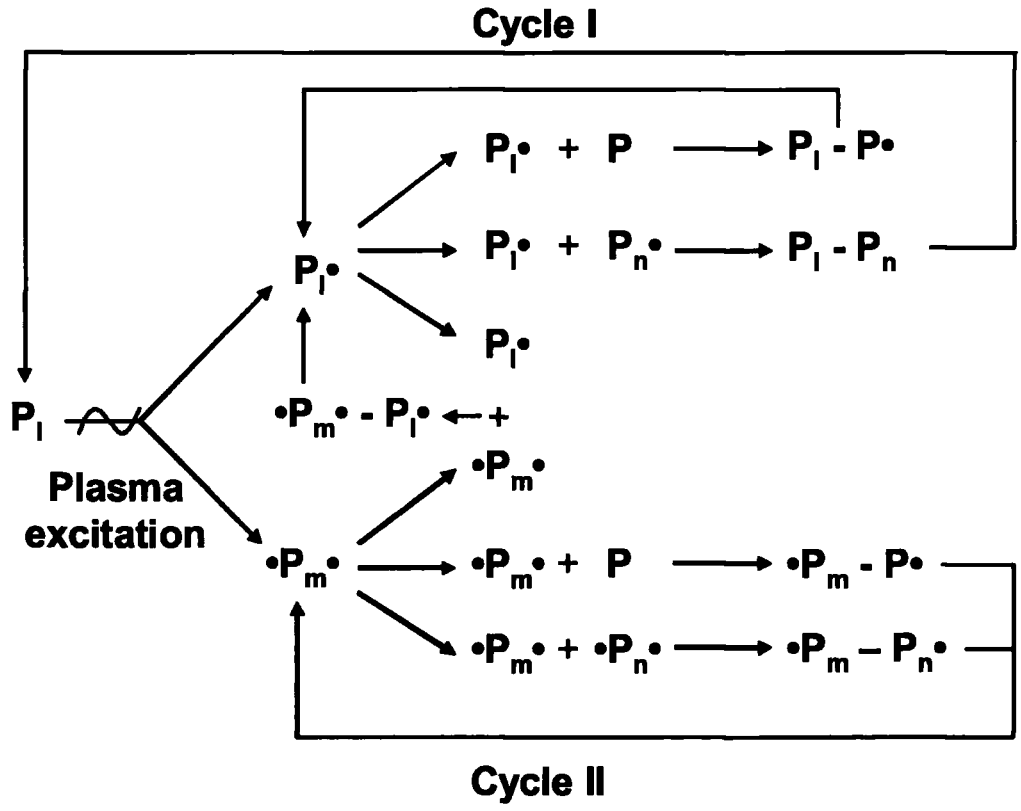

Figure 1.2 Mechanisms for rapid step growth polymerization: P_l, P_m, and P_n represent polymer chains of different length.

1.1.5 Pulsed Plasma Polymerization

Plasma polymerization is inherently destructive, with the formation of reactive products via collisions and fragmentation producing highly cross-linked materials. The polymer composition and cross linking is determined by a variety of parameters including substrate temperature, plasma zone substrate positioning, and reactor geometry.[36,37] A composite parameter *W/FM* (*W* represents power, *F* represents precursor flow rate, and *M* the precursor), determines the energy input per unit mass of precursor and is considered the determining parameter, with higher ratios inducing greater fragmentation.[9] Continuous wave plasma, when energy is supplied throughout the duration of plasma process, often generates excessive precursor fragmentation, increasing yield material cross linking. Pulsing of the power supply allows for lower average power inputs, effectively reducing the *W/FM* ratio and allowing for high levels of surface functionality as a consequence of reduced fragmentation and increased precursor structural retention,[38,39] Equation 1.2.

$$W_{eq} = \frac{T_{on}}{T_{on} + T_{off}} \bullet Peak\ Power \qquad \textbf{Equation 1.2}$$

W_{eq} = Equivalent power.

τ_{on} = Plasma on time.

τ_{off} = Plasma off time.

In varying the pulsed plasma duty cycle the on-time generates active sites in the gas phase and also at the growing film surface, followed by polymerization operating throughout the prolonged off-time in the absence of any UV, ion, or electron induced damage.[40,41] Furthermore, by programming the pulse duty cycle, the surface density of desired chemical groups can be tailored with examples including amine,[42] anhydride,[41] epoxide,[43] carboxylic acid,[44] cyano,[45] halide,[46] hydroxyl,[47] furfuryl,[48] perfluoroalkyl[33] and thiol groups.[30]

1.2 Surface Analysis

1.2.1 X-Ray Photoelectron Spectroscopy

1.2.1.1 Theory

X ray photoelectron spectroscopy (XPS) is a surface sensitive technique providing quantitative elemental information from the top 5 nm of a surface, furthermore, it can determine the chemical environment of the elements present, giving rise to the moniker 'electron spectroscopy for chemical analysis' or ESCA.[49]

The selectivity of XPS is a result of an elements unique binding energy. The binding energy is determined via irradiating a sample with high energy photons, resulting in ejection of core electrons by the photoelectric effect,[50] Figure 1.3.

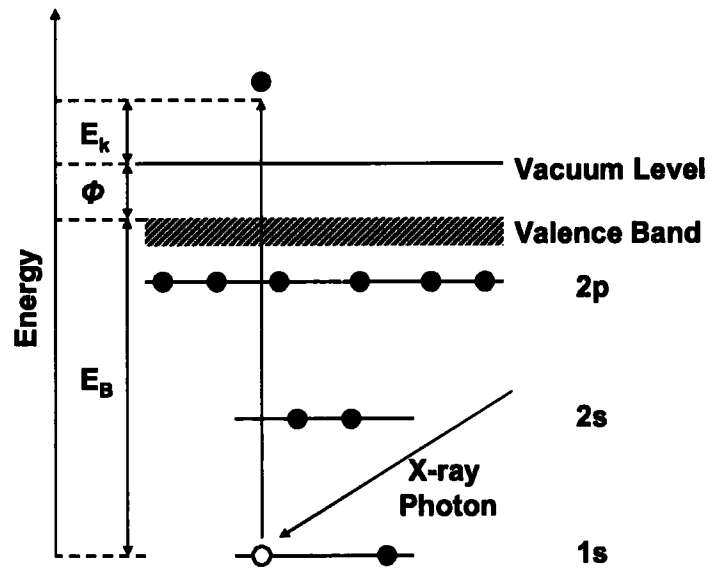

Figure 1.3 Ejection of a core 1s electron by an X-ray photon.

The kinetic energy of the core electrons is measured experimentally and used to determine the binding energy by applying the photoelectron equation,[51] Equation 1.3.

$$E_k = hv - E_B - \phi \qquad \textbf{Equation 1.3}$$

E_k = Photo-emitted electron kinetic energy.

E_B = Photo-emitted electron binding energy.

hv = Exciting photon energy.

Φ = Work function.

The precise core electron binding energies are sensitive to the chemical environment of the element. In general, the presence of electron withdrawing groups may leave atoms with a partial positive charge, leading to a shift in the core levels to higher binding energies as a result of an increase in electrostatic work done to remove the core electrons, therefore atoms in a high formal oxidation state will yield XPS peaks at higher binding energies relative to the same atom in a low oxidation state.[52] XPS spectra of elements exhibiting a range of oxidation states often appear as complex envelopes which can be deconvoluted into their component environments by a peak fitting procedure.[53] This allows for quantitative information on the chemical state of the elements present.

The surface sensitivity of XPS is derived from the inelastic mean free path (IMFP) of an electron travelling through the solid. The IMFP is an index of how far an electron can travel before losing energy via inelastic. XPS experiments in which the IMFP is low are highly surface sensitive. The IMFP is only weakly material dependent, however it is strongly dependent on electron energy, allowing for the formation of a 'universal curve' for materials, showing the IMFP as a function of electron energy,[54] Figure 1.4.

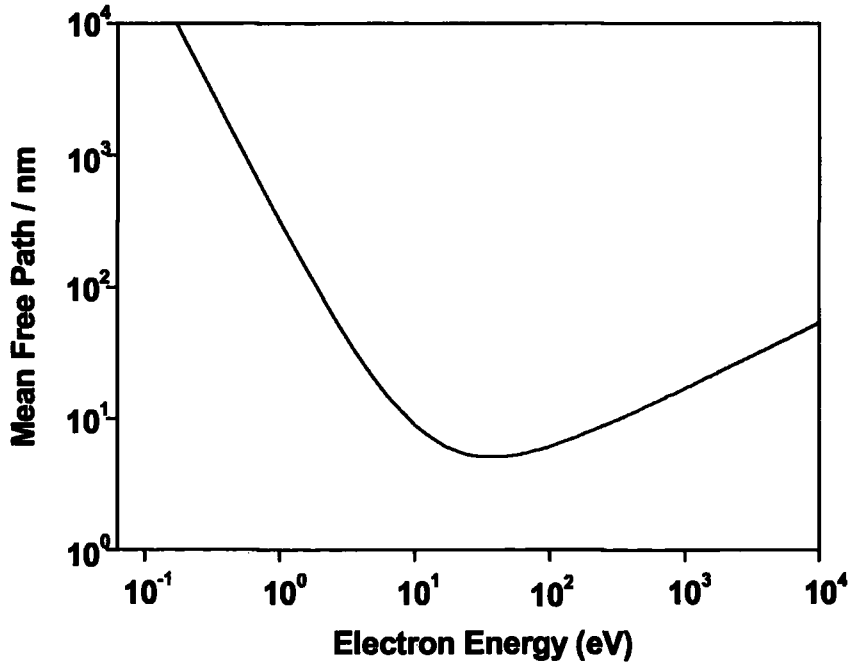

Figure 1.4 The dependence of inelastic mean free path on electron energy.

Low kinetic energy electrons possess insufficient energy to participate in energy loss processes so the IMFP is large. High energy electrons possess similarly low cross sections for IMFP. In contrast, electrons with medium kinetic energy (100 – 1000 eV), such as those generated by XPS have a high cross section for inelastic events. The resultant low escape depth gives XPS its surface sensitivity.

1.2.1.2 XPS Spectrometer

XPS analysis is carried out in ultra-high vacuum (UHV) to minimise sample contamination and to prevent scatter of photo-electrons prior to analysis. X-ray photons are usually created via the impaction of thermionic electrons on magnesium or aluminium coated anodes. The photons produced posses sufficient energy (Mg Kα: 1253.6 eV, Al Kα 1486.6 eV) to eject core electrons from a wide range of elements and possess a line width narrow enough (Mg Kα: 0.7 eV, Al Kα 0.85 eV) to permit high energy resolution analysis. Energy analysis of the photo-emitted electrons is normally accomplished using a concentric hemispherical analyser (CHA). The CHA, coupled with electronic lenses, filter electrons according to kinetic energy, before detection by a secondary electron multiplier.[52]

1.2.2 Fourier Transform Infrared (FT-IR) Spectroscopy

1.2.2.1 Theory

Chemical groups which contain a change in dipole moment may have a frequency that can be excited by an infra red photon.[55] Infrared spectroscopy is the IR absorption measurement of molecules containing these groups, with a comparison between the incident and transmitted IR beam allowing for a plot of the relative transmission at a given wavenumber.

Infrared spectra can be obtained by the dispersion of an infrared beam, via a grating, into its monochromated components, and slowly scanning the spectra through the sample, however this method can be time consuming. Fourier transform infrared spectroscopy varies from conventional IR by using a Michelson Interferometer. The interferometer consists of a standard IR source, a beamsplitter, a fixed mirror and a moving mirror. The beamsplitter reflects 50% of the beam to a stationary mirror and transmits 50% to a movable mirror, as the beams recombine interference fringes are produced. Varying the path length by moving the mirror results in an interferogram of intensity values against mirror distance travelled. Any sample placed in the path of the beam which absorbs infrared radiation modifies the interferogram according to the wavelengths absorbed. When the resultant interferogram undergoes a Fourier transform a spectra of intensity values versus wavenumber is obtained.[56]

The FT-IR method has the ability to scan a whole spectrum at once, reducing the time taken to acquire a spectrum with identical signal to noise ratio as a conventional IR spectrometer. Additionally, there are no slits required in the optics of the spectrometer resulting in a much higher radiation throughput, and the resolving power in a FT-IR instrument does not depend on wavenumber but remains constant.[57]

1.2.2.2 IR Surface Analysis

IR spectroscopy is normally performed in transmission mode, i.e. the radiation is passed through the sample. This is a bulk technique and inappropriate for detecting surface change. More suitable methods include attenuated total reflectance ATR-IR and specular reflectance FT-IR.

ATR-IR comprises an IR transparent crystal (e.g. KRS-5 or diamond) held in intimate contact with the sample. The difference in refractive indices between the optically dense crystal and the sample results in total internal reflection of the incident IR beam (I_o) at the surface, and also creates a standing wave at the crystal-surface interface. This standing wave penetrates into the sample, with penetration depth dependent upon incident wavelength but typical of the order of 2.5 to 25 μm in the mid IR range. The comparison of this wave with the incident beam allows for the formation of an FT-IR spectrum, Figure 1.5.[57]

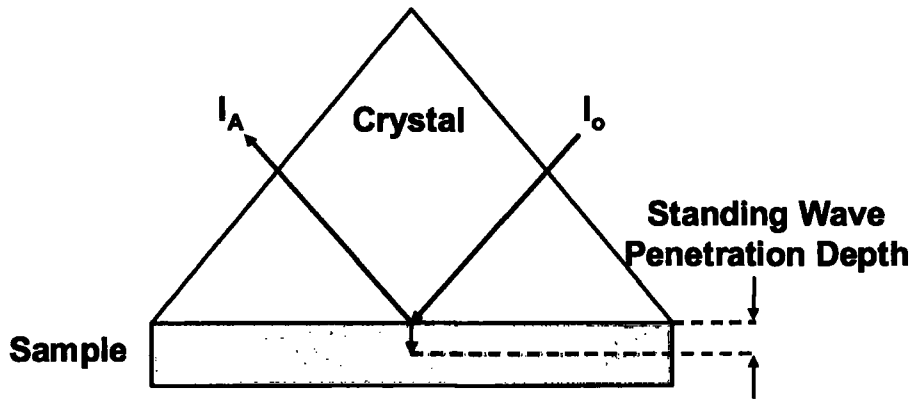

Figure 1.5 Total internal reflection of IR beam at the crystal surface interface propagating a standing wave into the sample surface.

Specular reflectance involves reflected energy measurement from a given surface at a given angle of incidence, Figure 1.6. When an incident FT-IR beam (I_o) illuminates a thin layer on a reflective substrate below the critical angle, some of the incident beam is reflected from the sample surface (I_R) and some is transmitted through the sample (I_T). When the beam exits the thin film it has passed through the film twice (I_A), with infrared energy absorbed at the characteristic wavelengths of the thin film.

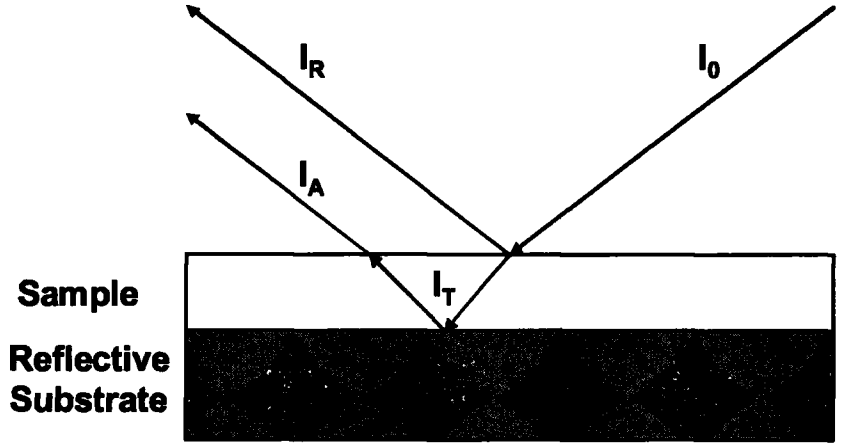

Figure 1.6 Specular reflectance of FT-IR beam incidented upon a thin film on a reflective substrate.

1.2.3 Fluorescence Microscopy

1.2.3.1 Photoluminescence

Fluorescence microscopy is a technique whereby fluorescent substances can be imaged. As many substances are fluorescent, or can be made so by fluorescent staining, and because fluorescence is observed as luminosity on a dark background, it is possible to differentiate between small features.[58]

The process of photoluminescence can be described as a stepwise mechanism consisting of the formation of one or more excited states by absorption of energy, followed by non-radiative transitions within the excited state, and finally, energy loss accompanied by emission of radiation,[59] Figure 1.7.

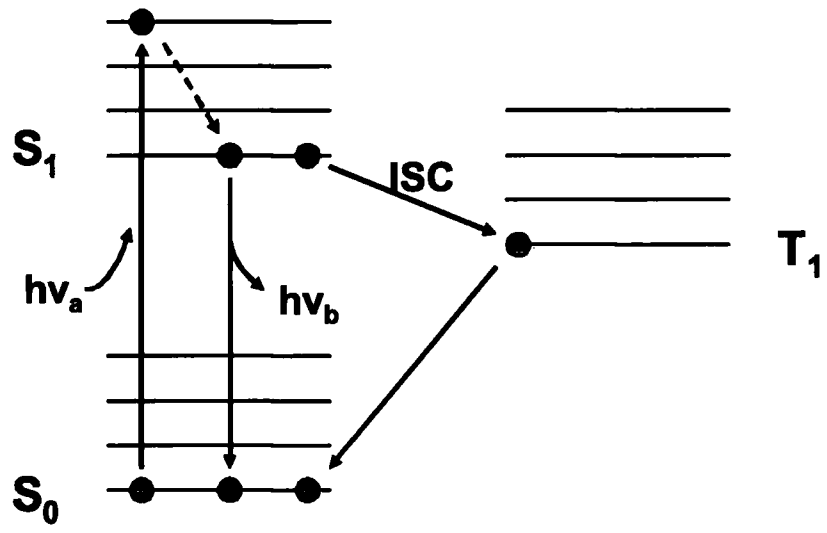

Figure 1.7 Jablonski diagram for photoluminescence were S_0 and S_1 are ground and excited triplet states respectively, and T_1 the associated triplet state

When a photon of energy hv_a is absorbed the material is excited from the ground singlet state S_0 to a vibronic sublevel of an excited state S_1. Non radiative decay brings the material down to the lowest sublevel in the excited state, leaving the material with less energy than absorbed (this

results in the emitted luminescence being of longer wavelength compared to the absorbed wavelength).[60] Photon emission of energy hv_b from the S_1 excited state to the S_0 ground state can takes place within nanoseconds, and is known as fluorescence.

The singlet excited state has a corresponding triplet state with slightly lower energy,[61,62] singlet-triplet state transitions are normally spin forbidden however it is possible to undergo intersystem crossing (ISC) into the triplet state. Furthermore, since the transition to the ground state is spin forbidden the microsecond lifetime of this state before photon emission allows for emission to proceed even after the excitation source has been removed, this is known as phosphorescence.

1.2.3.2 Microscope Design

A fluorescent microscope can be broken down into excitation source, contrast enhancement and emission detection, Figure 1.8. Typical excitation sources include lamps, lasers, and light emitting diodes, whose emission is collected into a lens and passed through a filter to allow light of only the desired wavelength to be focussed onto the sample. The emitted light from the sample is collected by a nearby objective and passed through another filter to improve the signal to noise ratio by removing any light of undesired wavelength. This light is focussed onto a photo-detector which can convert the light into a spatial image of fluorescence intensity.[63]

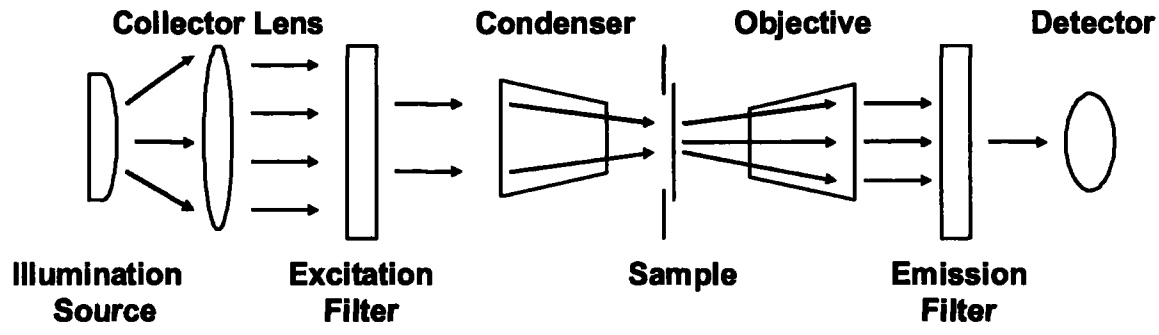

Figure 1.8 A schematic diagram of a fluorescence microscope.

1.2.4 Scanning Probe Microscopy

1.2.4.1 Development

The Atomic Force Microscope (AFM)[64] was developed from the Scanning Tunnelling Microscope[65] and can provide atomically resolved topographical images of conductors, insulators, organics, biological molecules, polymers and ceramics in different environments such as liquid, vacuum and low temperature.[66,67,68,69,70,71,72] The AFM can also provide information on adhesion,[73,74] electrostatic,[75,76] magnetic[77,78] and frictional forces[79,80] as well as surface wear[81,82]. Furthermore the AFM can be utilised as a lithographic tool.[83,84,85,86,87]

A basic AFM comprises of a sharp probing tip (~50 nm radius of curvature) located at the free end of a cantilever (~150 μm in length). The tip is scanned across the surface using an XYZ piezoelectric ceramic, providing movement with nanometer precision. The tip sample interactions create a change in cantilever properties which can be detected by various sensors including an STM tip positioned behind the cantilever,[64] optical interferometry[88] and laser beam deflection.[89] The changes in cantilever properties are fed into a feedback loop which changes the xyz piezo in order to keep a set point value constant.

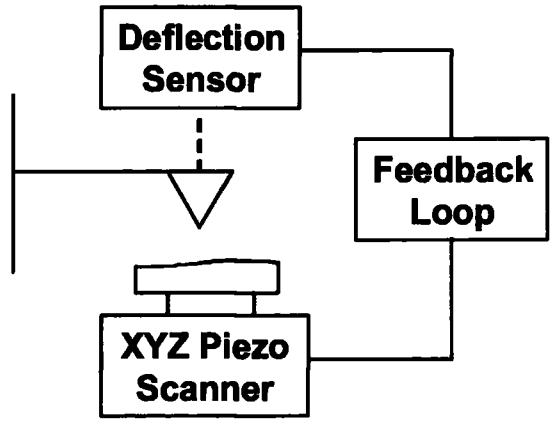

Figure 1.9 Schematic diagram showing the basic operating system of a scanning probe microscope.

Tip sample interactions are dependent upon the forces felt by the tip as a function of distance above the surface. The variation of force with distance from the surface allows the AFM to operate in three distinct regimes: contact, non-contact and intermittent contact,[90] Figure 1.10.

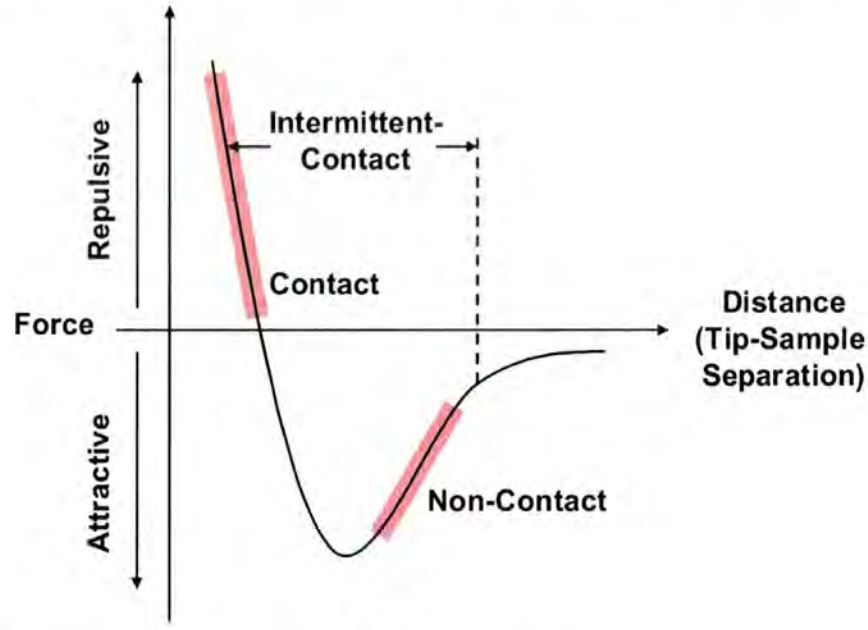

Figure 1.10 Interatomic force vs distance curve.

1.2.4.2 Contact Mode

In contact mode the AFM tip and sample are placed in "contact" and scanned across the surface,[91] here the tip is placed so close to the surface that the forces are repulsive, Figure 1.10. The curve in this section is extremely steep so when the cantilever pushes against the surface the magnitude of the repulsive force results in cantilever distortion rather than forcing the tip atoms closer to the surface atoms.

As the tip is rastered across the surface, topographical data can be collected in two ways. In the first, by maintaining the sample height at a constant value and scanning the tip over the surface, the spatial variation of the cantilever deflection can be used directly to generate a topographic image, this is known as constant-height mode. The second involves keeping the force between the sample and the tip constant by maintaining the deflection of the cantilever at a set point, as the tip is scanned across

the surface a feedback loop monitors the deflection and adjusts the tip-sample separation accordingly. The change in z-height, required to keep the set point constant, can then be used to generate a topographic image. However, in both methods, the dragging motion of the tip combined with the adhesive and lateral forces experienced can cause damage to soft samples.[92,93]

1.2.4.3 Non-Contact mode

When a tip is oscillated near its resonant frequency, at a distance of approximately 10 nm above the surface, the tip sample forces are considered attractive,[94] Figure 1.10. It is known that the resonant frequency of the oscillating tip varies with the spring constant of the cantilever, Equation 1.4.[95]

$$v = \frac{1}{2\pi}\sqrt{\frac{k}{m}} \qquad \textbf{Equation 1.4}$$

v = Cantilever resonant frequency.
k = Cantilever spring constant.
m = Cantilever mass.

Furthermore, the spring constant varies from its intrinsic value with the force gradient, Equation 1.5. Therefore, as the force gradient changes in the non-contact regime the resulting effect is a change in the resonant frequency of the cantilever. When a sample is scanned a feedback loop maintains the resonant frequency at a set point value by moving the z-piezo, allowing for the generation of a topographic image.

$$k_{eff} = k_0 - F \qquad \textbf{Equation 1.5}$$

k_{eff} = Effective spring constant.
k_0 = Spring constant in air.
F = Forces gradient.

Non-contact mode does not suffer from tip or sample degradation, however as non-contact interactions are very weak the change in resonance frequency is difficult to detect. Furthermore if condensed water monolayers are present on the surface the capillary forces can induce tip-sample artefacts as a result of the hydro-dynamic damping.[96]

1.2.4.4 Intermittent Contact mode

In intermittent contact mode the cantilever is vibrated near its resonant frequency and brought close to the sample so that it intermittently taps the surface. Each time the tip contacts the surface it loses energy and reduces the amplitude of modulation from that of the free amplitude in air. When scanning a surface, a set point amplitude is used in a feedback system so that any change will result in the movement of the z-piezo to restore the amplitude to its set-point, giving rise to a topographic imaging. Tapping mode does not suffer from the hydrodynamic damping as non-contact does and does not degrade the tip or sample like contact mode, allowing for the imaging of soft and biological samples in air.[97]

1.2.5 Contact Angle Analysis

The wettability of a sessile droplet on a surface is sensitive to changes in surface free energy and roughness. This makes contact angle an extremely surface sensitive (0.5 – 1 nm) means of characterizing a solid.[98]

As a sessile droplet of water is created on a surface a three phase boundary is created between the liquid, solid, and vapour, Figure 1.11 This can be described by three vector quantities: γ_{SV}, γ_{SL}, and γ_{LV} where γ is the surface tension and the subscripts SV, SL, LV refer to the solid-vapour, solid liquid and liquid vapour interfaces respectively.

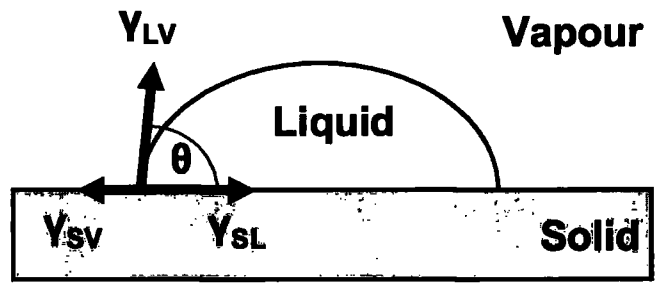

Figure 1.11 The three phase boundary by a liquid droplet on a solid surface.

The resolution of these interfacial tensions creates the balance of forces described by the Young's equation, where $\gamma_{LV}\cos\theta$ is the projection of γ_{LV} upon the surface Equation 1.7.[99]

$$\gamma_{sv} = \gamma_{sl} + \gamma_{lv}(\cos\theta) \qquad \textbf{Equation 1.7}$$

The contact angle can be empirically summarised using the Zisman plot. This assumes that the contact angle of any given solid ($\cos\theta$) is a linear function of γ_{LV} for a homologous series of liquids (e.g n-alkanes). Extrapolation of a graph of $\cos\theta$ against γ_{LV} to $\cos\theta = 1$ will yield a value of γ_{LV} at which the surface will become completely wetted. This is termed the critical surface tension γ_c, which is characteristic of the surface and considered to be a measure of the surface tension.[100]

Contact angle analysis is performed using a video contact angle (VCA) instrument. A motorised syringe deposits a droplet of known volume onto the sample surface. A snapshot of the droplet is then captured using a CCD camera and displayed on the interfaced PC. Accompanying image analysis software is then used to compute the contact angle.

1.2.6 Spectrophotometry

As monochromated light (I_o) is focused onto a thin film we get reflectance (I_R) and transmission (I_T) at phase boundaries, Figure 1.12. The interaction of the emergent waves creates interference fringes with varying intensities. Spectrophotometry allows the determination of optical properties, such as the refractive index and film thickness by fitting a Cauchy dispersion model[101] to acquired data, gathered by monitoring the reflectance and transmittance of a sample over a wavelength range of 300 to 1000 nm.

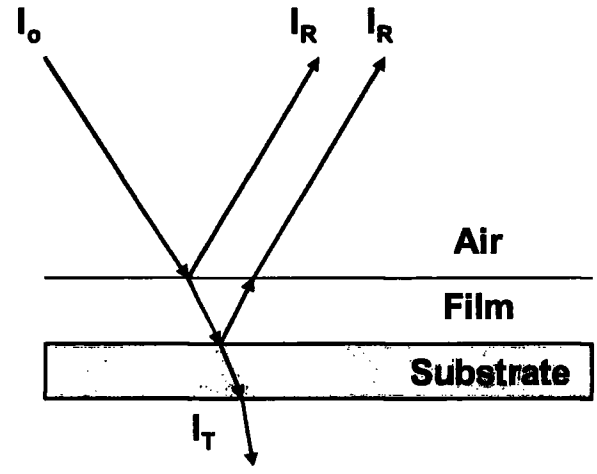

Figure 1.12 Reflection and transmission of monochromated light at phase boundaries to determine film properties.

1.3 References

(1) Langmuir, I. *Phys. Rev.* **1929**, *33,* 954.

(2) Grill, A. *Cold Plasma in Materials Technology*; IEEE press, Piscataway, 1994.

(3) Kanzawa, A. *Plasma Sources Sci. Technol.* **1993,** *2,* 58.

(4) Sturrock, P. A. *Plasma Physics*; Cambridge Univeristy Press, Cambridge, 1994.

(5) Latham, J.; Stromberg, M. Point-discharge. In *Lightning;* Golde, R. H., Eds.; Academic Press: New York, 1977; Chapter 4.

(6) Kapitza, P. L. *Rev. Mod. Phys* **1979**, *51,* 417.

(7) Bogaerts, A.; Neyts, E.; Gijbels, R.; van der Mullen, J. *Spectrochim. Acta,* Part B **2002,** *57,* 609.

(8) d, Agostino, R.; Favia, P.; Oehr, C.; Wertheimer, M. R. *Plasma Process. Polym.* **2005,** *2,* 7.

(9) Yasuda, H. *Plasma Polymerization;* Academic Press: New York, 1985.

(10) Manos, D. M.; Flamm, D. L. *Plasma Etching: An Introduction;* Academic Press: New York, 1989.

(11) Palmer, A. J.; *App. Phys. Lett.* **1974,** *25,* 138.

(12) Howatson, A. M. *An Introduction to Gas Discharges,* 2nd Ed; Pergamon Press: Oxford, 1976.

(13) Biederman, H.; Slavinska, D. *Surf. Coat. Technol.* **2000,** *125,* 371.

(14) Chan, C. M.; Ko, T. M.; Hiraoka, H. *Surf. Sci. Rep.* **1996,** *24,* 1.

(15) Gaur, S.; Vergason, G. Plasma Polymerization. Society of Vacuum Coaters 43rd Annual Technical Conference, Denver, 2000.

(16) Johnston, E. E.; Ratner, B. *J. Electron Spectrosc. Relat. Phenom.* **1996,** *81,* 303.

(17) Foest, R.; Adler, F.; Sigeneger, F.; Schmidt, M. *Surf. Coat. Technol.* **2003,** *163,* 323.

(18) Itatani, R. *Plasma & Ions* **1998,** *1,* 37.

(19) Barton, D.; Short, R. D.; Fraser, S.; Bradley, J. W. *Chem. Commun.* **2003,** 348.

(20) Guerin, D.; Hinshelwood, D. D.; Monolache, S.; Denes, F. S.; Shamamian, V. A. *Langmuir* **2003,** *18,* 4118.

(21) Evenson, S. A.; Fail, C. A.; Badyal, J. P. S. *Chem. Mater.* **2000,** *12,* 3038.

(22) Pan, Y. V.; Wesley, R. A.; Luginbuhl, R.; Denton, D. D.; Ratner, B. D. *Biomacromolecules* **2001,** *2,* 32.

(23) Tang, L.; Wu, Y.; Timmons, R. B. *J. Biomed. Mater. Res., Part A* **1998,** *1,* 156.

(24) Li, M.; Timmons, R. B.; Kinsel, G. R. *Anal. Chem.* **2005,** *77,* 350.

(25) Muguruma, H.; Hiratsuka, A.; Karube, I. *Anal. Chem.* **2000,** *72,* 2671.

(26) Kitade, T.; Kitamura, K.; Konishi, T.; Takegami, S.; Okuno, T.; Ishikawa, M.; Wakabayashi, M.; Nishikawa, K.; Muramatsu, Y. *Anal. Chem.* **2004,** *76,* 6802.

(27) Sadhir, R. K.; Schoch, K. F. *Chem. Mater.* **1996,** *8,* 1281.

(28) Denes, F. S.; Manolache, S. *Prog. Polym. Sci.* **2004,** *29,* 815.

(29) Schram, D. C. *Pure Appl. Chem.* **2002,** *74,* 369.

(30) Schofield, W. C. E.; McGettrick, J,; Bradley, T. J.; Badyal, J. P. S.; Przyborski, S. *J. Am. Chem. Soc.* **2006,** *128,* 2280.

(31) Matsuura, H.; Tanikawa, T.; Takaba, H.; Fujiwara, Y. *J. Phys. Chem. B.* **2004,** *108,* 17748.

(32) Coulson, S. R.; Woodward, I.; Badyal, J. P. S.; Brewer, S. A.; Willis, C. *J. Phys. Chem. B.* **2000,** *104,* 8836.

(33) Coulson S. R.; Woodward, I. S.; Badyal J. P. S.; Brewer, S. A.; Willis, C. *Langmuir* **2000,** *16,* 6287.

(34) Jiang, H.; Johnson, W. E.; Grant, J. T.; Eyink, K.; Johnson, E. M.; Tomlin, D. W.; Bunning, T. J. *Chem. Mater.* **2003,** *15,* 340.

(35) Teare, D. O. H.; Schofield, W. C. E.; Garrod, R. P.; Badyal, J. P. S. *J. Phys. Com. B* **2005,** *109,* 20923.

(36) Sproul, W. D. *Surf. Coat. Technol.* **1996,** *81,* 1.

(37) Shi, F. F. *Surf. Coat. Technol.* **1996,** *82,* 1.

(38) Han, L. M.; Timmons, R. B.; Bogdal, D.; Pielichowski, J. *Chem. Mater.* **1998,** *10,* 1422.

(39) Mackie, N. M.; Castner, D. G.; Fischer, E. R. *Langmuir* **1998,** *14,* 1227.

(40) Badyal, J. P. S. *Chem. Br.* **2001,** *37,* 45.

(41) Ryan, M. E.; Hynes, A. M.; Badyal J. P. S.; *Chem. Mater.* **1996,** *8,* 37.

(42) Oye, G.; Roucoules, V.; Oates, L. J.; Cameron, A. M.; Cameron N. R.; Steel P. G.; Davis, B. G.; Coe, D. M.; Cox, R. A.; Badyal, J. P. S. *J. Phys. Chem. B.* **2003,** *107,* 3496.

(43) Tarducci, C.; Kinmond, E.; Brewer, S.; Willis, C.; Badyal J. P. S. *Chem. Mater.* **2000,** *12,* 1884.

(44) Hutton, S. J.; Crowther, J. M.; Badyal, J. P. S. *Chem. Mater.* **2000,** *12,* 2282.

(45) Tarducci, C.; Schofield, W. C. E.; Brewer, S.; Willis, C.; Badyal, J. P. S. *Chem. Mater.* **2001,** *13,* 1800.

(46) Teare, D. O. H.; Barwick, D. C.; Schofield, W. C. E.; Garrod, R. P.; Ward, L. J.; Badyal, J. P. S. *Langmuir* **2005,** *21,* 11425.

(47) Tarducci, C.; Schofield W. C. E.; Brewer, S. A.; Willis, C.; Badyal, J. P. S. *Chem. Mater.* **2002,** *14,* 2541.

(48) Tarducci, C.; Brewer, S. A.; Willis, C.; Badyal, J. P. S. *Chem. Comm.* **2005,** *3,* 406.

(49) Siegbahn, K. *Rev. Mod. Phys* **1982,** *54,* 709.

(50) Kibel, M. H. X-Ray Photoelectron Spectroscopy. In *Surface Analysis Methods in Materials Science*; O'Connor, D. J., Sexton, B. A., Smart, R. St. C., Eds.; Springer-Verlag: Berlin, 1992; Chapter 7.

(51) Moulder, J. F.; Stickle, W. F.; Sobol, P. E.; Bomben, K. D. *Handbook of X-rat Photoelectron Spectroscopy*; Perkin-Elmer: Minnesota, 1992.

(52) Briggs, D.; Riviere, J. C. Spectral Interpretation. In *Practical Surface Analysis Volume 1 – Auger and X-ray Photoelectron Spectroscopy*, 2nd ed.; Briggs, D., Seah, M. P., Eds.; Wiley: Chichester, 1990; Chapter 5.

(53) Beamson, G.; Briggs, D. *High Resolution XPS of Organic Polymers*; Wiley: Chichester, 1992.

(54) Seah, M. H.; Dench, W. A. *Surf. Interface. Anal.* **1979,** *1,* 2.

(55) Colthup, N. B.; Daly, L. H.; Wiberley, S. E. *Introduction To Infrared And Raman Spectroscopy*; Academic Press: New York, 1990.

(56) Williams, D. H.; Fleming, I. *Spectroscopic Methods in Organic Chemistry*, 5th ed; McGraw-Hill: London, 1995; Chapter 2.

(57) Roberts, N. K. Fourier Transform Infrared Spectroscopy of Surfaces. In *Surface Analysis Methods in Materials Science*; O'Connor, D. J., Sexton, B. A., Smart, R. St. C., Eds.; Springer-Verlag: Berlin, 1992; Chapter 8.

(58) Rost, F. W. D. *Fluorescence Microscopy Volume 1;* Cambridge University Press: Cambridge, 1992.

(59) White, N. S.; Errington, R. J. *Adv. Drug Delivery Rev.* **2005,** *57,* 17.

(60) Atkins, P. A.; de Paula, J. *Atkins Physical Chemistry, 7th Ed;* Oxford University Press: Oxford, 2002, Chapter 17.

(61) Snow, R. L.; Bills, J. L. *J. Chem. Educ.* **1974,** *51,* 585.

(62) Liu, R. S. H. *J. Chem. Educ.* **2005,** *82,* 585.

(63) Michalet, X.; Kapanidis, A. N.; Laurence, T.; Pinaud, F.; Doose, S.; Pfughoefft, M.; Weiss, S. *Annu. Rev. Biophys. Biomol. Struct.* **2003,** *32,* 161.

(64) Binnig, G.; Quate, C. F.; Gerder, C. *Phys. Rev. Lett.* **1986,** *56,* 930.

(65) Binnig, G.; Rohrer, H.; Gerber, C.; Weibel, E. *Phys. Rev. Lett.* **1982,** *49,* 57.

(66) Anderson, M. W. *Curr. Opin. Solid State Mater. Sci.* **2001,** *5,* 407

(67) Lang, H, P.; Hegner, M.; Meyer, E.; Gerber, C. *Nanotech.* **2002,** *13,* R29.

(68) Maganov, S. N.; Reneker, D. H. *Annu. Rev. Mater. Sci.* **1997,** *27,* 175.

(69) Giessibl, F. J. *Rev. Mod. Phys.* **2003,** *75,* 949.

(70) Colton, R. J.; Baselt, D. R.; Dufrene, Y. F.; Green, J. B. D.; Lee, G. U. *Curr. Opin. Chem. Biol.* **1997,** *1,* 370.

(71) Engel, A.; Gaub, H. E.; Muller, D. J. *Curr. Bio.* **1999,** *9,* R133.

(72) Birdi, K. S. *Scanning Probe Microscopes;* CRC Press: Florida, 2003.

(73) Avci, R.; Schweitzer, M.; Boyd, R. D.; Wittmeyer, J.; Steele, A.; Toporski, J.; Beech, I.; Arce, F. T.; Spangler, B.; Cole, K. M.; McKay, D. S. *Langmuir* **2004,** *20,* 11053.

(74) Yoon, E. S.; Yang, S. O.; Han, H. G.; Kong, H. *Wear* **2003,** 974.

(75) Jiang, J.; Krauss, T. D.; Brus, L. E. *J. Phys. Chem. B.* **2000,** *104,* 11936.

(76) Knite, M.; Teteris, V.; Polyakov, B.; Erts, D. *Mater. Sci. Eng., C* **2002,** *19,* 15.

(77) Koblischka, M. R.; Hartmann, U. *Ultramicroscopy* **2003,** *97,* 103.

(78) Proksch, R. *Curr. Opin. Solid State Mater. Sci.* **1999,** *4,* 231.

(79) Liang, Q.; Li, H.; Xu, Y.; Xiao, X. *J. Phys. Chem. B.* **2006,** *110,* 403.

(80) Lio, A.; Morant, C.; Ogletree, D. F.; Salmeron, M. *J. Phys. Chem. B.* **1997,** *101,* 4767.

(81) Dinelli, F.; Leggett, G. J.; Alexander, M. R. *J. Appl. Phys.* **2002,** *91,* 2002.

(82) Dinelli, F.; Leggett, G. J.; Shipway, P. H. *Nanotech.* **2005,** *16,* 675.

(83) Xu, S.; Miller, S.; Laibinis, P. E.; Liu. G. Y. *Langmuir* **1999,** *15,* 7244.

(84) Ginger, D. S.; Zhang, H.; Mirkin, C. A. *Angew. Chem. Int. Ed.* **2004**, *43,* 30.

(85) Cai, Y.; Ocko, B. M. *J. Am. Chem. Soc.* **2005**, *127,* 16287.

(86) Martin, C.; Rius, G.; Borrrise, X.; Perez-Murano, F. *Nanotech,* **2005**, *16,* 1016.

(87) King, W. P.; Kenny, T. W.; Goodson, K. E.; Cross, G.; Despont, M.; Durig, U.; Rothuzien, H.; Binnig, G. K.; Vettifer, P. *Appl. Phys. Lett.* **2001**, *78,* 1300.

(88) Rugar, D.; Mamin, H. J.; Guethner, P. *Appl. Phys. Lett.* **1989,** *55,* 2588.

(89) Meyer, G.; Amer, N. M. *Appl. Phys. Lett.* **1988,** *53,* 1045.

(90) Capella, B.; Dietler, G. *Surf. Sci. Rep.* **1999,** *34,* 1.

(91) Meyer, E. *Prog. Surf. Sci.* **1992,** *41,* 3.

(92) Sommer, F.; Duc, M. T.; Pirri, R.; Meunier, G.; Quet, C. *Langmuir* **1995,** *11,* 440.

(93) Weisenhorn, A. L.; Khorsandi, M.; Kasas, S.; Gotzos, V.; Butt, H. J. *Nanotech.* **1993,** *4,* 106

(94) Martin, Y.; Williams, C. C.; Wickramasinghe, H. K. *J. Appl. Phys.* **1987,** *61,* 4723.

(95) Attard, G.; Barnes, C. *Surfaces;* Oxford University Press: Oxford, 2001.

(96) Hansma, H. G.; Hoh, J. H. *Ann. Rev. Biophys. Biomol. Stuct.* **1994,** *23,* 115.

(97) Zhong, Q.; Innis, D.; Kjollerm K.; Ellings, V. B. *Surf. Sci.* **1993**, *14,* 3045.

(98) Domingue, J. *American Laboratory* **1990,** *22,* 50.

(99) Good, R. J. Contact Angle, wetting and adhesion: a critical review. In *Contact Angle, Wettability and Adhesion*; MIttal, K., Ed.; VSP: Utrecht, 1993.

(100) Kabza, K.; Gestwicki, J. E.; McGrath, J. L. *J. Chem. Ed.* **2000**, *77,* 63.

(101) Tabet, M. F.; McGahan, W. *Thin Solid Films* **2000,** *370,* 122.

CHAPTER 2

MOLECULAR SCRATCHCARDS FOR PROTEOMICS AND GENOMICS

2.1 Introduction

Functional patterning of solid surfaces is of key importance for technological applications such as thin film transistors,[1] solar cells,[2] genomics,[3,4,5] proteomics,[6,7,8] microelectronics,[9,10,11] sensors[12] and microfluidics.[13,14,15] A plethora of techniques has been devised for this purpose based on top down, bottom up, or a combination of both approaches.[16,17] These include light stamping,[18] microcontact printing,[19,20,21,22,23] microarraying,[24,25,26] e-beam lithography,[27,28,29] polymer blend phase separation,[30,31,32] UV patterning[33,34,35] and exposure through a mask to a reactive medium.[36,37,38] Furthermore, the utilisation of scanning probe tips for patterning on the nanoscale has emerged as a promising alternative. This encompasses dip pen nanolithography,[39,40,41] electro pen nanolithography,[42] local anodic oxidation,[43,44,45,46,47] nanoshaving[48,49,50,51,52,53] and thermal scribing.[54,55] Generically, such scanning probe patterning techniques comprise either direct surface modification or partial removal of a surface layer to reveal the underlying substrate (which can then be subjected to further functionalization). Dip pen nanolithography[39,40,41] is an example of the former approach – where ink is transferred from a scanning probe tip onto a surface; associated drawbacks include the prerequisite of tip modification prior to use, and the reliance on specific ink-substrate interactions (e.g. gold-thiol coupling for the generation of self-assembled monolayers (SAMs)[56,57,58,59,60]). The alternative variant, where SAMs are directly removed by the tip,[48,49,50,51,63] also suffers from substrate specificity and poor shelf-life attributable to the oxidation and desorption processes of Au-S bond at the gold surface.[61]

In this study, a new and relatively straightforward approach for chemically patterning solid surfaces on both the micro- and nano- scales is introduced, which is based upon plasmachemical nanolayering to construct multi-functional stacks, with subsequent nanoscale scratching or puncturing down to the appropriate depth in order to expose the desired functionality, Figure 2.1.

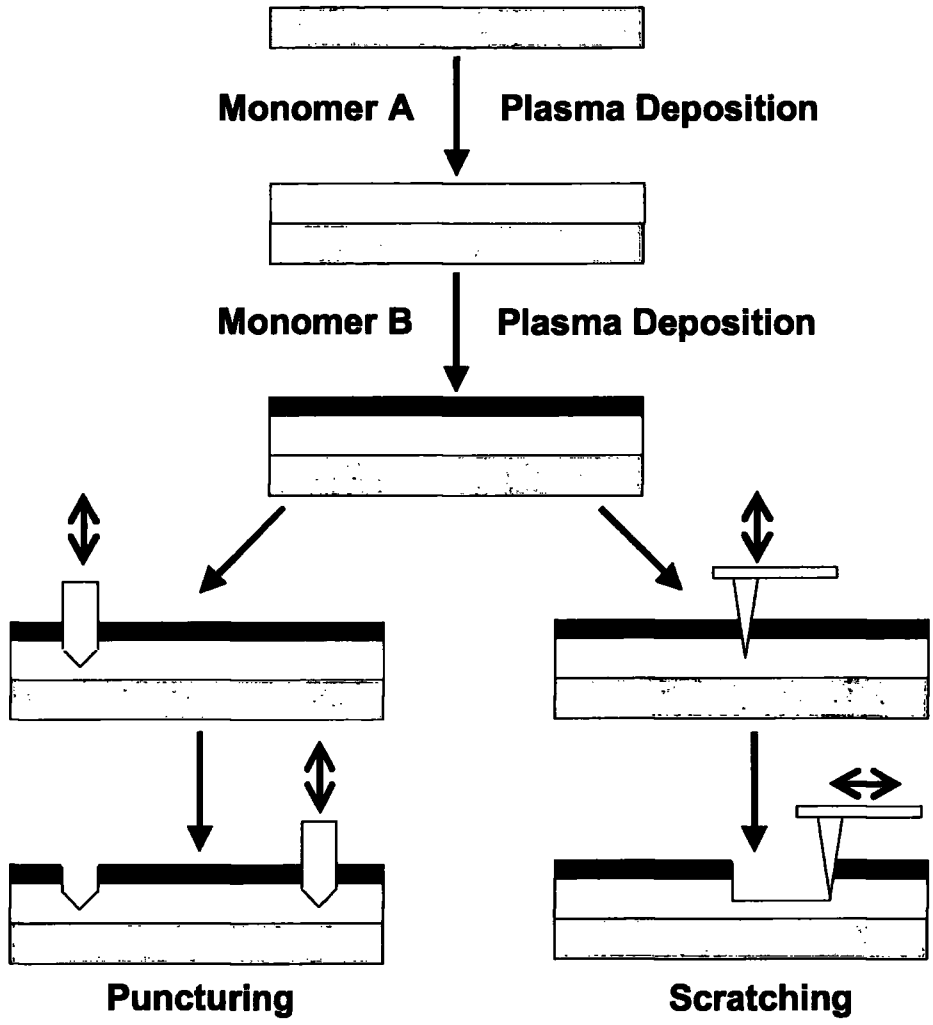

Figure 2.1 Molecular scratchcard fabrication followed by either robotic micropin puncturing or SPM tip scratching.

Previous attempts to fabricate multilayer functional stacks have tended to be cumbersome and reliant upon complex and expensive syntheses.[62] Here, functional nanolayering is readily achieved by switching monomers during pulsed plasma depositions. Subsequent removal of the outermost passivation layer leaves behind a patterned multi-functional surface. The major attributes envisaged include substrate independence, high throughputs and the scope for multifunctional (multiplex) surfaces.

2.2 Experimental

2.2.1 Plasmachemical Nanolayering

Plasma polymerization was carried out in a cylindrical glass reactor (4.5 cm diameter, 460 cm^3 volume) located inside a Faraday cage and evacuated by a 30 L min^{-1} rotary pump via a liquid nitrogen cold trap (2 x 10^{-3} mbar base pressure and better than 1.2 x 10^{-9} mol s^{-1} leak rate). A copper coil (4 mm diameter, 10 turns, located 15 cm away from the precursor inlet) was connected to a 13.56 MHz radio frequency supply via an LC matching network. System pressure was monitored with a Pirani gauge. All fittings were grease free. During pulsed plasma deposition, the RF source was triggered by a signal generator, and the pulse shape monitored with an oscilloscope. Prior to each experiment the apparatus was scrubbed with detergent, rinsed with propan-2-ol, and oven dried. Further cleaning entailed running a 40 W continuous wave air plasma at 0.2 mbar pressure for 20 min. At this stage, each monomer was loaded into a sealable glass tube and further purified using multiple freeze-pump-thaw cycles. The substrate of interest was placed into the centre of the reactor, and the system evacuated to base pressure. For each functional monomer, a continuous flow of vapour was introduced via a fine needle control valve at a pressure of 0.2 mbar and 1.5 x 10^{-7} mol s^{-1} flow rate for 5 min prior to electrical discharge ignition. Optimum pulsed plasma duty cycle parameters for each precursor are listed in Table 2.1. Upon completion of deposition, the RF power source was switched off and the monomer allowed to continue to purge though the system for a further 5 min prior to evacuation to base pressure and venting to atmosphere.

Precursor	Reactor Temp / °C	Pulse Duty Cycle / µs		Deposition Rate / nm min^{-1}
		Time On	Time Off	
Glycidyl methacrylate (+97%,SigmaAldrich)	22	20	20000	16
N–acryloylsarcosine methyl ester (+97%, Lancaster)	50	20	5000	9
Allylmercaptan (+80%, Sigma-Aldrich)	22	100	4000	10

Table 2.1 Optimum parameters for pulsed plasma polymerization of each monomer.

2.2.2 Protein Arrays

A difunctional stack comprising pulsed plasma deposited poly(*N*-acryloylsarcosine methyl ester) on top of poly(glycidyl methacrylate) was employed for the preparation of protein arrays. Micron-scale protein patterns were fabricated using a computer-controlled robotic microarrayer (Genetix Inc) equipped with micro-machined pins delivering ~1 nL of protein solution onto the reactive pulsed plasma poly(glycidyl methacrylate) underlayer by puncturing the pulsed plasma poly(*N*–acryloylsarcosine methyl ester) protein-resistant top layer. Typical circular spots with diameters of 100 to 150 µm could be routinely prepared. Protein I and Protein III solutions were prepared by diluting in phosphate buffered saline (pH 7.0, Sigma-Aldrich) containing 40% v/v glycerol (+99%, Sigma Aldrich) to a final concentration of 20 µg mL^{-1}, Table 2.2. The spotted surfaces were incubated for 16 h at 22 °C in a humidified chamber (70% relative humidity). Protein immobilization occurred via reaction between the biomolecule amine groups and epoxide centres exposed during concurrent puncturing and liquid delivery.

Protein	Label	Fluorophore
Protein G from streptococcus sp (Sigma-Aldrich)	Protein I	N/A
Goat antimouse IgG (H + L) (Sigma-Aldrich)	Protein II	Alexa fluor 633 (Abs 632 nm, Em 650 nm)
IgG from equine serum, salt-free (Molecular Probes)	Protein III	N/A
Protein A from staphylococcus aureus (Sigma-Aldrich)	Protein IV	FITC (Abs 494 nm, Em 518 nm)

Table 2.2 Proteins and associated fluorophores employed in this study with their absorption (Abs) and emission (Em) maxima.

Microarrays of Protein I and Protein III were subsequently exposed to solutions of fluorescently tagged complementary Protein II and Protein IV respectively (20 μg mL^{-1} in phosphate buffered saline) for 60 min. This was followed by successive rinses in phosphate buffered saline, phosphate buffered saline diluted to 50% v/v with de-ionized water, and finally washed twice with de-ionized water.

Sub-micron scale protein immobilization entailed loading a molecular scratchcard onto an atomic force microscope stage (Digital Instruments Nanoscope III control module, extender electronics, and signal access module, Santa Barbara, CA). The protein-resistant pulsed plasma poly(*N*–acryloylsarcosine methyl ester) top layer was scratched away using a tapping mode tip (Nanoprobe, spring constant 42 - 83 Nm^{-1}) applied in contact mode. The movement of the tip in the x, y, and z plane was controlled by Veeco Nanolithography Software (Version 5.30r1). The patterned molecular scratchcard was immersed in a solution of Protein I for 60 min at room temperature followed by successive rinses in phosphate buffered saline, phosphate buffered saline diluted to 50% v/v with de-ionized water, and twice with de-ionized water. The sample was then exposed to a complementary solution of Protein II (20 μg mL^{-1} in

phosphate buffered saline) for 60 min followed by successive rinses in phosphate buffered saline, phosphate buffered saline diluted to 50% v/v with de-ionized water, and finally washed twice with de-ionized water.

2.2.3 DNA Arrays

For the DNA arrays, poly(glycidyl methacrylate) was employed as the passivation top layer, with poly(allylmercaptan) serving as the reactive underlayer. Scanning probe lithography was performed as described above. The patterned scratchcard was then immersed in a solution of thiol terminated Cy5 tagged 15 base oligonucleotide (5' – AACGATGCACGAGCA – 3') diluted to a concentration of 400 nM in a 3 M Sodium Chloride (+99 %, Sigma Aldrich)/0.5 M Sodium Citrate Dihydrate (+99%, Sigma Aldrich) (SSC) buffer solution for 12 h at room temperature. This was followed by successive rinses in SSC, SSC diluted 50% v/v with de-ionized water, and twice with de-ionized water. Surface immobilization of the oligonucleotides occurred via di-sulfide bridge formation.[63]

2.2.4 Surface Characterization

X-ray photoelectron spectroscopy (XPS) was undertaken using an electron spectrometer (VG ESCALAB MK II) equipped with a non-monochromated Mg $K\alpha_{1,2}$ X-ray source (1253.6 eV) and a concentric hemispherical analyser. Photo-emitted electrons were collected at a take-off angle of 30° from the substrate normal, with electron detection in the constant analyser energy mode (CAE, pass energy = 20 eV). The XPS spectra were charge referenced to the C(1s) peak at 285.0 eV and fitted with a linear background and equal full-width-at-half-maximum (FWHM) Gaussian components[64] using Marquardt minimization computer software. Instrument sensitivity (multiplication) factors derived from chemical standards were taken as being C(1s): S(2p): O(1s): N(1s): equals 1.00: 0.52: 0.63: 0.45.

Fourier transform infrared (FTIR) analysis of the films was carried out using a Perkin-Elmer Spectrum One spectrometer equipped with a liquid nitrogen cooled MCT detector operating across the 700 – 4000 cm^{-1} range. Reflection–absorption (RAIRS) measurements were performed using a variable angle accessory (Specac) set at 86° on an Au substrate in conjunction with a KRS-5 polarizer fitted to remove the s–polarized component. All spectra were averaged over 10,000 scans at resolution of 1 cm^{-1}.

Contact angle analysis of the plasma-deposited films was carried out with a video capture system (ASE Products, model VCA2500XE) using 2.0 μL droplets of de-ionized water.

Film thickness measurements were carried out using an nkd-6000 spectrophotometer (Aquila Instruments Ltd). Transmittance-reflectance curves (over the 350-1000 nm wavelength range) were fitted to the Cauchy model for dielectric materials using a modified Levenburg-Marquardt method.[65]

AFM micrographs of each surface were acquired in tapping mode[66] operating in air at room temperature (Digital Instruments Nanoscope III control module, extender electronics, and signal access module, Santa Barbara, CA).

Fluorescence microscopy was performed using an Olympus IX–70 system (DeltaVision RT, Applied Precision, WA). Image data was collected using excitation wavelengths at 525 nm and 633 nm corresponding to the absorption maxima of the dye molecules, FITC and Alexa Fluor 633 respectively.

2.3 Results

2.3.1 Protein Arrays

The XPS elemental stoichiometry of the pulsed plasma deposited poly(*N*–acryloylsarcosine methyl ester) protein-resistant film closely resembles the predicted theoretical composition calculated from the monomer structure, Table 2.3. Further confirmation of the high level of retained functionality was evident from the six C(1s) spectra hydrocarbon environments: $\underline{C}_xH_y$ (285.0 eV, α), $\underline{C}$-C=O (285.7 eV, β), $\underline{C}$-N (286.2 eV, ε), $\underline{C}$-O (286.6 eV, μ), N-$\underline{C}$=O (288.0 eV, δ), O-$\underline{C}$=O (289.3 eV, θ), Figure 2.2(a), and the characteristic infrared spectra absorbances at 1749 cm^{-1} (ester carbonyl), 1653 cm^{-1} (amide), and 1212 cm^{-1} (ester C–O),[67] Figure 2.3(a). Presence of the nanolayer only at the surface was confirmed by the absence of the Si(2p) peak from the underlying silicon substrate.

Pulsed Plasma Polymer(s)	Contact Angle / °	Elemental Composition		
		C %	N %	O %
N-acryloylsarcosine methyl ester	48.1 ± 3.2	63.1 ± 1.3	9.9 ± 0.4	26.9 ± 1.4
Theoretical *N*-acryloylsarcosine methyl ester	N/A	64	9	27
Glycidyl methacrylate	58.4 ± 1.3	68.9 ± 1.4	-	31.3 ± 1.3
Theoretical glycidyl methacrylate	N/A	70	0	30
N-acryloylsarcosine methyl ester + Glycidyl methacrylate	49.4 ± 4.2	63.1 ± 0.5	9.9 ± 0.3	26.9 ± 0.7

Table 2.3 Contact angle and XPS elemental composition of pulsed plasma deposited poly(*N*–acryloylsarcosine methyl ester), poly(glycidyl methacrylate), and poly(*N*–acryloylsarcosine methyl ester) deposited on top of poly(glycidyl methacrylate).

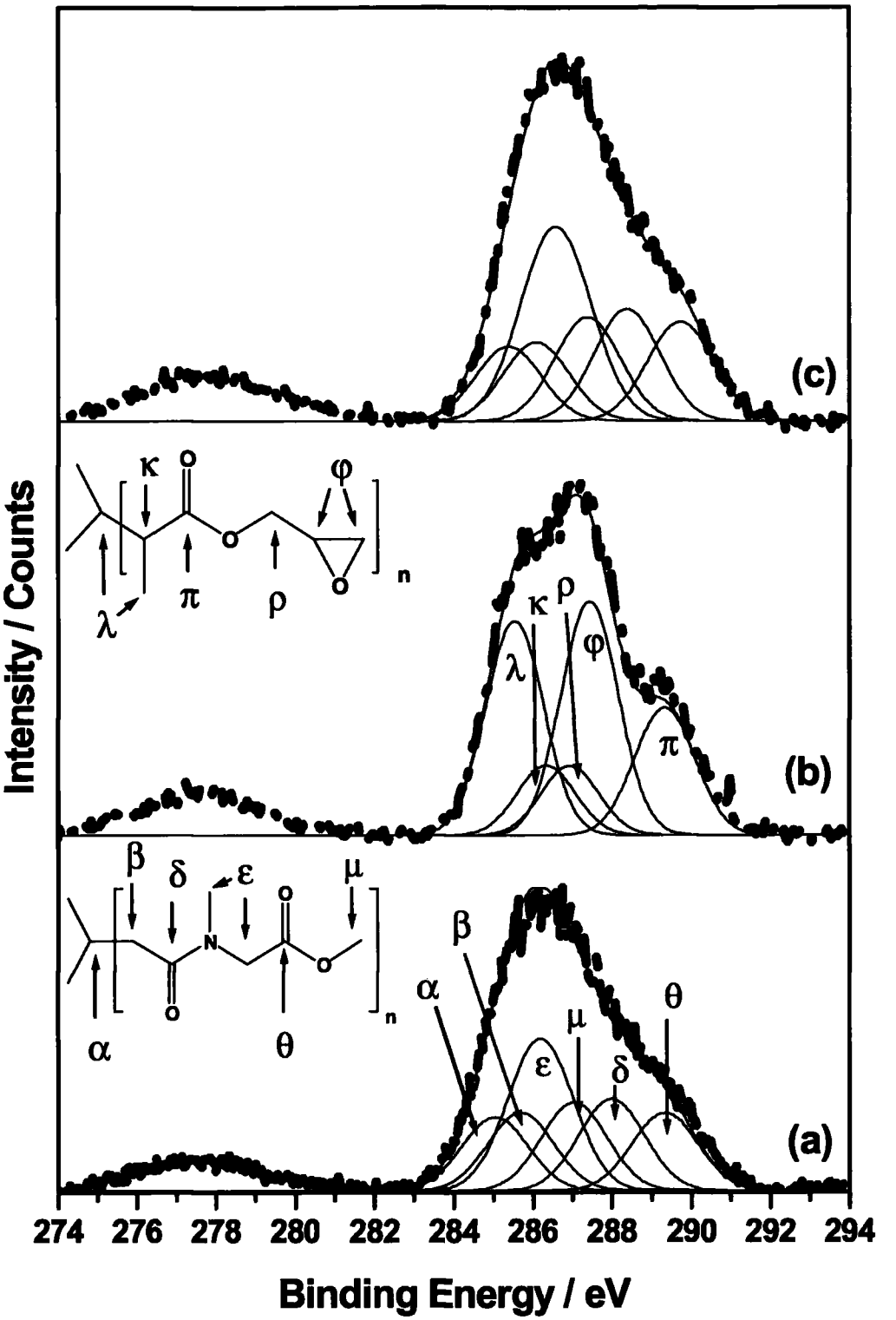

Figure 2.2 C(1s) XPS peak fitting of pulsed plasma deposited: (a) 20 nm poly(*N*–acryloylsarcosine methyl ester) protein-resistant layer; (b) 300 nm poly(glycidyl methacrylate) protein-binding layer; and (c) 20 nm poly(*N*–acryloylsarcosine methyl ester) on top of a 300 nm poly(glycidyl methacrylate) layer.

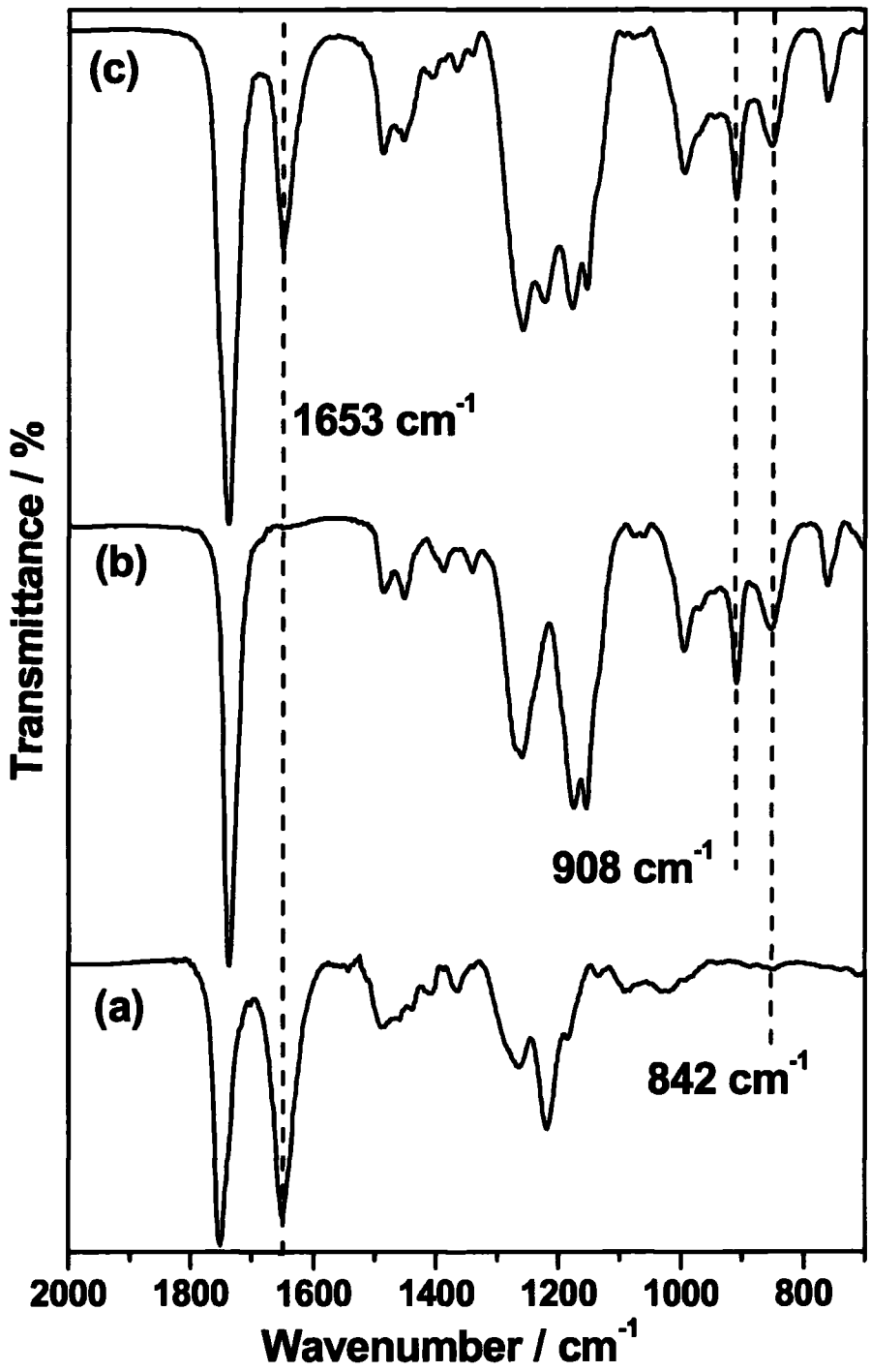

Figure 2.3 Infrared spectra of pulsed plasma deposited: (a) 20 nm poly(*N*–acryloylsarcosine methyl ester) protein-resistant layer; (b) 300 nm poly(glycidyl methacrylate) protein-binding layer; and (c) 20 nm poly(*N*–acryloylsarcosine methyl ester) on top of a 300 nm poly(glycidyl methacrylate) layer.

A similar trend is observed for the pulsed plasma deposited poly(glycidyl methacrylate) protein-binding layer, where XPS stoichiometry closely resembles the monomer composition, Table 2.3. C(1s) peak fitting displays five environments: $\underline{C}_xH_y$ (285.0, eV, λ), $\underline{C}$-C=0 (285.7 eV, κ), O-$\underline{C}$-C-O (286.7 eV, ρ), epoxide carbons (287.2 eV, φ), and O-$\underline{C}$=O (289.1 eV, π), Figure 2.2(b). Infrared spectroscopy indicates fingerprint absorption bands at 1728 cm^{-1} (ester carbonyl), 908 cm^{-1} (antisymmetric epoxide ring deformation), and 842 cm^{-1} (symmetric epoxide ring deformation), Figure 2.3 (b).[68,69]

Consecutive pulsed plasma deposition of a 300 nm thick poly(glycidyl methacrylate) layer followed by 20 nm of poly(*N*-acryloylsarcosine methyl ester) in the absence of cross-contamination was verified by infrared spectroscopy, and C(1s) XPS spectra peak fitting, Figure 2.2(c) and 2.3(c) respectively.

The antisymmetric epoxide ring deformation (908 cm^{-1}) and symmetric epoxide ring deformation (842 cm^{-1}) of poly(glycidyl methacrylate) are clearly visible, as well as the characteristic amide (1653 cm^{-1}) band of poly(*N*–acryloylsarcosine methyl ester). The XPS C(1s) spectra environments, elemental composition, and contact angle values of this bilayer stack were measured to be identical to those obtained for poly(*N*–acryloylsarcosine methyl ester), Table 2.3.

A regular 5 x 5 array of epoxide functionalities exposed through the protein-resistant layer was created by rastering an SPM tip across the bilayer surface to scratch either 500 nm x 500 nm squares or 5 μm x 5 μm squares, Figures 2.4(a) and (b), respectively. Exposure of these functionally patterned surfaces to solutions containing Protein I and then complementary fluorescent Protein II verified that protein attachment to the exposed epoxide functionalities occurs in the correct configuration, Table 2.2 and Figures 2.4 (c) - (d).

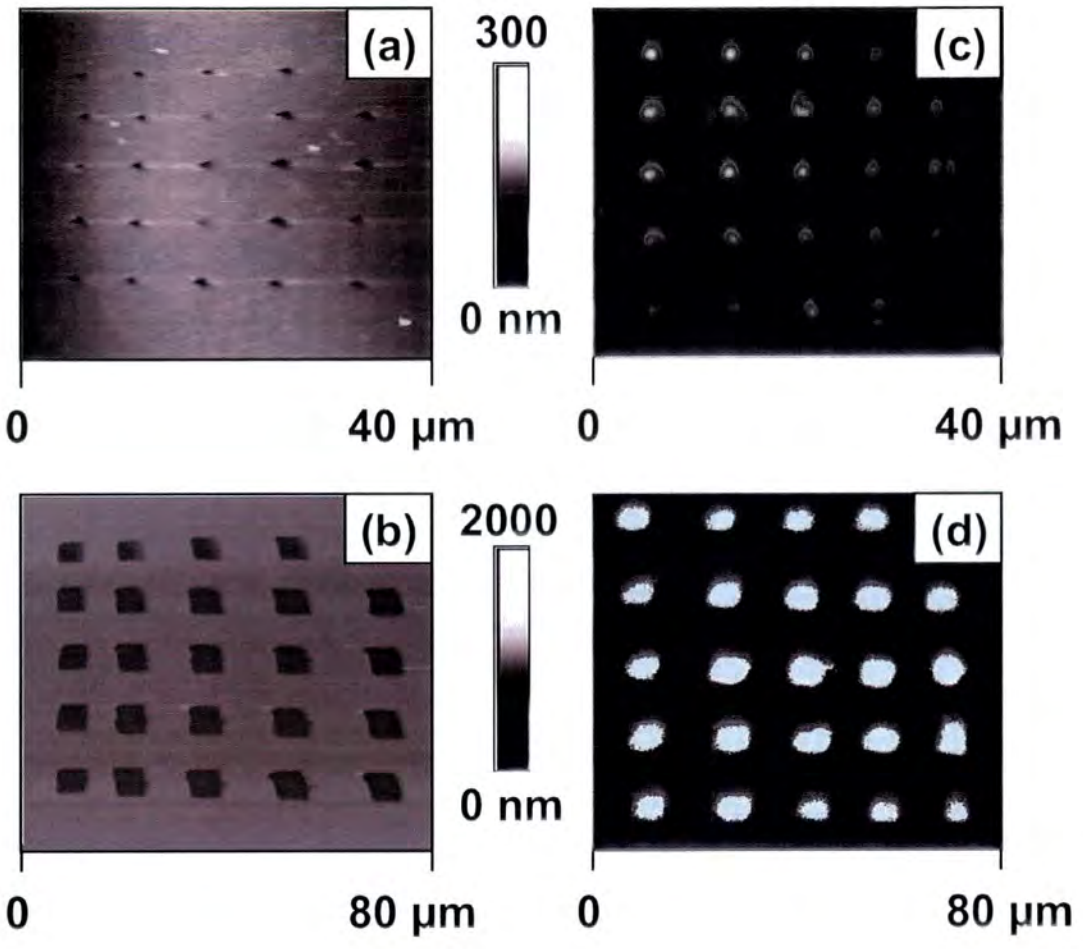

Figure 2.4 AFM micrographs of 5 x 5 arrays of exposed epoxide functionalities surrounded by a protein-resistant background: (a) 500 nm x 500 nm squares, and (b) 5 µm x 5 µm squares. Corresponding fluorescence images following immersion of the functional array in Protein I, and then complementary fluorescent Protein II, are shown in (c) and (d), respectively.

Similarly, an alternating pattern of immobilized Protein I and Protein III, was prepared by concurrently puncturing the protein-resistant poly(*N*-acryloylsarcosine methyl ester) top layer and delivering the respective protein solution using a robotic microarrayer pin. Subsequent immersion in fluorescent Protein II solution displayed binding to Protein I only, Figure 2.5(a), whereas exposure of the protein array to fluorescent Protein IV solution gave rise to exclusive binding to Protein III spots, Figure 2.5(b).

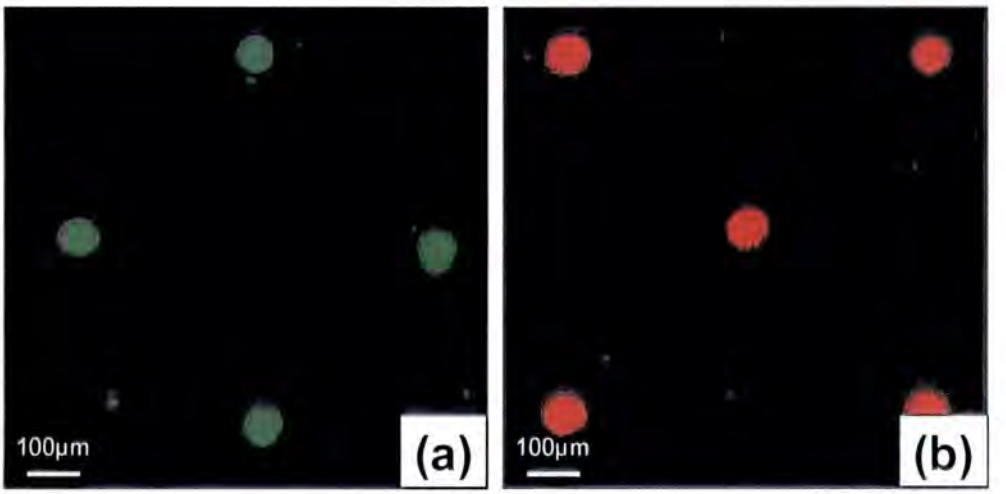

Figure 2.5 Fluorescence images of an alternating pattern of Protein I and Protein III after exposure to: (a) Protein II; and (b) Protein IV (scale bar is 100 μm).

2.3.2 DNA Arrays

XPS elemental analysis and C(1s) peak fitting of pulsed plasma deposited poly(glycidyl methacrylate) and poly(allylmercaptan) films was found to be in good agreement with the theoretical precursor compositions, Table 2.4 and Figure 2.6(a) and (b) respectively.[30,68]

Pulsed plasma deposition of a 300 nm thick poly(allylmercaptan) DNA binding layer, followed by a 20 nm thick poly(glycidyl methacrylate) non-binding film was verified by C(1s) XPS spectra peak fitting, elemental composition, and contact angle values of the bilayer stack matching poly(glycidyl methacrylate), Table 2.4, and Figure 2.6(c).

Pulsed Plasma Polymer(s)	**Contact Angle / °**	**Elemental Composition**		
		C %	**S %**	**O %**
Allylmercaptan	83.2 ± 4.5	72.4 ± 2.2	27.6 ± 2.2	0
Theoretical allylmercaptan	N/A	75	25	0
Glycidyl methacrylate	59.5 ± 2.3	66.9 ± 1.1	0	33.1 ± 1.1
Theoretical glycidyl methacrylate	N/A	70	9	30
Glycidyl methacrylate + allylmercaptan	61.5 ± 2.3	66.6 ± 0.3	0	33.3 ± 0.6

Table 2.4 Experimental contact angle and composition of pulsed plasma deposited poly(allylmercaptan), poly(glycidyl methacrylate), and poly(glycidyl methacrylate) pulsed plasma deposited onto poly(allylmercaptan).

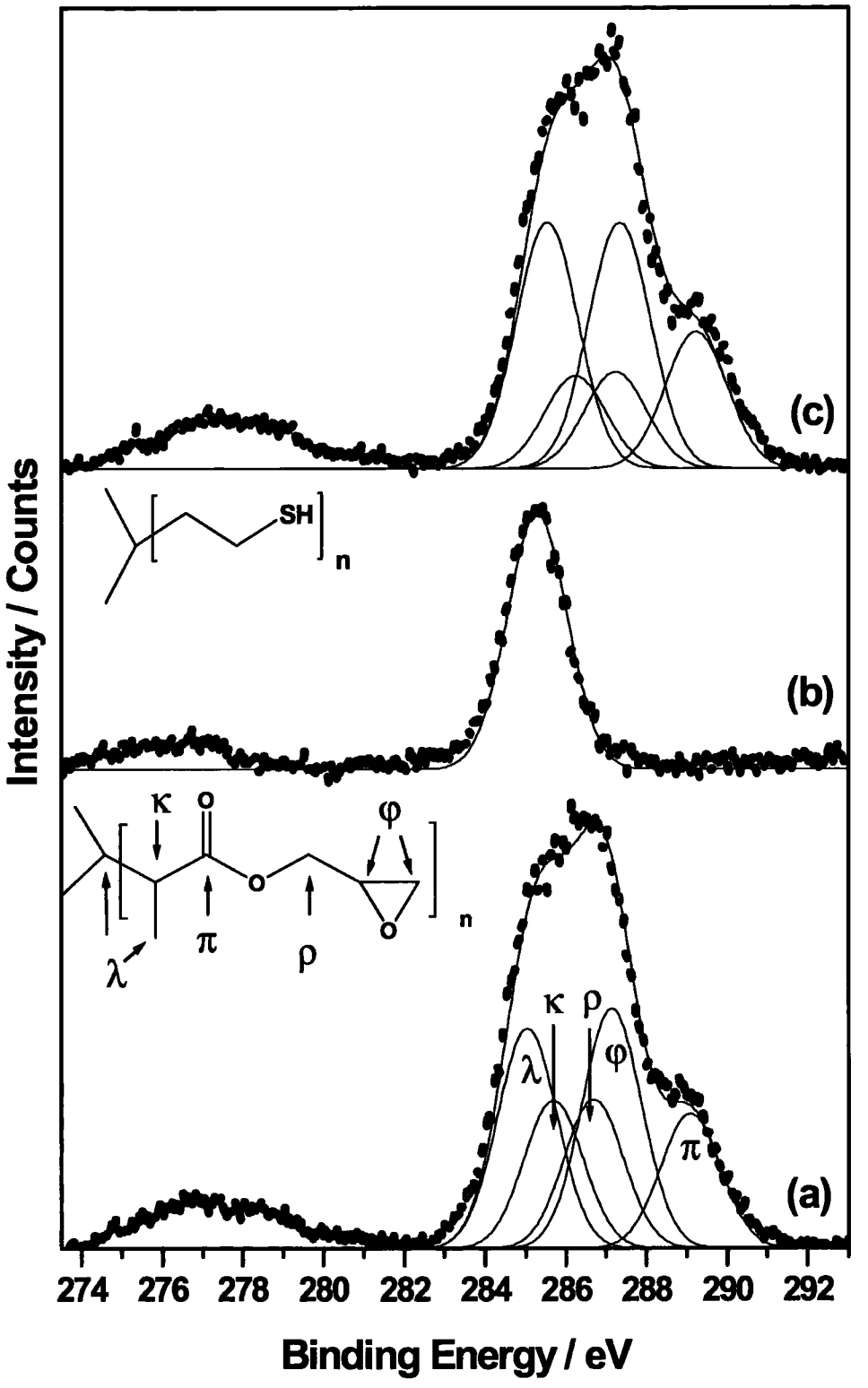

Figure 2.6 C(1s) XPS peak fitting of pulsed plasma deposited: (a) 20 nm poly(glycidyl methacrylate); (b) 300 nm poly(allylmercaptan); and (c) 20 nm poly(glycidyl methacrylate) on top of a 300 nm poly(allylmercaptan) layer.

A regular 5 x 5 array of exposed thiol functionalities was created by rastering an SPM tip to scratch either 5 μm x 5 μm or 500 nm x 500 nm squares, Figure 2.7(a) and (b), respectively. Exposure of these patterned surfaces to thiol terminated, Cy5 tagged, oligonucleotide demonstrated the reactivity of the exposed poly(allylmercaptan) pixels, Figure 2.7(c) and (d), respectively. Clearly, such arrays can be utilised for DNA hybridization re-writing as applications by using previously reported protocols.[30]

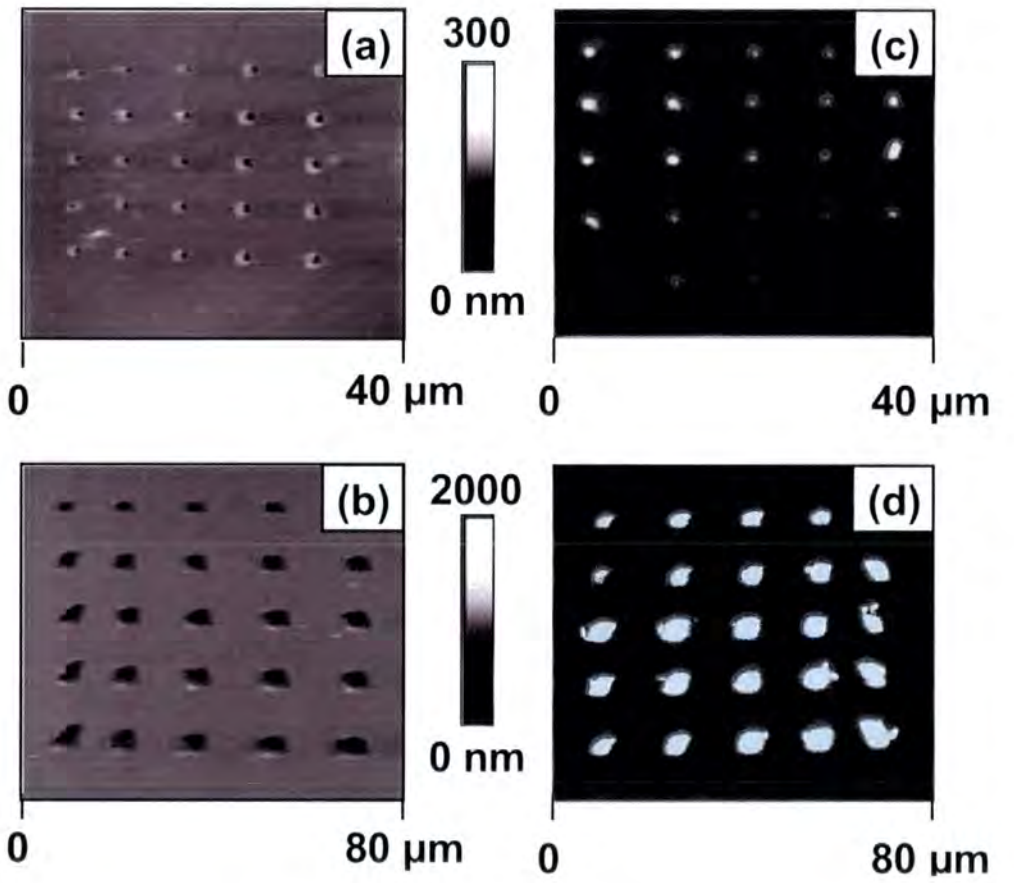

Figure 2.7 AFM micrographs showing a 5 x 5 array of exposed thiol functionalities surrounded by epoxide background: (a) 500 nm x 500 nm squares, and (b) 5 μm x 5 μm squares. Corresponding fluorescence images following immersion in Cy5 tagged thiol terminated DNA are shown in (c) and (d) respectively.

2.4 Discussion

A functional protein array typically comprises a series of protein spots immobilized onto a solid surface whilst retaining biological functionality.[6,7,8] Numerous approaches have been devised to facilitate this,[70] including covalent attachment to activated surfaces through reactive linker groups,[71, 72] gel-coated slides[73] and affinity capture of proteins via biomolecular interactions.[74] However, all of these methods suffer from either restriction to the utilisation of only one protein,[75] or the limitation of non-specific protein adsorption onto the surrounding background[76,77] leading to a reduction in background fluorescence (rather than complete elimination of non-specific protein binding). The molecular scratchcard protein arrays described utilise a bifunctional nanolayer stack comprising a 20 nm pulsed plasma deposited poly(*N*–acryloylsarcosine methyl ester) protein-resistant top coating[67] and a 300 nm pulsed plasma deposited poly(glycidyl methacrylate) underlayer containing reactive epoxide groups amenable to binding primary amine groups belonging to the protein[78,79] via nucleophilic attack. It has been shown that the top layer can be pierced using a robotic microarrayer pin to concurrently deliver approximately 1 nl droplets of protein solution direct to the underlying reactive epoxide surface. Retention of protein functionality has been demonstrated by generating an alternating array of Protein I and Protein III, which bind selectively to fluorescently labelled Protein II[80] and Protein IV,[81] respectively, Figure 2.5. An important attribute of this nanolayered functional stack is that it benefits from low background fluorescence due to the elimination of non-specific protein adsorption as a consequence of the protein-resistant top layer. In a similar fashion, the utilisation of an SPM probe tip can provide much smaller (higher density) arrays, Figure 2.4. The variation of spot intensity of the high density arrays is a consequence of the pixels being at slightly different focal lengths due to uneven sample mounting. The variation in pixel shape is an artefact resulting from the lack of a closed loop scanner in the multimode scanner leading to poor linearity. Further variants could include the marrying of this molecular scratchcard concept with dip pen

nanolithography. Also, smaller scale features are feasible by utilising sharper SPM tips (e.g. carbon nanotubes).

To demonstrate the versatility of molecular scratchcards, the immobilization of deoxyribonucleic acid (DNA) has also been performed. The fabricated molecular scratchcard DNA array utilises a dual nanolayer stack comprising a 300 nm pulsed plasma poly(allylmercaptan) underlayer possessing reactive thiol groups amenable to binding to thiol terminated DNA strands, and a 20 nm pulsed plasma top-coating of poly(glycidyl methacrylate), which does not bind to thiol terminated DNA under the applied reaction conditions (thus acting as a passivation layer). Selective removal of the poly(glycidyl methacrylate) outer layer exposes the underlying thiol linker groups. Fluorescently tagged thiol terminated DNA strands have been shown to readily react with these sites via di-sulfide bridge formation. Such immobilized DNA strands can then undergo hybridization with their complementary strands.[30]

2.5 Conclusions

Pulsed plasmachemical nanolayering is a relatively straightforward method for the fabrication of multilayer functional stacks. Sequential deposition of a reactive layer and then a passivation layer, followed by selective localized unveiling of the underlying reactive groups by piercing the passive top layer has been shown to be an effective way of preparing protein and oligonucleotide arrays.

2.6 References

(1) Whang, Z.; Zhang, J.; Xing, R.; Yuan, J.; Yan, D.; Han, Y. *J. Am. Chem. Soc.* **2003,** *125,* 15278.

(2) Jiang, P.; McFarland, M. J. *J. Am. Chem. Soc.* **2005,** *127,* 3710.

(3) Peterlinz, K. A.; Georgiadis, R. M.; Herne, Tarlov M. J. *J. Am. Chem. Soc.* **1997,** *119,* 3401.

(4) Schena, M.; Shalon, D.; Davis, R. W.; Brown, P. O. *Science* **1995,** *270,* 467.

(5) Georgiadis, R.; Peterlinz, K. P.; Peterson, A. W. *J. Am. Chem. Soc.* **2000,** *122,* 3166.

(6) MacBeath, G.; Schreiber, S. L. *Science* **2000,** *289,* 1760.

(7) Kane, R. S.; Takayama, S.; Ostuni, E.; Ingber, D. E.; Whitesides, G. M. *Biomaterials* **1999,** *20,* 2363.

(8) Zhou, H.; Baldini, L.; Hong, J.; Wilson, A. J.; Hamilton, A. D. *J. Am. Chem. Soc.* **2006,** *128,* 2421.

(9) Zhong, Z.; Wang, D.; Cui, Y.; Bockrath, M. W.; Lieber, C. M. *Science* **2003,** *302,* 1377.

(10) Filho, F. H. D.; Mauricio, M. H. P.; Ponciano, C. R.; Prioli, R. *Mat. Sci. Eng., B* **2004,** *112,* 194.

(11) Wallraff, G. M.; Hinsberg, W. D. *Chem. Rev.* **1999,** *99,* 1801.

(12) Wei, C.; Dai, L.; Roy, A.; Tolle, T. B. *J. Am. Chem. Soc.* **2006,** *128,* 1412.

(13) Kline, R. T.; Paxton, F. W.; Wang, Y.; Velegol, D.; Mallouk, T. E.; Sen, A. *J. Am. Chem. Soc.* **2005,** *127,* 17150.

(14) Beebe, D. J.; Moore, J. S.; Yu, Q.; Liu, R.; Kraft, M. L.; Jo, B.; Devadoss, C. *Proc. Natl. Acad. Sci.* **2000,** *97,* 13488.

(15) Beebe, D. J.; Mensing, G. A.; Walker, G. M. *Ann. Rev. Biomed. Eng.* **2002,** *4,* 261.

(16) Heath, J. R. Acc. *Chem. Res* **1999,** *32,* 388.

(17) Du, P.; Mingqi, L.; Douki, K.; Li, X.; Garcia, C. B. W.; Jain, A.; Smilgies D. M.; Fetters L. J.; Gruner, S. M.; Wiesner, U.; Ober, C. K. *Adv. Mater.* **2004,** *16,* 953.

(18) Park, K. S.; Seo, E. K.; Do, Y. R.; Kim, K.; Sung, M. M. *J. Am. Chem. Soc.* **2006,** *128,* 858.

(19) Xia, Y.; Whitesides, G. M. *Angew. Chem. Int. Ed.* **1998,** *37,* 550.

(20) Lackowski, W. M.; Ghosh, P.; Crooks, R. M. *J. Am. Chem. Soc.* **1999,** *121,* 1419.

(21) Tan, J. L.; Tien, J.; Chen, C. S. *Langmuir* **2002,** *18,* 519.

(22) Yu, A. A.; Savas, T.; Cabrini, S.; diFabrizio, E.; Smith, H. I.; Stellacci, F. *J. Am. Chem. Soc.* **2005,** *127,* 16774.

(23) Langowski, B. A.; Uhrich, K. E. *Langmuir* **2005,** *21,* 10509.

(24) Rupcich, N.; Goldstein, A.; Brennan, J. D. *Chem. Mater.* **2003,** *15,* 1803.

(25) Lin, H.; Sun, L.; Crooks, R. M. *J. Am. Chem. Soc.* **2005,** *127,* 11210.

(26) MacBeath, G.; Koehler, A. N.; Schreiber, S. L. *J. Am. Chem. Soc.* **1999,** *121,* 7967.

(27) Mendes, P. M.; Jacke, S.; Critchley, K.; Plaza, J.; Chen, Y.; Nikitin, K.; Palmer, R. E.; Preece, J. A.; Evans, S. D.; Fitzmaurice, D. *Langmuir* **2004,** *20,* 3766.

(28) Sondag-Huethorst, J. A. M.; Fokkink, L. G. *Langmuir* **1995,** *11,* 4823.

(29) Kim, J. M.; Jung, H. S.; Park, J. W.; Yukimasa, T.; Oka, H.; Lee, H. Y.; Kawai, T. *J. Am. Chem. Soc.* **2005,** *127,* 2358.

(30) Zhao, B.; Zhu, L. *J. Am. Chem. Soc.* **2006,** *128,* 4574.

(31) Wang, C. W.; Moffit, M. G. Chem. Mater. **2005,** *17,* 3871.

(32) Minelli, C.; Hinderling, C.; Heinzelmann, H.; Pugin, R.; Liley, M. *Langmuir* **2005,** *21,* 7080.

(33) Behm, J. M.; Lykke, K. R.; Pellin, M. J.; Hemminger, J. C. *Langmuir* **1996,** *12,* 2124.

(34) Anderson, J. R.; Chiu, D. T.; Jackmann, R. J.; Cherniavskaya, O.; McDonald, J. C.; Wu, H.; Whitesides, S. H.; Whitesides, G. M. *Anal. Chem.* **2000,** *72,* 3158.

(35) Zhou, C.; Nagy, G.; Walker, A. V. *J. Am. Chem, Soc.* **2005,** *127,* 12160.

(36) Lejeune, M.; Valsesia, A.; Kormunda, M.; Colpo, P.; Rossi, F. *Surf. Sci.* **2005,** *583,* L142.

(37) Choi, Y. K.; Zhu, J.; Grunes, J.; Bokor, J.; Somorjai, G. A. J. *Phys. Chem. B.* **2003,** *107,* 3340.

(38) Korczagin, I.; Golze, S.; Hempenius M. A.; Vansco, G. J. *Chem. Mater.* **2003,** *15,* 3663.

(39) Davis, J. J. ; Coleman, K. S.; Busuttil, K. L.; Bagshaw, C. B. *J. Am. Chem. Soc.* **2005,** *127,* 13082.

(40) Ginger, D. S.; Zhang, H.; Mirkin, C. A. *Angew. Chem. Int. Ed.* **2004,** *43,* 30.

(41) Lee, K. B.; Lin, J. H.; Mirkin, C. A. *J. Am. Chem. Soc.* **2003,** *125,* 5588.

(42) Cai, Y.; Ocko, B. M. *J. Am. Chem. Soc.* **2005,** *127,* 16287.

(43) Xie, X. N.; Deng, M.; Xu, H.; Yang, S. W.; Qi, D. C.; Gao, X. Y.; Chung, H. J.; Sow, C. H.; Tan, V. B. C.; Wee, T. S. W. *J. Am. Chem. Soc.* **2006,** *128,* 2738.

(44) Tella, M.; Garcia, R. *Appl. Phys. Lett.* **2001,** *79,* 424.

(45) Dagata, J. A.; Scheir, J.; Harary, H. H.; Evans, C. J.; Postek, M. T.; Bennet, J. *Appl. Phys. Lett.* **1990,** *56,* 2001.

(46) Dagata, J. A.; Perez-Murano, F.; Abadal, G.; Morimoto, K.; Inoue, T.; Itoh, J.; Yokoyama, H. *Appl. Phys. Lett.* **2000,** *76,* 2710.

(47) Martin, C.; Rius, G.; Borrrise, X.; Perez-Murano, F. *Nanotech* **2005,** *16,* 1016.

(48) Seo, K.; Borguet, E. *Langmuir* **2006,** *22,* 1388.

(49) Sung, I. H.; Kim, D. E.; *Appl. Surf. Sci.* **2005,** *239,* 209.

(50) Headrick, J. E.; Armstrong, M.; Cratty, J.; Hammond, S.; Sheriff, B. A.; Berrie, C. L. *Langmuir* **2005,** *21,* 4117.

(51) Nuraje, N.; Banerjee, I. A.; MacCuspie, R. I.; Lingtao, Y.; Matsui, H. *J. Am. Chem. Soc.* **2004,** *126,* 8088.

(52) Liu, G. Y.; Xu, S.; Qian, Y. *Acc. Chem. Res.* **2000,** *33,* 457.66

(53) Xu, S.; Miller, S.; Laibinis, P. E.; Liu. G. Y. *Langmuir* **1999,** *15,* 7244.

(54) Lutwyche, M. I.; Despont, M.; Dreschler, U.; Durig, U.; Haberle, W.; Rothuizen, H.; Stutz, R.; Widmer, R.; Binning, G. K.; Vettiger, P. *Appl. Phys. Lett.* **2000,** *77,* 3299.

(55) King, W. P.; Kenny, T. W.; Goodson, K. E.; Cross, G.; Despont, M.; Durig, U.; Rothuzien, H.; Binnig, G. K.; Vettifer, P. *Appl. Phys. Lett.* **2001,** *78,* 1300.

(56) Xiao, X.; Hu, J.; Charych, D. H.; Salmeron, M. *Langmuir* **1996,** *12,* 235.

(57) Mrksich, M.; Sigal, G. B.; Whitesides, G. M. *Langmuir* **1995,** *11,* 4383.

(58) Ostuni, E.; Chapman, R. G.; Holmlin, R. E.; Takayama, S.; Whitesides, G. M. *Langmuir* **2001,** *17,* 5605.

(59) Chapman, R. G.; Ostuni, E.; Yan, L.; Whitesides G. M. *Langmuir* **2000,** *16,* 6927.

(60) Gates, B. D.; Xu, Q.; Love, J.; Wolfe, D. B.; Whitesides, G. M. *Ann. Rev. Mater. Res.* **2004,** *34,* 339.

(61) Flynn, N. T.; Tran, T. N. T.; Cima, M. J.; Langer, R. *Langmuir* **2003,** *19,* 10909.

(62) Wanunu, M.; Vaskevich, A.; Cohen, R. S.; Hagai, C.; Arad-Yellin, R.; Shanzer, A.; Rubinstein I. *J. Am. Chem. Soc.* **2005,** *127,* 17877.

(63) Schofield, W. C. E.; McGettrick, J.; Bradley, T. J.; Przyborski, S.; Badyal, J. P. S. *J. Am. Chem. Soc.* **2006,** *128,* 2280.

(64) Evans, J. F.; Gibson, J. H.; Moulder, J. F.; Hammond, J. S.; Goretzki, H. *Fresenius J. Anal. Chem.* **1984,** *319,* 841.

(65) Tabet, M. F.; McGahan, W. A. *Thin Solid Film* **2000,** *370,* 122

(66) Zhong, Q.; Innis, D.; Kjollerm K.; Ellings, V. B. *Surf. Sci.* **1993,** *14,* 3045.

(67) Teare, D. O. H.; Schofield, W. C. E.; Garrod, R. P.; Badyal, J. P. S. *J. Phys. Chem. B* **2005,** *109,* 20923.

(68) Tarducci, C.; Kinmond, E.; Brewer, S.; Willis, C.; Badyal J. P. S. *Chem. Mater.* **2000,** *12,* 1884.

(69) Beamson, G. P.; Brigss, D. *High Resolution XPS of Organic Polymers, The Scienta ESCA 300 Database*; John Wiley & Sons: New York, 1992: p130.

(70) Heng, Z.; Snyder, M. *Curr. Opin. Chem. Biol.* **2003,** *7,* 55.

(71) Zhu, H.; Klemic, J. F.; Chang, S.; Bertone, P.; Casamayor, A.; Klemic, K. G.; Smith, D.; Gerstein, M.; Reed, M. A.; Snyder, M. *Nat. Genet.* **2000,** *26,* 283.

(72) Wilson, D. S.; Nock, S. *Curr. Opin. Chem. Biol.* **2001,** *6,* 81.

(73) Arenkhov, P.; Kukhtin, A.; Gemmell, A.; Voloschuck, S.; Chupeeva, V.; Mirzabekov, A. *Anal. Biochem.* **2000,** *278,* 123.

(74) Zhu, H.; Bilgin, M.; Bangham, R.; Hall, D.; Casamayor, A.; Bertone, P.; Lan, N.; Jansen, R.; Bidlingmaier, S.; Houfek, T.; Mitchell, T.; Miller, P.; Dean, R. A.; Gerstein, M.; Snyder, M. *Science,* **2001,** *293,* 2101.

(75) Lee, S. W.; Oh, B. K.; Sanedrin, R. G.; Salaita, K.; Fujigaya, T.; Mirkin, C. A. *Adv. Mater.* **2006,** *18,* 1133.

(76) Vroman, L.; Adams, A. L.; Fischer, G. C.; Munoz, P. C. *Blood* **1980,** *55,* 156.

(77) Wang, M. S.; Palmer, L. B.; Schwarts, J. D.; Razatos, A. *Langmuir* **2004,** *20,* 7753.

(78) Deng, Y.; Zhu, W. Y.; Kienlen, T.; Guo, Q. *J. Am. Chem. Soc.* **2006,** *128,* 2768.

(79) Mateo, C.; Torres, R.; Fernandez-Lorente, G.; Ortiz, C.; Fuentes, M.; Hidalgo, A.; Lopez-Gallego, F.; Abian, O.; Palomo, J. M.; Guisan, J. M.; Betancor, L.; Pessela, B. C. C.; Fernandez-Lafuente, R. *Biomacromolecules* **2003,** *4,* 772.

(80) Lindmark, R.; Thoren-Tolling, K.; Sjoquist, J. J. *Immunol. Methods* **1983,** *62,* 1.

(81) Bjorck, L.; Kronvall, G. *J. Immunol.* **1984,** *133,* 969.

CHAPTER 3

RE-WRITABLE SUGAR ARRAYS FOR FUNCTIONAL GLYCOMICS

3.1 Introduction

Sugar-protein interactions mediate a whole host of biological systems including those responsible for viral infection,[1,2] cancer metastasis,[3,4] peptide conformation,[5] enzyme activity,[6] cell-cell recognition,[7,8] cell adhesion[9,10] and cell development.[11] The current techniques utilised to monitor these interactions include electrospray ionisation mass spectrometry,[12] fluorescence microscopy,[13] chromatography,[14] X-ray crystallography[15,16] and NMR.[17] Although well understood, these methods can be time consuming, expensive and technically demanding. An alternative low cost, high-throughput diagnostics solution is to screen molecular arrays of sugars in a similar mode d'emploi to DNA[18,19,20] and protein[21,22,23] chips.

Two generic approaches exist to facilitate the prerequisite sugar immobilization. Firstly there is non-covalent attachment to the substrate, which includes thiol terminated sugar self assembled monolayers (SAMs) on gold,[24,25,26] Diels-Alder coupling of sugar–cyclopentadiene conjugates to bezoquinone SAMs,[27,28] hydrophobic attachment of $C_{13} - C_{15}$ saturated alkyl terminated sugars to polystyrene microtiter plates,[29,30,31,32] arraying onto nitrocellulose membranes,[33] and electrostatic immobilization.[34] Alternatively there is direct covalent immobilization of modified sugars onto functionalized glass slides[35,36,37,38,39,40,41,42] or silicon.[43,44] However, many of these approaches suffer from drawbacks such as poor shelf-life e.g. SAM's,[24,25,26,27,28] attributable to oxidation and desorption processes of the Au-S bond at the gold surface,[45] the dependency of electrostatic attractions upon molecular size,[33,34] limiting the possible range of immobilized sugars,[46] and the substrate dependant nature of the specific covalent attachment chemistries[35-44] prohibiting application to a wide range of materials.

In this study two substrate independent plasmachemical methodologies for the fabrication of re-writable sugar micro-arrays based on disulfide bridge formation between glycomethanethiosulfonate[47,48,49] terminated sugars and thiol functionalized pulsed plasma deposited poly(allylmercaptan) nanolayers,[50] Figure 3.1, or alternatively Schiff base

imine[51] formation between the aldehyde terminus present in reducing sugars and surface amine groups presented by pulsed plasma deposited poly(4-vinylaniline) nanolayers, Figure 3.2

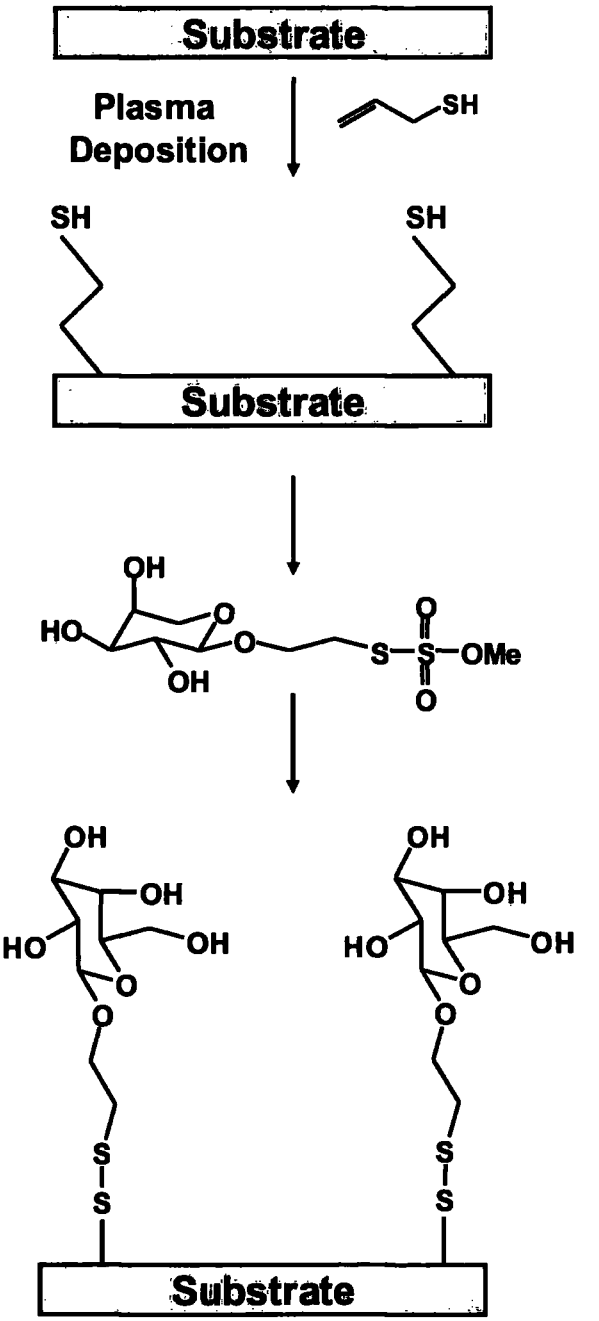

Figure 3.1 Glycomethanethiosulfonate functionalization of pulsed plasma deposited poly(allylmercaptan).

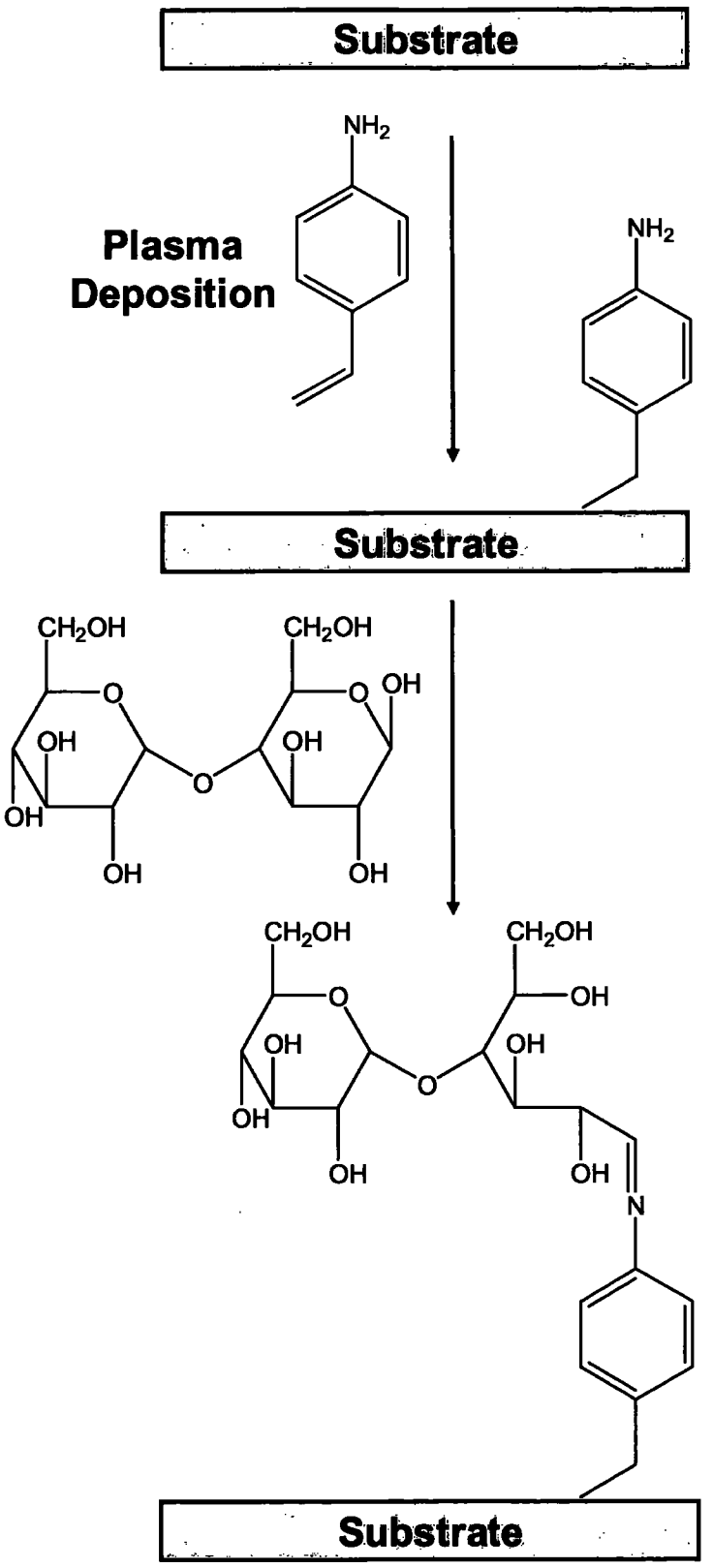

Figure 3.2 D-Maltose functionalization of pulsed plasma deposited poly(4-vinylaniline).

In addition, the utilisation of a molecular scratchcard comprising upper protein-resistant nanolayers deposited over a sugar binding layer for the detection of protein-sugar interactions is demonstrated, Figure 3.3. Finally a multiplex surface is created for binding of different sugars by sequential deposition of different functionalities through a mask, Figure 3.4.

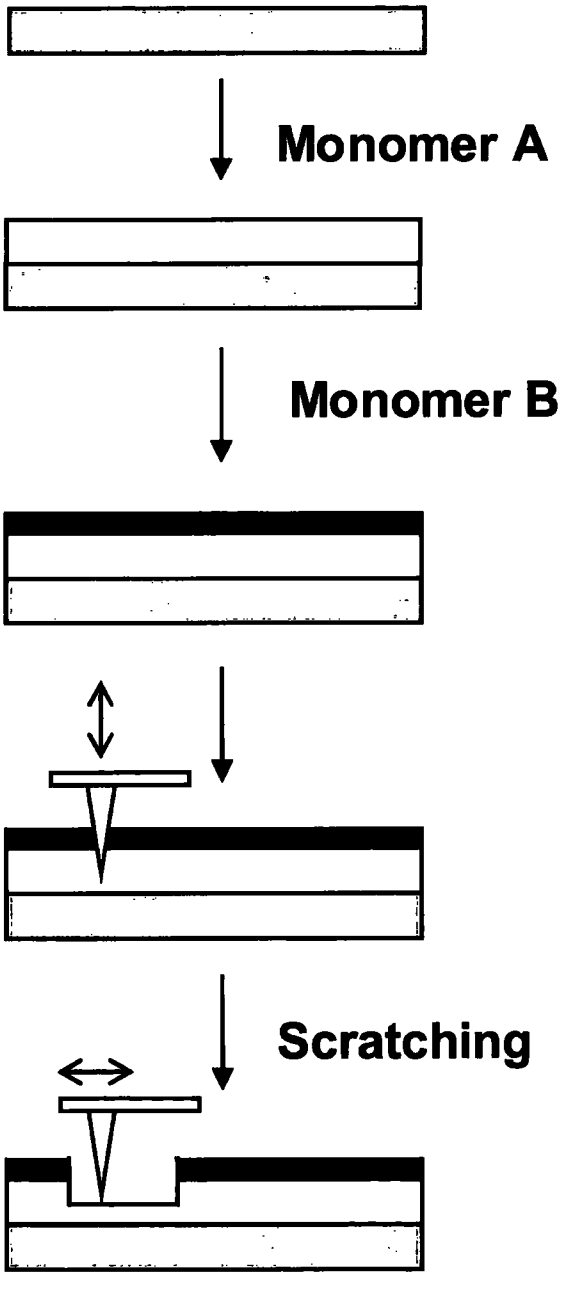

Figure 3.3 Molecular scratchcard fabrication followed by SPM tip scratching where monomer A is sugar binding and monomer B is protein resistant.

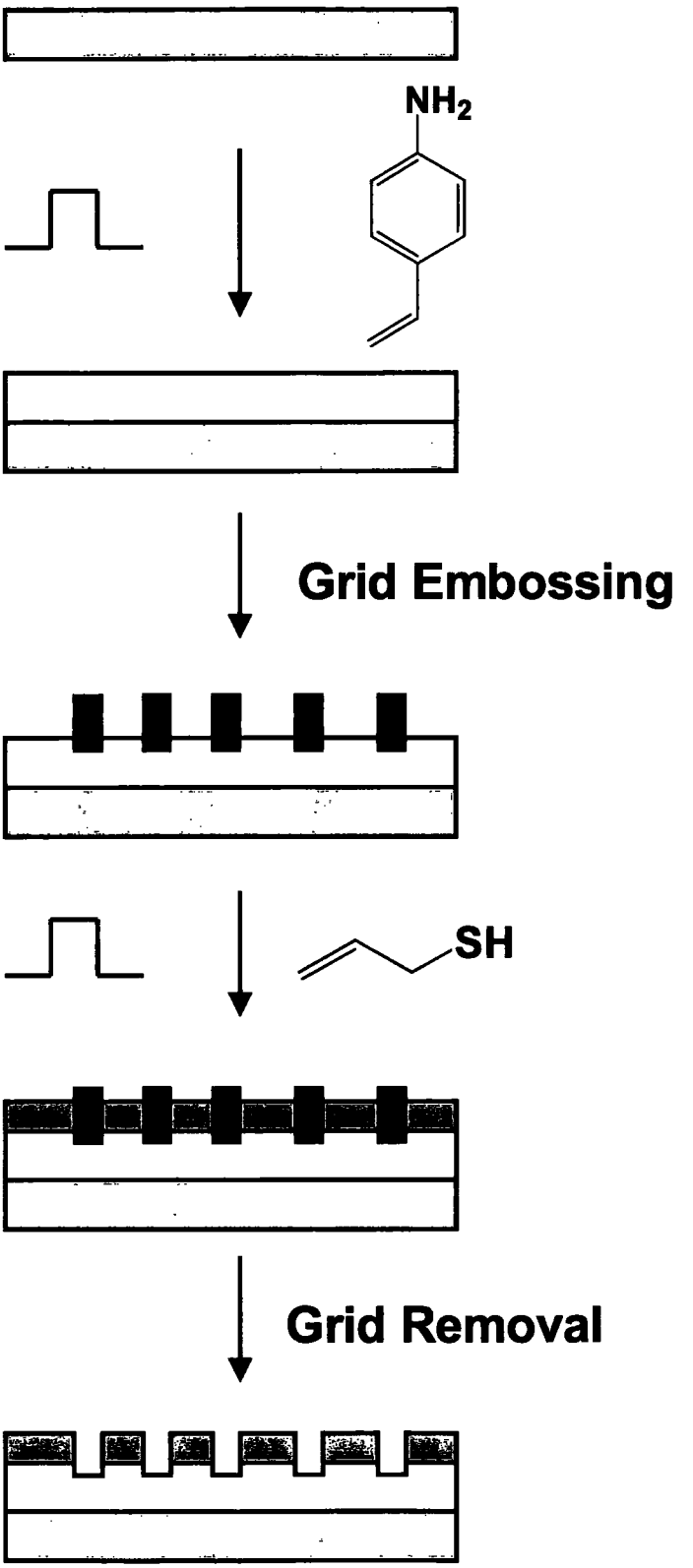

Figure 3.3 Formation of multi-functional surface via an embossed grid to immobilize biologically differing sugars

3.2 Experimental

3.2.1 Plasmachemical Nanolayering

Plasma polymerization was carried out in a cylindrical glass reactor (4.5 cm diameter, 460 cm^3 volume) located inside a Faraday cage and evacuated by a 30 L min^{-1} rotary pump via a liquid nitrogen cold trap (2 x 10^{-3} mbar base pressure and better than 1.2 x 10^{-9} mol s^{-1} leak rate). A copper coil (4 mm diameter, 10 turns, located 15 cm away from the precursor inlet) was connected to a 13.56 MHz radio frequency supply via an LC matching network. System pressure was monitored with a Pirani gauge. All fittings were grease free. During pulsed plasma deposition, the RF source was triggered by a signal generator, and the pulse shape monitored with an oscilloscope. Prior to each experiment the apparatus was scrubbed with detergent, rinsed with propan-2-ol, and oven dried. Further cleaning entailed running a 40 W continuous wave air plasma at 0.2 mbar pressure for 20 min. At this stage, each monomer was loaded into a sealable glass tube and further purified using multiple freeze-pump-thaw cycles. The substrate of interest was placed into the centre of the reactor, and the system evacuated to base pressure. For each functional monomer, a continuous flow of vapour was introduced via a fine needle control valve at a pressure of 0.2 mbar and 2.2 x 10^{-7} mol s^{-1} flow rate for 5 min prior to electrical discharge ignition. Optimum pulsed plasma duty cycle parameters for each precursor are listed in Table 3.1. Upon completion of deposition, the RF power source was switched off and the monomer allowed to continue to purge though the system for a further 5 min prior to evacuation to base pressure and venting to atmosphere. Multiplex surface generation entailed embossing a grid (2000 Mesh, Agar) at 400MPa for 10s onto pulsed plasma deposited poly(4-vinyalaniline), followed by the deposition of allylmercaptan and grid removal to leave 10 μm pulsed plasma deposited poly(allylmercaptan) squares separated via 2 μm pulsed plasma deposited poly(4-vinylaniline) bars.

Precursor	Reactor Temp / °C	Pulse Duty Cycle / µs		Deposition Rate / nm min^{-1}
		Time On	Time Off	
Allylmercaptan (+80%, Sigma-Aldrich)	22	100	4000	10
4-vinylaniline (+97%, Sigma-Aldrich)	40	100	4000	20
N–acryloylsarcosine methyl ester (+97%, Lancaster)	50	20	5000	9

Table 3.1 Optimum parameters for pulsed plasma polymerization of each monomer.

3.2.2 Sugar Functionalization

Sugar microarrays were fabricated using a robotic microarrayer (Genetix Inc) equipped with 1 nL delivery micro-machined pins. Sugar solutions of A and B were spotted onto pulsed plasma poly(allylmercaptan) and (4-vinylaniline) coated glass slides (18 × 18 × 0.17 mm, BDH) respectively, Table 3.2. Circular spots with diameters ranging from 100 to 125 µm could be routinely obtained. After spotting, the slides of immobilized sugar A and B were kept in a humidity chamber for 12 h at 32 ^{o}C and 36 h at 70 ^{o}C respectively. The slides were subsequently washed with CHES buffer, CHES buffer diluted to 50% v/v with de-ionized water, and twice with de-ionized water.

Sugar	Concentration	Label
β-D-galacto-methanethiosulfonate (Ben Davis, Oxford University)	1μm in 70mM CHES buffer (+99%, Sigma Aldrich)	A
D-Maltose (+90%, Sigma-Aldrich)	1μm in Formamide (Sigma-Aldrich)	B

Table 3.2 Sugar solutions employed in this study.

Microarrays of sugar A and B were exposed to a complementary solution of Protein I (20 μg mL^{-1} in phosphate buffered saline) and Protein II (20 μg mL^{-1} in phosphate buffered saline) respectively for 60 min at room temperature followed by successive rinses in phosphate buffered saline, phosphate buffered saline diluted to 50% v/v with de-ionized water, and finally washed twice with de-ionized water, Table 3.3.

Protein	Fluorophore	Label
Peanut Agglutinin (Molecular Probes)	Alexa Fluor 488	Protein I
Concanavalin A (Molecular Probes)	Alexa Fluor 647	Protein II

Table 3.3 Proteins and their associated fluorophores employed in this study.

Stripping of bound sugars A and B from the pulsed plasma poly(allylmercaptan) and poly(4-vinylaniline) respectively was investigated by placing the chips in a boiling solution of 200 nM TrisCl pH 7.0, 0.03 M SSC and 0.1% (w/v) SDS for 10 min. Followed by re-immobilization according to the above protocols.

Sugar immobilization onto a multiplex surface formed via deposition though a grid entailed exposure to sequential solutions of sugar A and B for 12 h at 32 ^{O}C and 36 h at 70 ^{O}C respectively The slides were subsequently washed with CHES buffer, CHES buffer diluted to 50% v/v with de-ionized water, and twice with de-ionized water. Functionalized multiplex surfaces were subsequently exposed to a complementary solution of Protein I and Protein II (20 μg mL^{-1} per protein in phosphate buffered saline) for 60 min at room temperature followed by successive rinses in phosphate buffered saline, phosphate buffered saline diluted to 50% v/v with de-ionized water, and finally washed twice with de-ionized water.

Sugar immobilization via a molecular scratchcard entailed mounting a bilayer stack comprising of 20 nm pulsed plasma deposited poly(*N*- acryloylsarcosine methyl ester) on top a 300 nm pulsed plasma deposited binding layer, onto an atomic force microscope stage (Digital Instruments Nanoscope III control module, extender electronics, and signal access module, Santa Barbara, CA). The protein-resistant pulsed plasma poly(*N*–acryloylsarcosine methyl ester) top layer was scratched away using a tapping mode tip (Nanoprobe, spring constant 42 - 83 Nm^{-1}) applied in contact mode. The movement of the tip in the x, y, and z plane was controlled by Veeco Nanolithography Software (Version 5.30r1). The patterned molecular scratchcard was immersed in a solution of sugar A or B for 12 h at 32 ^{O}C or 36 h at 70 ^{O}C respectively followed by successive rinses in CHES buffered, CHES buffer diluted to 50% v/v with de-ionized water, and twice with de-ionized water. Functionalized molecular scratchcards were then exposed to a complementary solution of Protein I (20 μg mL^{-1} in phosphate buffered saline) and Protein II (20 μg mL^{-1} in phosphate buffered saline) respectively for 60 min at room temperature followed by successive rinses in phosphate buffered saline, phosphate buffered saline diluted to 50% v/v with de-ionized water, and finally washed twice with de-ionized water.

3.2.3 Surface Characterization

X-ray photoelectron spectroscopy (XPS) was undertaken using an electron spectrometer (VG ESCALAB MK II) equipped with a non-monochromated Mg $K\alpha_{1,2}$ X-ray source (1253.6 eV) and a concentric hemispherical analyser. Photo-emitted electrons were collected at a take-off angle of 30° from the substrate normal, with electron detection in the constant analyser energy mode (CAE, pass energy = 20 eV). The XPS spectra were charge referenced to the C(1s) peak at 285.0 eV and fitted with a linear background and equal full-width-at-half-maximum (FWHM) Gaussian components[52] using Marquardt minimization computer software. Instrument sensitivity (multiplication) factors derived from chemical standards were taken as being C(1s): S(2p): O(1s): N(1s): equals 1.00: 0.52: 0.63: 0.45.

Fourier transform infrared (FTIR) analysis of the films was carried out using a Perkin-Elmer Spectrum One spectrometer equipped with a liquid nitrogen cooled MCT detector operating across the 700 – 4000 cm^{-1} range. Reflection–absorption (RAIRS) measurements were performed using a variable angle accessory (Specac) set at 86° on an Au substrate in conjunction with a KRS-5 polarizer fitted to remove the s–polarized component. All spectra were averaged over 10,000 scans at resolution of 1 cm^{-1}.

Contact angle analysis of the plasma-deposited films was carried out with a video capture system (ASE Products, model VCA2500XE) using 2.0 µL droplets of de-ionized water.

Film thickness measurements were carried out using an nkd-6000 spectrophotometer (Aquila Instruments Ltd). Transmittance-reflectance curves (over the 350-1000 nm wavelength range) were fitted to the Cauchy model for dielectric materials using a modified Levenburg-Marquardt method.[53]

AFM micrographs of each surface were acquired in tapping mode[54] operating in air at room temperature (Digital Instruments Nanoscope III control module, extender electronics, and signal access module, Santa Barbara, CA).

Fluorescence microscopy was performed using an Olympus IX–70 system (DeltaVision RT, Applied Precision, WA). Image data was collected using excitation wavelengths at 490 nm and 633 nm.

3.3 Results

3.3.1 Sugar Microarrays

Evidence for di-sulfide bridge formation required for β-D-galacto-methanethiosulfonate immobilization and Schiff base imine formation in the case of D-maltose immobilization onto solid supports for microarrays, was obtained using XPS, FT-IR and fluorescence studies.

XPS characterization of the pulsed plasma deposited poly(allylmercaptan) and poly(4-vinylaniline) nano-layers, with close resemblance to the theoretical composition calculated from the monomer structure, was confirmed by the presence of the nanolayer only at the surface, with no Si(2p) signal from the underlying silicon substrate showing through, Table 3.4. Further confirmation of the high level of retained functionality was evident from the C(1s) spectra of the pulsed plasma deposited poly(allylmercaptan), Figure 3.5(b), and the three C(1s) spectra environments of pulsed plasma deposited poly(4-vinylaniline) including: aromatic $\underline{C}_xH_y$ (284.7 eV, λ), $\underline{C}_xH_y$ (285.0 eV, κ) and $\underline{C}$-N (285.9 eV, π), Figure 3.6(b)

Pulsed Plasma Polymer(s)	Contact Angle / °	Elemental Composition			
		C %	N %	O %	S%
N-acryloylsarcosine methyl ester	51.7 ± 2.6	63.9 ± 1.9	9.6 ± 0.7	26.5 ± 1.4	-
Theoretical *N*-acryloylsarcosine methyl ester	N/A	64	9	27	-
Allylmercaptan	81.5 ± 1.2	73.5 ± 1.4	-	-	26.5 ± 1.4
Theoretical allylmercaptan	N/A	75	0	0	25
N-acryloylsarcosine methyl ester + allylmercaptan	52.6 ± 1.9	64.0 ± 0.6	9.7 ± 0.5	26.3 ± 0.6	-
4-vinylaniline	71.1 ± 1.9	87.8 ± 0.2	12.3 ± 0.2	-	-
Theoretical 4-vinylaniline	N/A	88.8	11.2	-	-
N-acryloylsarcosine methyl ester + 4-vinylaniline	52.7 ± 3.2	64.8 ± 1.1	9.6 ± 0.4	25.6 ± 1.4	

Table 3.4 Contact angle and XPS elemental composition of pulsed plasma deposited poly(*N*–acryloylsarcosine methyl ester), poly(allylmercaptan), poly(4-vinylaniline) and poly(*N*–acryloylsarcosine methyl ester) deposited on top of poly(allylmercaptan) or poly(4-vinylaniline).

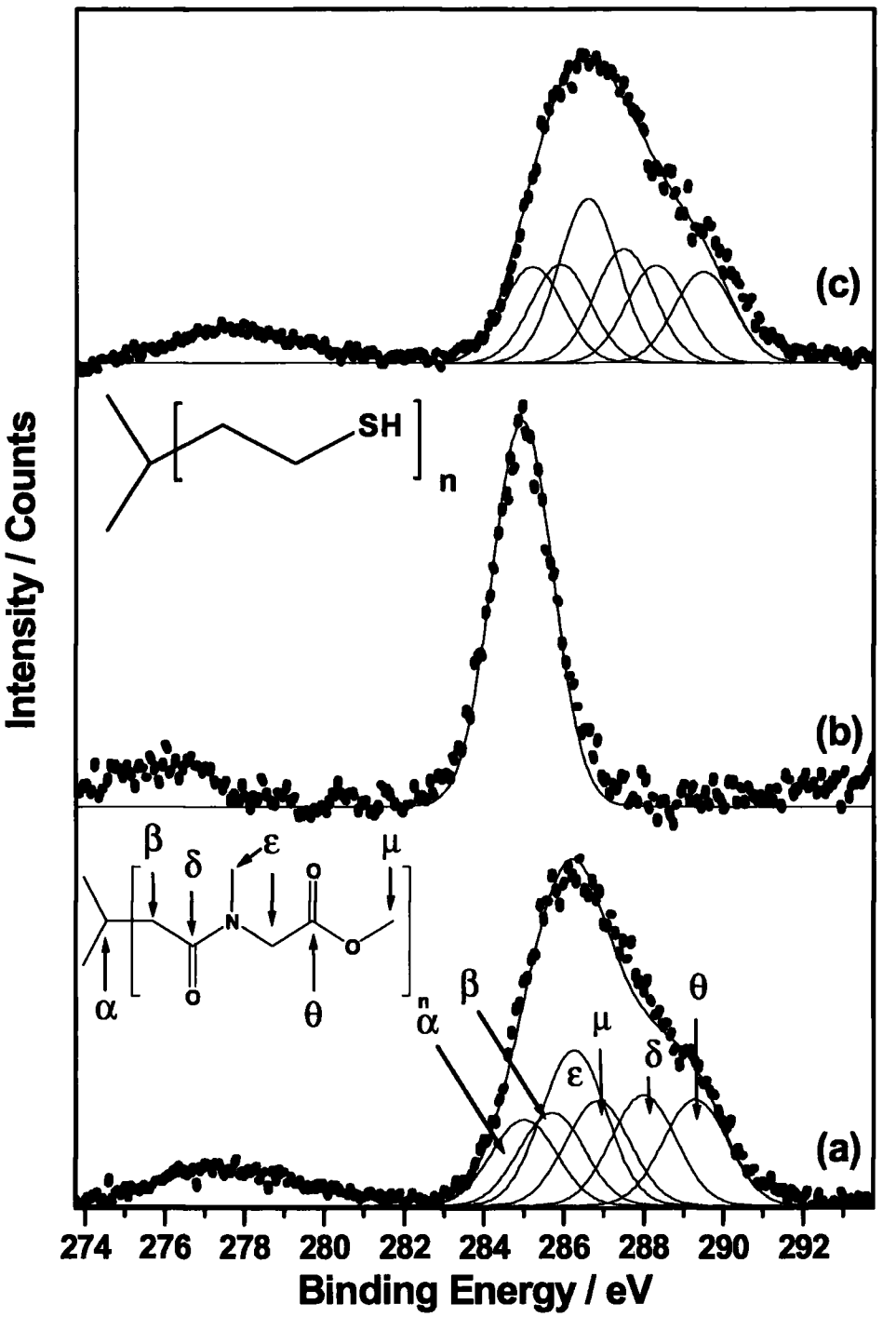

Figure 3.5 C(1s) XPS peak fitting of pulsed plasma deposited: (a) 20 nm poly(*N*–acryloylsarcosine methyl ester) protein resistant layer; (b) 300 nm poly(allylmercaptan) GMS binding layer, and (c) 20 nm poly(*N*–acryloylsarcosine methyl ester) on top of a 300 nm poly(allylmercaptan).

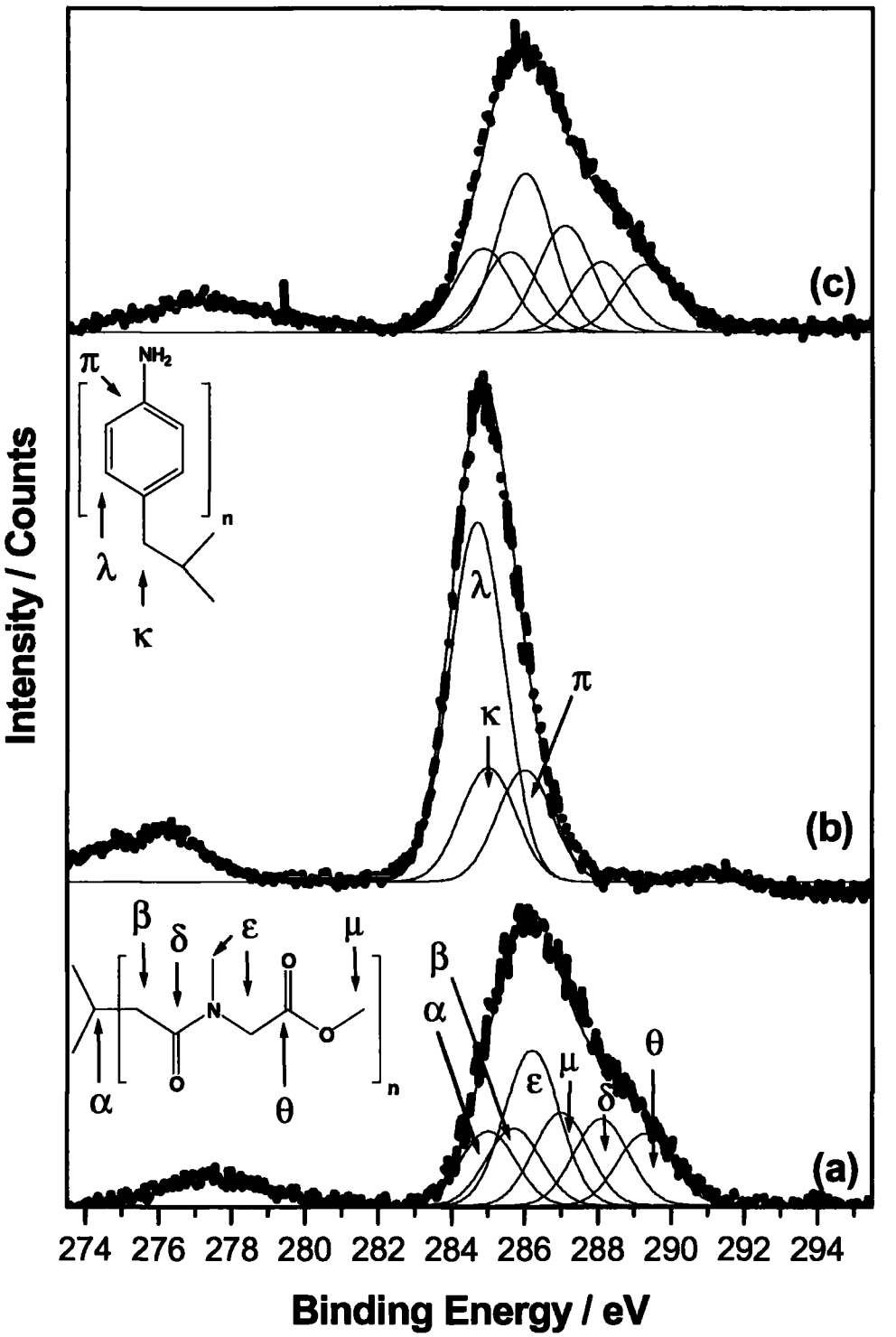

Figure 3.6 C(1s) XPS peak fitting of pulsed plasma deposited: (a) 20 nm poly(*N*–acryloylsarcosine methyl ester) protein resistant layer; (b) 300 nm poly(4-vinylaniline) D-Maltose binding layer; and (C) 20 nm poly(*N*–acryloylsarcosine methyl ester) on top of a 300 nm poly(4-vinylaniline).

Further confirmation of the high level of functional retention was evident from infrared spectroscopy. Allylmercaptan precursor displays absorbance corresponding to allyl C-H stretching (3080 cm^{-1}), allyl CH_2 stretching (3031 cm^{-1}), alkyl CH_2 stretching (2891 cm^{-1}), thiol S-H stretching (2555 cm^{-1}) and allyl C=C stretching (1634 cm^{-1}), Figure 3.7(a). All of these features are clearly discernable following pulsed plasma polymerization, except for the allyl carbon-carbon double bond stretches, which have disappeared as a consequence of polymerization, Figure 3.7(b). Exposure to β-D-galacto-methanethiosulfonate gives rise to an attenuation of the thiol S-H stretch (2555 cm^{-1}) and appearance of the OH stretch (3300 cm^{-1}) which can be taken as being indicative of di-thiol formation between sugar and surface, Figure 3.7(c)

The characteristic infrared bands for the 4-vinylaniline monomer are: asymmetric amine stretching (3440 cm^{-1}), symmetric amine stretching (3350 cm^{-1}), aromatic CH stretching (3090 cm^{-1}), ring summation (1880 cm^{-1}), C=C stretching (1625 cm^{-1}), NH_2 deformations (1615 cm^{-1}), para substituted aromatic ring stretching (1500 cm^{-1}), $=CH_2$ deformations (1415 cm^{-1}), aromatic C-N stretching (1300 cm^{-1}), para substituted benzene ring stretching (1170 cm^{-1}), HC=CH trans wagging (990 cm^{-1}), $=CH_2$ wagging (910 cm^{-1}) and NH_2 wagging (850 cm^{-1}) [55], Figure 3.8(a). All of these features are clearly discernible following pulsed plasma polymerization, except for the vinyl carbon-carbon double bond features, which disappear during polymerization, Figure 3.8(b). Subsequent exposure to D-maltose leads to an attenuation of the amine NH_2 wag (850 cm^{-1}), NH_2 deformation (1615 cm^{-1}) intensities; also there is the appearance of OH stretching (3250 cm^{-1}) and C=N stretching (1630 cm^{-1}) stretches due to Schiff base imine formation between the sugar and poly(4-vinylaniline), Figure 3.8(c). The NH_2 wag, bend and para substituted aromatic ring stretching (1500 cm^{-1}) are still visible as they remain present in the bulk of the nano-film.

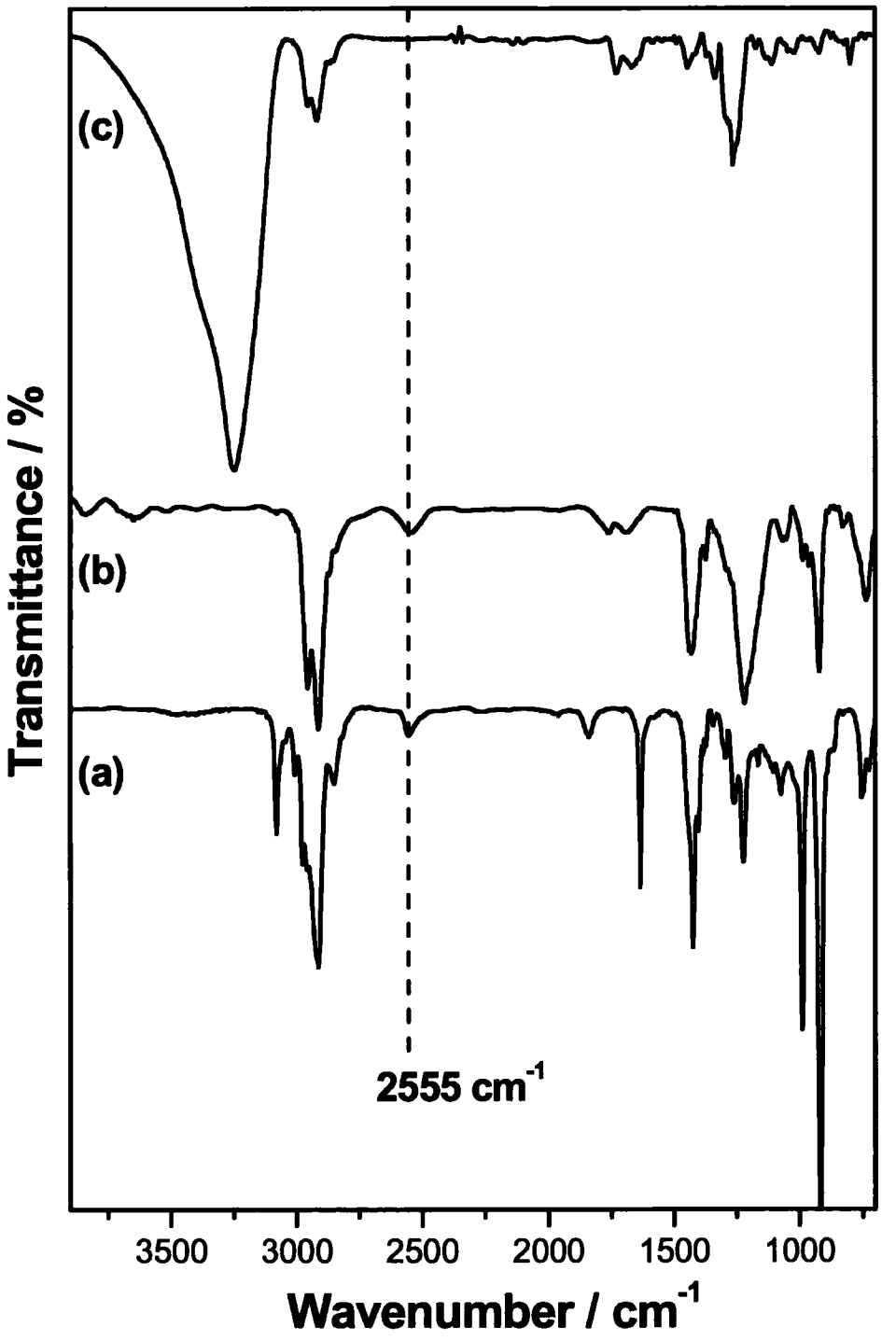

Figure 3.7 Infrared spectra of: (a) allylmercaptan monomer; (b) pulsed plasma polymerised poly(allylmercaptan); and (c) β-D-galacto-methanethiosulfonate bound to poly(allylmercaptan).

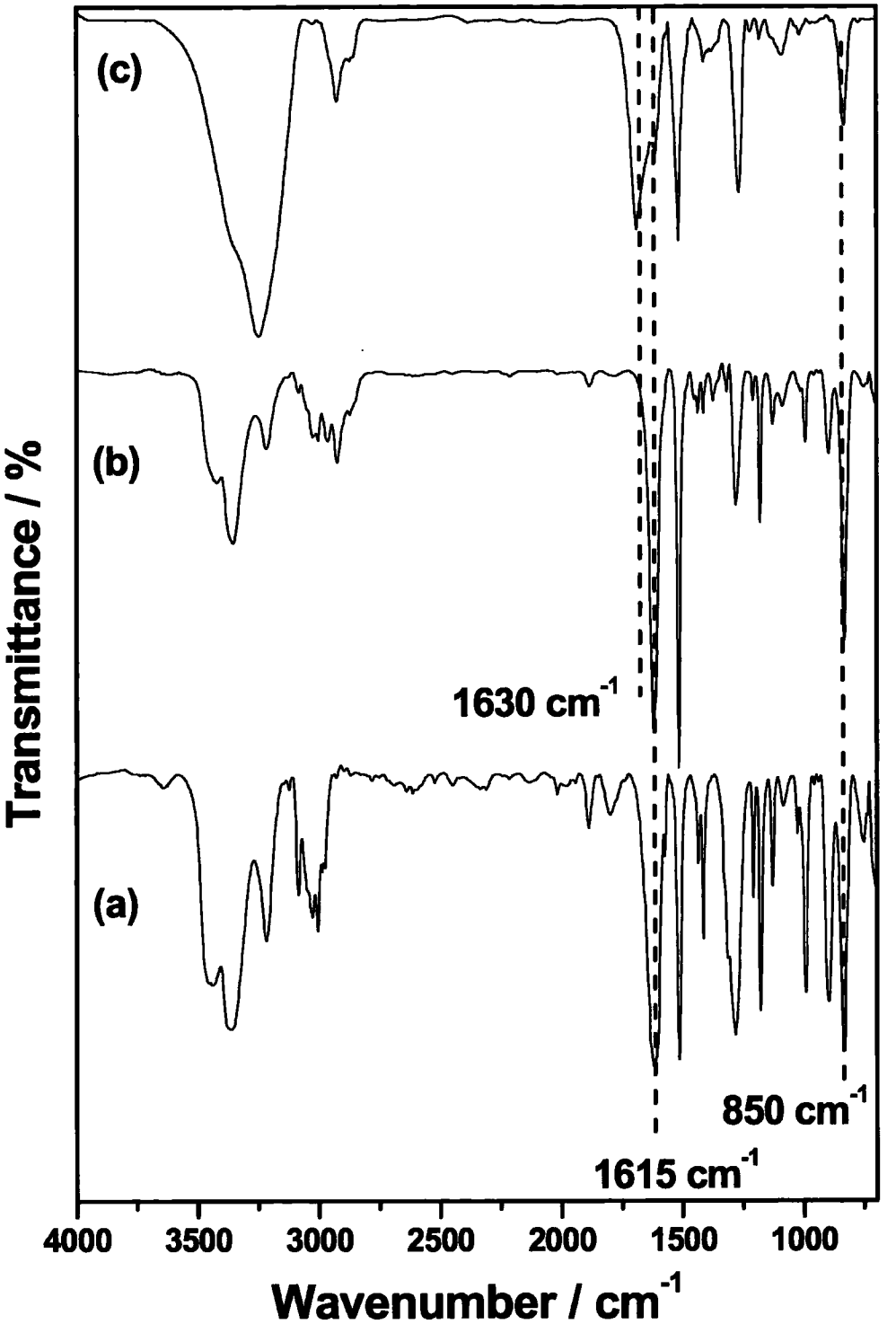

Figure 3.8 Infra red spectra of: (a) 4-vinylaniline monomer; (b) pulsed plasma deposited poly(4-vinyalaniline); and (c) D-maltose bound to poly(4-vinylaniline).

Retention of the sugar biological specificity upon immobilization onto a pulsed plasma deposited binding nanolayer was verified by fluorescence studies. This indicated selective binding of Protein I to regions of immobilized β-D-galacto-methanethiosulfonate, Figure 3.9(a), and selective binding of Protein II to regions of D-maltose, Figure 3.9(b).

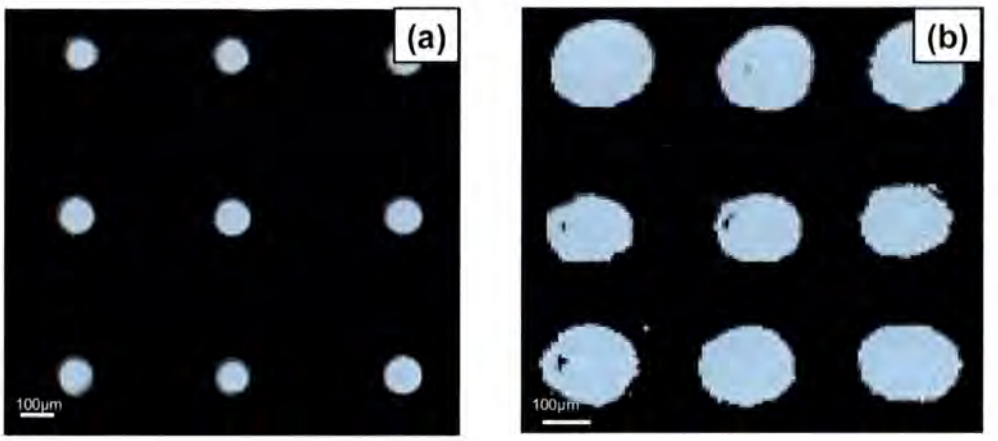

Figure 3.9 Fluorescent image of a micro-spotted array of (a) β-D-galacto-methanethiosulfonate array after exposure to complementary Protein I and (b) D-maltose array after exposure to complementary Protein II.

The potential for reusability of these sugar microarrays was investigated by using high-stringency washes to remove immobilized sugars from the surface. The removal of the immobilized sugar by stripping was followed by repeat immobilization procedures. The fluorescent intensity remained approximately constant for the five prints for both β-D-galacto-methanethiosulfonate and D-maltose immobilized arrays as a function of times the surface bound sugars are stripped, Figure 3.10(a) and (b) respectively.

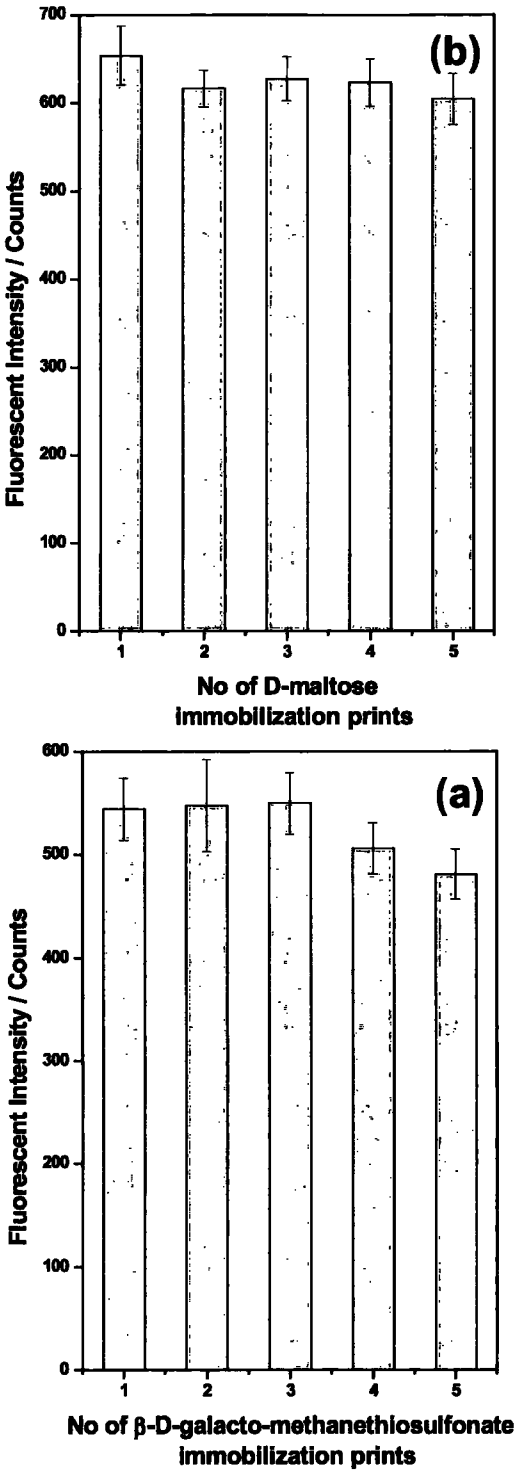

Figure 3.10 Fluorescence intensity following stripping and re-immobilization of: (a) β-D-galacto-methanethiosulfonate after exposure to Protein I; and (b) immobilization of D-maltose after exposure to Protein II. The fluorescence signal dropped to the background level for each fully stripped/denatured sample in rewriting of the respective sugar.

3.3.2 Sugar Molecular Scratchcards

The viability of plasmachemical nanolayering for the fabrication of a molecular scratchcard entailed the pulsed plasma deposition of a poly(allylmercaptan) β-D-galacto-methanethiosulfonate binding layer or a poly(4-vinylaniline) D-maltose binding layer; followed by the overcoating of a 20 nm poly(*N*–acryloylsarcosine methyl ester) film. The absence of cross contamination was verified by the measured XPS elemental composition and contact angles for each bilayer stack matching those of the bilayer stack poly(*N*–acryloylsarcosine methyl ester), Table 3.4 Further evidence is provided from the C(1s) peak fitting of the poly(*N*–acryloylsarcosine methyl ester) protein resistant layer deposited onto poly(allylmercaptan) and poly(4-vinylaniline) matching that of poly(*N*–acryloylsarcosine methyl ester) with six C(1s) spectra environments present in both: $\underline{C}_xH_y$ (285.0 eV, α), $\underline{C}$-C=O (285.7 eV, β), $\underline{C}$-N (286.2 eV, ε), $\underline{C}$-O (286.6 eV, μ), N-$\underline{C}$=O (288.0 eV, δ), O-$\underline{C}$=O (289.3 eV, θ), Figure 3.5(c) and 3.6(c).

Subsequent rastering of an SPM tip to scratch 1 μm x 1 μm squares was used to create a regular 4 x 4 array of exposed sugar functionalities, Figure 3.11. Exposure to β-D-galacto-methanethiosulfonate and Protein I demonstrates the reactivity of the thiol pixels whilst sequential exposure to D-maltose and Protein II exemplifies the reactivity of the exposed amine pixels, Figure 3.11

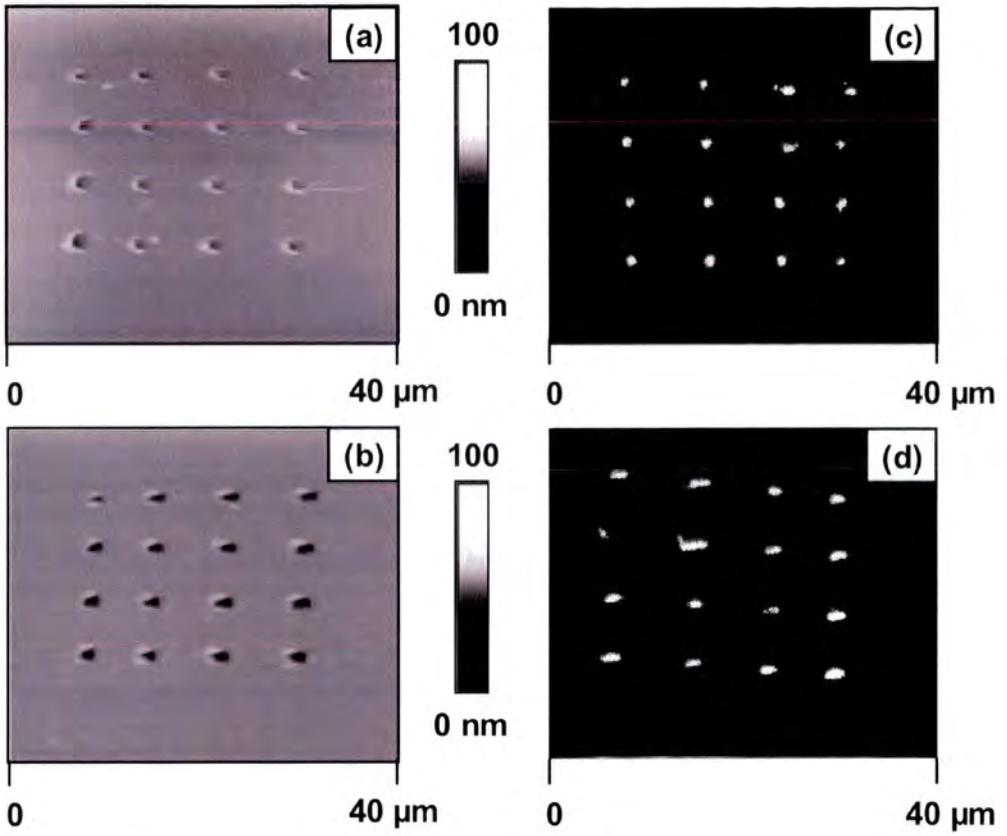

Figure 3.11 AFM micrographs of a 4 x 4 array surrounded by a protein-resistant background: (a) thiol functionalities; and (B) amine functionalities. The corresponding fluorescence images following: (c) β-D-galacto-methanethiosulfonate and Protein I; and (d) D-maltose and Protein II.

3.3.3 Multiplex Patterning

Sequential pulsed plasma deposition of poly(4-vinylaniline) followed by a poly(allylmercaptan) coating through an embossed grid gave rise to a bifunctional surface amenable to the immobilization of D-maltose and β-D-galacto-methanethiosulfonate. Retention of biological selectivity was demonstrated by exposure to a mixed solution of Protein I and Protein II. These indicated that upon exposure to a combined solution binding of Protein I is shown to occur to regions of β-D-galacto-methanethiosulfonate functionalized poly(allylmercaptan), whilst binding of Protein II is exclusive to areas of D-maltose functionalized poly(4-vinylaniline) Figure 3.12 (a) and (b). The high degree of sugar selectivity towards protein binding is evident from the absence of cross contamination between areas of alternating sugar functionalization, Figure 8(c).

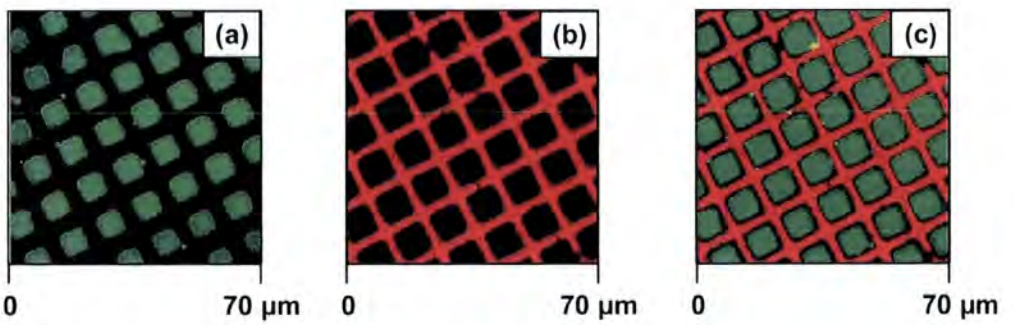

Figure 3.12 β-D-galacto-methanethiosulfonate functionalized poly(allyl-mercaptan) squares and D-Maltose functionalized poly(4-vinylaniline) bars. Fluorescence microscopy following exposure to: (a) Protein I; (b) Protein II and (c) a mixture of Protein I and Protein II.

3.4 Discussion

The structural diversity of sugars allows for their participation in a plethora of biologically important events.[56,57] Glycomic arrays are a very powerful tool for gaining a biomolecular level of understanding of these complex systems. Therefore, it is essential to produce robust, reproducible sugar arrays tethered to solid substrates where sugar biological activity is maintained. Although numerous approaches have been developed for this purpose, these are known to either restrict the range of sugars which can be immobilized[32-33] or suffer from non-transferable surface chemistries.[24-32,35-44] The described pulsed plasma chemical functionalization approach provides a substrate-independent scaffold for the immobilization of sugars This has been demonstrated by generating poly(allylmercaptan) thiol surfaces which readily undergo di-sulfide bridge formation with β-D-galacto-methanethiosulfonate[58] and poly(4-vinylanilne) amine surfaces amenable to Schiff base imine formation with the aldehyde terminus of D-maltose. Retention of biological activity has been exemplified by the binding of the fluorescently labelled galactose binding lectin PNA (Protein I),[59,60] and maltose binding lectin concanavalin A (Protein II),[61,62] Figure 3.9. The change in spot size is a result of the print pitch (distance between spot centres) being altered between samples.

The use of a sequential depositions of poly(allylmercaptan) and poly(4-vinylaniline) to create a multiplex surface comprising 10 μm poly(allylmercaptan) squares separated by 2 μm poly(4-vinylaniline) bars has been shown to be effective for selective sugar immobilization, with retention of respective biological selectivity, Figure 3.12.

An alternative approach for patterning protein onto solid surfaces has entailed creating molecular scratchcards. This type of nanolayered functional stack benefits from low background fluorescence due to the elimination of non-specific protein adsorption as a consequence of the protein-resistant top layer.[63] Bilayer stacks comprising off 20 nm pulsed plasma protein resistant poly(*N*–acryloylsarcosine methyl ester) on top of pulsed plasma poly(allylmercaptan) or pulsed plasma poly(4-Vinylaniline) underlayers were fabricated. Subsequent removal of the protein resistant

top layer to reveal reactive thiol or amine groups was carried out using an SPM tip, followed by immobilization with either β-D-galacto-methanethiosulfonate or D-maltose. In each case, retention of biological selectivity was demonstrated by the binding of fluorescent Proteins I and II respectively, Figures 3.11.

The regeneration/reusability of the functional surfaces was confirmed by subjecting the chips to the conditions of standard stripping and then rewriting the sugar micro-arrays without significant loss of immobilization binding efficiencies, Figure 3.10. Therefore, in principle, multiple sugar probes can be patterned simultaneously or consecutively onto a surface using a simple robotic liquid-delivering system, in the absence of cross-contamination between different probes. An array-manufacturing process employing this chemistry could be easily automated and scaled up.

3.5 Conclusions

Thiol and amine functionalized pulsed plasma nanolayers can be utilised for the immobilization of sugars amenable to protein binding. The sequential deposition of a reactive layer and then a passivation layer, followed by localized mechanical unveiling of the underlying reactive groups by piercing the passive top layer has been shown to be an effective way of preparing sugar arrays surrounding by a protein-resistant background. The reported thiol and amine functionalized nanolayers have been found to be highly stable towards stripping and re-writing of sugar arrays.

3.6 References

(1) Dwek, R. A. *Chem. Rev.* **1996,** *96,* 683.

(2) Kitov, P. I.; Sadowska, J. M.; Mulvey, G.; Armstrong, G. D.; Ling, H.; Pannu, N. S.; Read, R. J.; Bundle, D. R. *Nature* **2000,** *403,* 669.

(3) Joo, K. L.; Mao, S.; Sun, C.; Gao, C.; Blixt, O.; Arrues, S.; Hom, L. G.; Kaufmann, G. F.; Hofmann, T. Z.; Coyle, A. R.; Paulson, J.; Felding-Habermann, B.; Janda, K. D. *J. Am. Chem. Soc.* **2002,** *124,* 12439.

(4) McCever, R. P. *Glycoconjugate J.* **1997,** *14,* 585.

(5) Bosques, C. J.; Tschampel, S. M.; Woods, R. J.; Imperiali, B. *J. Am. Chem. Soc.* **2004,** *126,* 8421.

(6) Major, L. L.; Wolucka, B. A.; Naismith, J. H. *J. Am. Chem. Soc* **2005,** *127,* 18309.

(7) Lis, H.; Sharon, N. *Chem. Rev.* **1998,** *98,* 637.

(8) Flitsch, S. L.; Ulijn, R. V. *Nature,* **2003,** *421,* 219.

(9) Dove, A. *Nature* **2000,** *19,* 913.

(10) Disney, M. D.; Zheng, J.; Swager, T. M.; Seeberger, P. H. J. Am. Chem. Soc. 2004, *126,* 13343.

(11) Bertozzi, C. R.; Kiessling, L. L. *Science* **2001,** *291,* 2357.

(12) Sun, J.; Kitova, E. N.; Wang, W.; Klassen, J. S.; *Anal. Chem.* **2006,** *78,* 3010.

(13) Liao, J. H.; Chen, C. T.; Chou, H. C.; Cheng, C. C. ; Chou, P. T. ; Fang, J. M. ; Slanina, Z.; Chow, T. J. *Org. Lett.* **2002,** *4,* 3107.

(14) Striegle, A. M. *J. Am. Chem. Soc.* **2003,** *125,* 4146.

(15) Olsen, L. R.; Dessen, A.; Gupta, D.; Sabesan, S.; Sacchettini, J. C.; Brewer, C. F. *Biochemistry* **1997,** *36,* 15073.

(16) Vyas, N. K.; Meenakshi, N. V.; Chervenak, M. C. ; Johnson, M. A. ; Mario Pinto, B. ; Bundle, D. R.; Quiocho, F. A. *Biochemistry* **2002,** *41,* 13575.

(17) Haselhorst, T.; Weimar, T.; Peters, T. *J. Am. Chem. Soc.* **2001,** *123,* 10705.

(18) Peterlinz, K. A.; Georgiadis, R. M.; Herne, Tarlov, M. J. *J. Am. Chem. Soc.* **1997,** *119,* 3401.

(19) Schena, M.; Shalon, D.; Davis, R. W.; Brown, P. O. *Science* **1995,** *270,* 467.

(20) Georgiadis, R.; Peterlinz, K. P.; Peterson, A. W. *J. Am. Chem. Soc.* **2000,** *122,* 3166.

(21) MacBeath, G.; Schreiber, S. L. *Science* **2000,** *289,* 1760.

(22) Kane, R. S.; Takayama, S.; Ostuni, E.; Ingber, D. E.; Whitesides, G. M. *Biomaterials* **1999,** *20,* 2363.

(23) Zhou, H.; Baldini, L;. Hong, J.; Wilson, A. J.; Hamilton, A. D. *J. Am. Chem. Soc.* ***2006,*** *128,* 2421.

(24) Fritz, M. C.; Hahner, G.; Spencer, N. D. *Langmuir* **1996,** *12,* 6074.

(25) Smith, E. A.; Thomas, W. D.; Kiessling, L. L.; Corn, R. M. *J. Am. Chem. Soc* **2003,** *125,* 6140.

(26) Hederos, M.; Konradsson, P.; Liedberg, B. *Langmuir* **2005,** *21,* 2971.

(27) Houseman, B. T.; Mrksich, M. *Chem. Biol.* **2002,** *9,* 443.

(28) Houseman, B. T.; Gawalt, E. S.; Mrksich, M. *Langmuir* **2003,** *19,* 1522.

(29) Bryan, M. C.; Plettenburg, O.; Sears, P.; Rabuka, D.; Wacowich-Sgarbi, S.; Wong, C. H. *Chem. Biol.* **2002,** *9,* 713.

(30) Bryan, M. C.; Wong, C. H. *Tett. Lett.* **2004,** *45,* 3639.

(31) Fazio, F.; Bryan, M. C.; Blixt, O.; Paulson, J. C.; Wong, C. H. *J. Am. Chem. Soc.* **2002,** *124,* 14397.

(32) Fazio, F.; Bryan, M. C.; Lee, H. K.; Chang, A.; Wong, C. H. *Tett Lett* **2004,** *45,* 2689.

(33) Fukui, S.; Feizi, T.; Galustian, C.; Lawson, A. M.; Chai, W. *Nat. Biotec.* **2002,** *20,* 1011.

(34) Short, R.; Buttle, D.; Day, A. Sugar Binding Surface. WO2004/04038 A1, 2004.

(35) Stevens, J.; Blixt, O.; Glaser, L.; Taubenberger, P. P.; Paulson, J. C.; Wilson, I. A. *J. Mol. Biol.* **2006,** *355,* 1143.

(36) Blixt, O.; Head, S.; Mondala, T.; Scanlan, T.; Huflejt, M. E.; Alvarez, R.; Bryan, C. M.; Fazio, F.; Calarese, D.; Stevens, J.; Razi, N.; Stevens, D. J.; Skehel, J. J.; van Die, I.; Burton, D. R.; Wilson, I. A.; Cummings, R.; Bovin, N.; Wong, C. H.; Paulson, J. C. *Proc. Natl. Acad. Sci.* **2004,** *7,* 17033.

(37) Zhou, X.; Zhou, J.; *Biosens. Bioelectron.* **2006,** *21,* 1451.

(38) Yates, E. A.; Jones, M. O.; Clarke, C. E.; Powell, A. K.; Simon, R. J.; Porch, A.; Edwards, P. P.; Turnbull, A. K. *J. Mat. Chem.* **2003,** *13,* 2061.

(39) Schwarz, M.; Spector, L.; Gargir, A.; Avraham, S.; Gortler, M.; Altstock, R. T.; Avinoam, A. D.; Dotan, N. *Glycobiol.* **2003,** *13,* 749.

(40) Adams, E. W.; Ratner, D. M.; Bokesch, H. R.; McMahon, J. B.; O'Keefe, B, R.; Seeberger, P. H.; *Chem. Biol.* **2004,** *11,* 876.

(41) Park, S.; Lee, M. R.; Pyo, S. J.; Shin, I. *J. Am. Chem. Soc.* **2003,** *126,* 4812.

(42) Park, S.; Shin, I. *Angew. Chemie. Int. Ed.* **2002,** *41,* 3180

(43) Shirahata, N.; Hozumi, A.; Miura, Y.; Kobayashi, K.; Sakka, Y.; Yonezawa, T. *Thin Solid Films* **2006,** *499,* 213.

(44) De Smet, L. C. P. M.; Stork, G. A.; Hurenkamp, G. H. F.; Sun, Q. Y.; Huseyin, T.; Vronen, P. J. E.; Sieval, A. B.; Wright, A.; Visser, G. M.; Zulihoff, H.; Sudholter, E. J. R. *J. Am. Chem. Soc.* **2003,** *125,* 13916.

(45) Flynn, N. T.; Tran, T. N. T.; Cima, M. J.; Langer, R. *Langmuir* 2003, *19,* 10909.

(46) Disney, M. D.; Seeberger, P. H. *Drug Discov. Today Targets* **2004,** *3,* 151.

(47) Davis, B. G.; Maughan, M. A. T.; Green, M. P.; Ullman, A.; Jones, J. B. *Tetrahedron: Asymmetry* **2000,** *11,* 245.

(48) Matsumoto, K.; Davis, B. G.; Jones, J. B. *Chem. Commun.* **2001,** 903.

(49) Davis B. G.; Ward, S. J.; Rendle, P. M. *Chem. Commun.* **2001,** 189.

(50) Schofield, W. C. E.; McGettrick, J., Bradley, T. J.; Badyal, J. P. S.; Przyborski, S. *J. Am. Chem. Soc.* **2006,** *128,* 2280.

(51) Clayden, J.; Greeves, N.; Warren, S.; Wothers, P. *Organic Chemistry;* Oxford University Press: Oxford, 2001.

(52) Evans, J. F.; Gibson, J. H.; Moulder, J. F.; Hammond, J. S.; Goretzki, H. *Fresenius J. Anal. Chem.* **1984**, *319*, 841.

(53) Tabet, M. F.; McGahan, W. A. *Thin Solid Film* **2000**, *370,* 122.

(54) Zhong, Q.; Innis, D.; Kjollerm K.; Ellings, V. B. *Surf. Sci.* **1993**, *14,* 3045.

(55) Colthup, N. B.; Daly, L. H.; Wiberley, S. E. *Introduction To Infrared And Raman Spectroscopy*; Academic Press: New York, 1990.

(56) Kim, J. H.; Yanh, H.; Park, J.; Boons, G. J. J. Am. Chem. Soc. **2005**, *127,* 12090.

(57) Nagahori, N.; Nishimura, S. I. Biomacromolecules **2001**, *2,* 22.

(58) Wynn, R.; Richard, F. M. *Methods Enzymol.* **1995,** *251,* 351.

(59) Gunther, G. R.; Wang, J. L.; Yahara, I.; Cunningham, B. A.; Edelman, G. M. *Proc. Nat. Acad. Sci.* **1973,** *70,* 1012.

(60) Mandal, D. K.; Brewer, C. F. *Biochemistry* **1993**, *31,* 5116.

(61) Lotan, R.; Skutelsky, E.; Danon, D.; Sharon, N. *J. Biol. Chem.* **1975,** *250,* 8518.

(62) Liener, I. E.; Sharon, N., Goldstein, I. J. *The Lectins;* Academic Press: New York, 1986.

(63) Vroman, L.; Adams, A. L.; Fischer, G. C.; Munoz, P. C. *Blood* **1980**, *55,* 156.

CHAPTER 4

DIGITAL MOLECULAR INFORMATION LAYERS FOR SENSORS AND DIAGNOSTICS

4.1 Introduction

Intelligent diagnostic devices provide high-throughput analysis for combinatorial chemistry,[1,2,3] genomics,[4,5,6] epigenomics[7,8,9] and proteomics.[10,11,12] A plethora of techniques have been devised for these purposes including fluorescence spectroscopy,[13,14,15] immunoassays,[16,17,18] infrared spectroscopy,[19,20,21] mass spectrometry,[22,23,24] and nuclear magnetic resonance.[25,26,27] However the expense and technical expertise demanded by these methods precludes their application in most laboratories. An alternative method immobilizes biomolecules onto the surface of compact discs,[28,29,30,31,32, 33, 34, 35] providing a potential route for the development of high density diagnostic sensors. As compact discs are a globally accessible, inexpensive and durable medium this technique provides an economically attractive alternative to current methods.

Described by ISO9660,[36] compact discs comprise a clear 1.2 mm thick polycarbonate substrate, a reflective metallized layer and a protective lacquer coating. Data is stored as a series of undulations, approximately 195 nm in height, embossed onto one face of the polycarbonate substrate. These follow a thin, 500 nm spiral track from the centre of the disk outwards, with an aluminium coating deposited on top. A polarized laser (λ = 780 nm) traverses over the compact disc and upon reaching an undulation zenith reflects onto a photodiode. Conversely when the laser reaches an undulation nadir the laser is reflected away from the photodiode, Figure 4.1(a). Recordable compact discs vary from standard compact discs by replacing the undulations with a thin film of photosensitive dye, placed over the aluminium layer, Figure 4.1(b). An additional, more powerful write-laser is used to record data by producing opaque islands in the transparent dye, when the laser traverses over the compact disc the opaque regions prevent laser reflections. The on/off nature of laser detection at the photodiode produces a binary output which can be converted, via suitable software, into

various formats. This method has allowed the compact disc to become a popular method of data storage.[37]

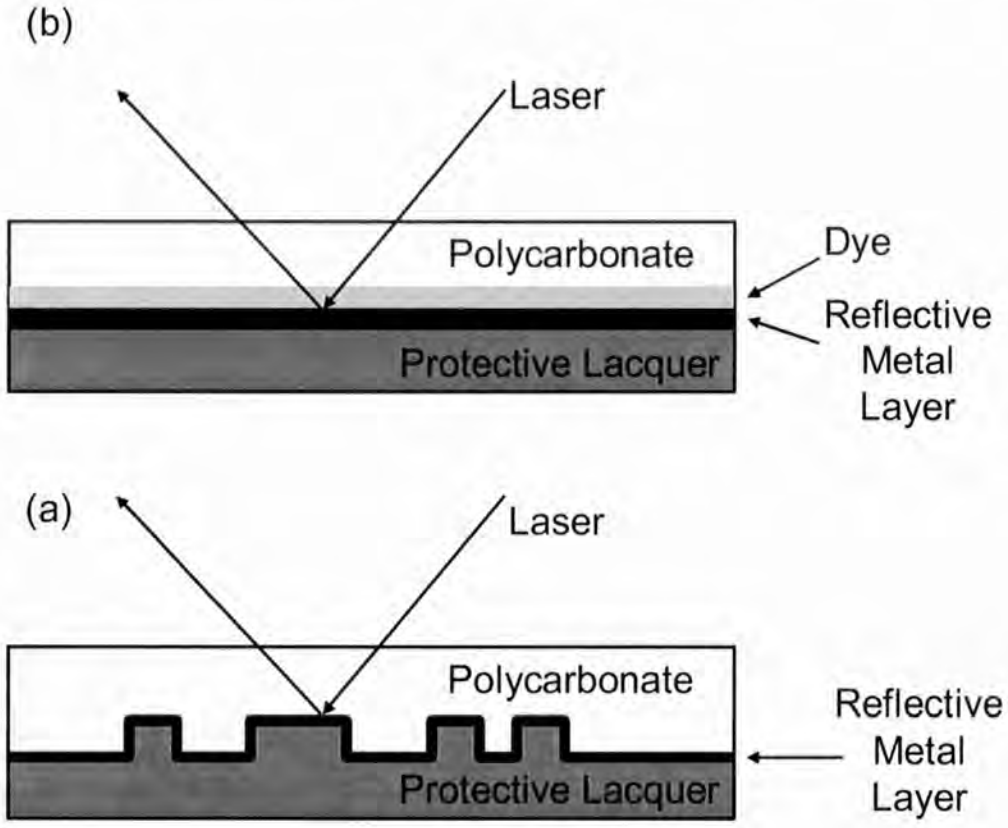

Figure 4.1 Cross section showing laser reflections from: (a) a metal layer on a standard compact disc; and (b) a recordable compact disc.

As the data in a compact disc is formed via the modulation of laser reflections as a function of height change in a series of undulations, it follows that the binding of an entity (biological or chemical) to the compact disc surface, when of sufficient size, may interfere with the optical transmission of this data. This is comparable to a stain on a compact disc encoded with music creating an error that may result in the data no longer being interpreted correctly i.e. as unintended audible clicks within a musical track.

It is these changes in data content, upon binding, that potentially allows compact discs to be utilised as diagnostic devices. However, a process is required to link the information stored in the compact disc to the molecular binding at the surface. To facilitate this a number of steps must be followed:

1. Burning data onto a compact disc.
2. Activation of compact disc surface to allow for attachment of suitable markers.
3. Immobilization of a screening library onto the compact disc in a spatially addressed manner.
4. Exposure to unknown biomolecules.
5. Reading of data after molecular binding.
6. Data visualisation to show if the information content has changed upon molecular binding in steps 3 and 4.

Current methods devised to develop diagnostic compact discs involve prerequisite wet chemical modification steps of the polycarbonate surface. This limits the range of ligands that may be screened,[32,35] furthermore the use of templates to immobilize ligands in a uniform pattern can limit the biomolecule density on the surface.[34,35] In this study, pulsed plasma polymerization onto a compact disc, coupled with software development, has created a diagnostic device without the need for wet chemical modification and masks.

The initial step of this method comprises burning into the compact disc, a series of tracks that each representing a different biomolecule. This is followed by the pulsed plasma deposition of glycidyl methacrylate to create a surface presenting reactive epoxy groups amenable to biomolecule binding.[38,39] At this stage the data is read by a standard CD-Rom drive to establish any changes that have occurred as a result of polymer formation. This step is followed by the inkjet deposition[40,41,42] of albumin bovine serum onto one half of the data tracks, and high purity water onto the remaining

half, followed by a further inkjet deposition where the positions of albumin bovine serum and high purity water are reversed. The compact disc is read after each inkjet deposition, monitoring any change in data. It is envisaged that the visualisations will show a change in data with albumin bovine serum due to interference with the optical transmission of the laser.[43, 44] This change in data will be presented in a series of visualisations developed to display the extent and position of data change on the compact disc surface, throughout the process, Figure 4.2

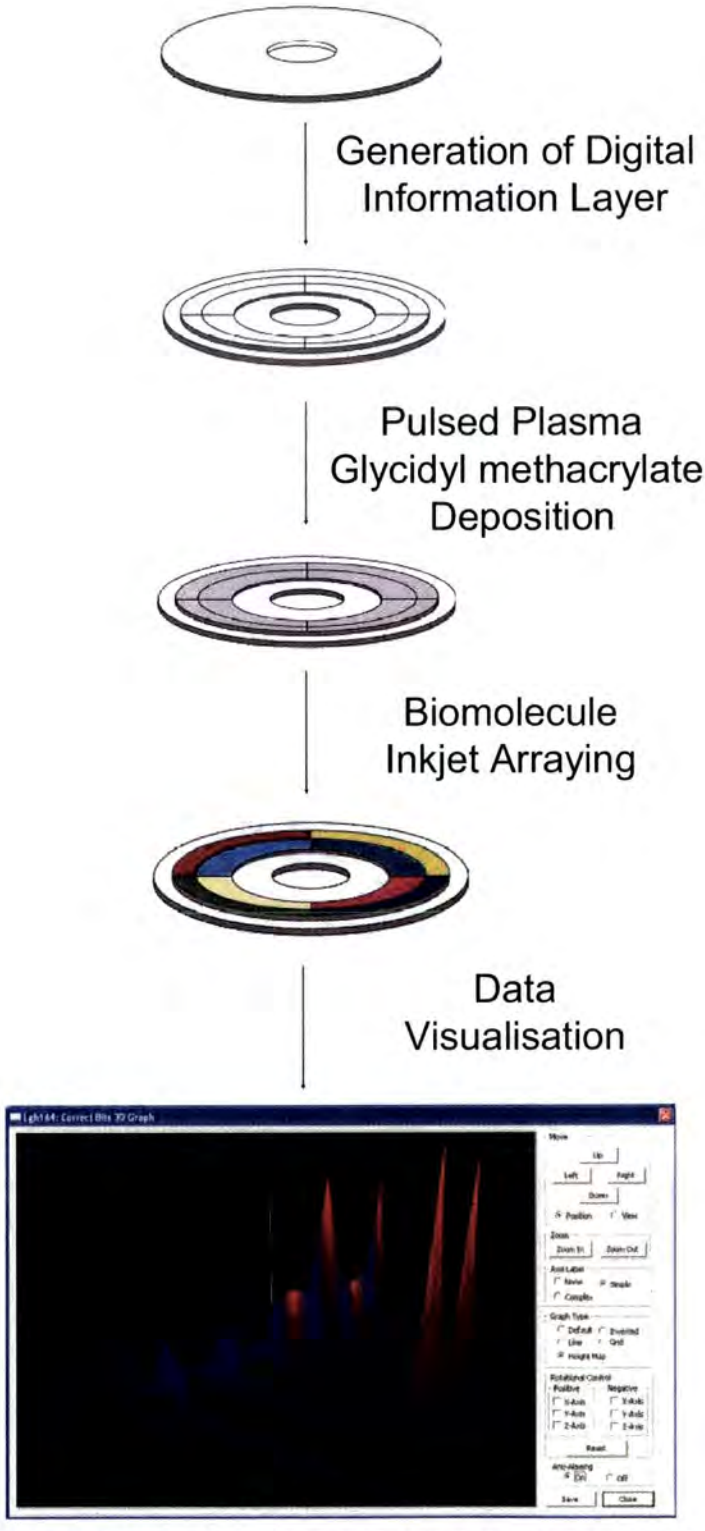

Figure 4.2 Formation of a bio-molecular compact disc for molecular diagnostics.

4.2 Experimental

4.2.1 Graphical User Interface Development

A software package, known as CD-Mol,[45] was written in Java to provide a data pattern and subsequently read, interpret and display the data generated in a series of differing visualisations. The creation of data entailed burning an alternating sequence of buffer and data tracks into a recordable compact disc. Each data track is 1, 048, 576 bytes (1 MB) in size where each byte consists of an array of 8 consecutive alternating bits (0101010101) and each buffer track consists of 104, 857, 600 bytes (100 MB). The start of each track contains a header and sync to provide geographical identification. The compact disc was written with alternate buffer and data tracks, with an additional buffer track at the beginning and the end. This results in a total of 13 tracks being written, Figure 4.3(a)

Each data track was assigned one of six colours corresponding to the colours available on an inkjet printer (black, cyan, light cyan, magenta, light magenta and yellow). The data tracks were written in concentric circles and converted to a .jpg image to provide guidance for the inkjet printing, Figure 4.3(b). A CD-R (Imation, 700 MB / 80 min) was loaded into a Toshiba DVD-ROM SD-R1002 drive and each track was burned with a 780 nm diode laser contained within the DVD-ROM drive. The data layer pattern was confirmed by reading the data on the compact disc using the same DVD-ROM drive.

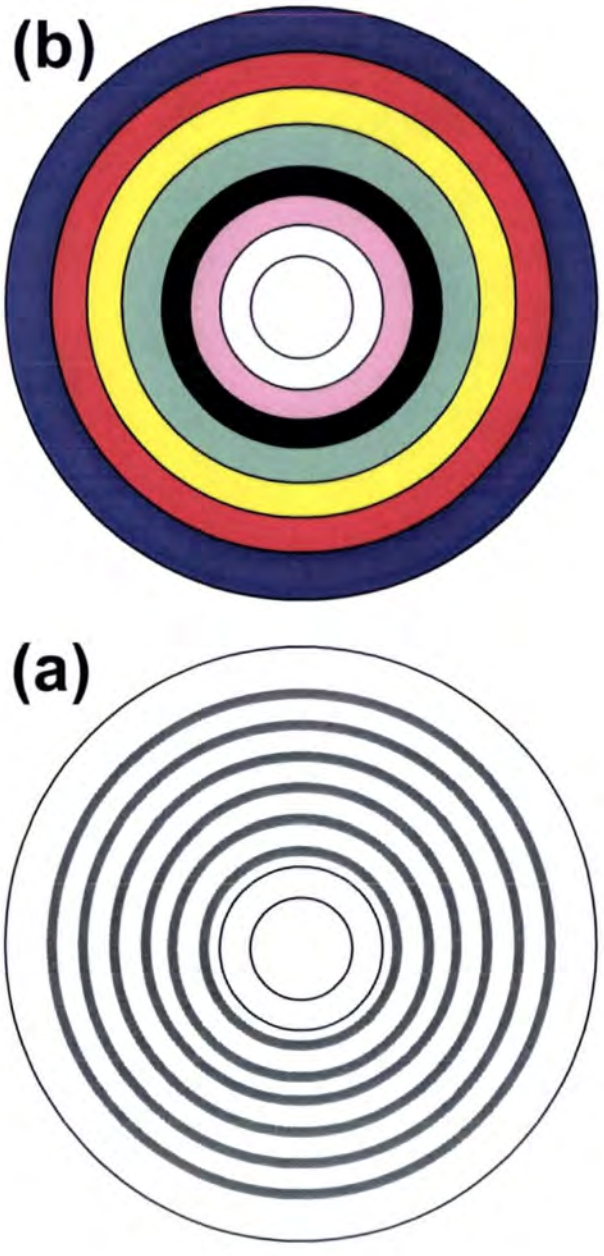

Figure 4.3 Patterned compact disc comprising of: (a) Alternating data and buffer tracks (data tracks in grey, buffer in white); and (b) the associated inkjet printer pattern designed to place a individual colour over each data track, from inside to out: light magenta, black, light cyan, yellow, magenta, cyan.

4.2.2 Plasmachemical Functionalization

Plasma polymerization was carried out in a cylindrical glass reactor (16 cm diameter, 5000 cm^3 volume) located inside a Faraday cage and evacuated by a 30 L min^{-1} rotary pump via a liquid nitrogen cold trap (2 x 10^{-3} mbar base pressure and better than 5.6 x 10^{-9} mol s^{-1} leak rate). A copper coil (4 mm diameter, 6 turns, located 23 cm away from the precursor inlet) was connected to a 13.56 MHz radio frequency supply via an LC matching network. System pressure was monitored with a Pirani gauge. All fittings were grease free. During pulsed plasma deposition, the RF source was triggered by a signal generator, and the pulse shape monitored with an oscilloscope. Prior to each experiment the apparatus was scrubbed with detergent, rinsed with propan-2-ol, and oven dried. Further cleaning entailed running a 40 W continuous wave air plasma at 0.2 mbar pressure for 20 min. At this stage, glycidyl methacrylate (+97%, Sigma-Aldrich) was loaded into a sealable glass tube and further purified using multiple freeze-pump-thaw cycles. The compact disc was placed into the centre of the reactor, and the system evacuated to base pressure. A continuous flow of glycidyl methacrylate vapour was introduced via a fine needle control valve at a pressure of 0.2 mbar and 8.2 x 10^{-8} mol s^{-1} flow rate for 5 min prior to electrical discharge ignition. The optimum pulsed plasma duty cycle corresponded to 40 W peak power continuous wave bursts lasting 20 µs and 20 ms off. Upon completion of deposition, the RF power source was switched off and the monomer allowed to continue to purge though the system for a further 5 min prior to evacuation to base pressure and venting to atmosphere, Figure 4.4.

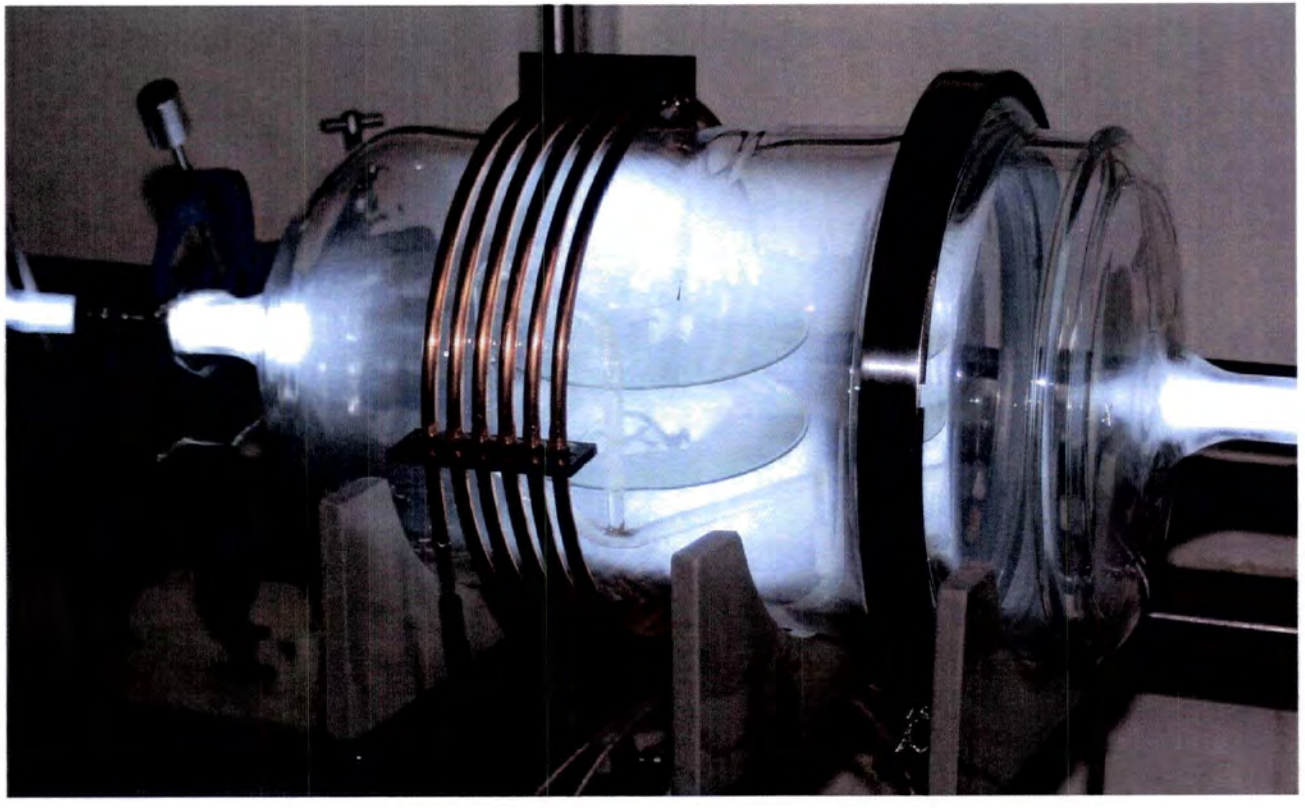

Figure 4.4 Pulsed Plasma glycidyl methacrylate deposition onto a compact disc.

4.2.3 Bio-molecule Functionalization

Biomolecule immobilization onto the compact disc surface utilised a continuous ink supply system (Consumables Café) coupled to an EPSON R200 CD printer. Prior to use ink cartridges were drained and rinsed with high purity water. Cartridges 1, 2, 3 (light magenta, light cyan, black) were then filled with high purity water and cartridges 4, 5, 6 (yellow, magenta, cyan) filled with bovine serum albumin (BSA) 5 mg ml^{-1} in phosphate buffered saline (>96% Sigma-Aldrich) containing 20% v/v glycerol, and purged three times before use. The software generated pattern, Figure 4.3, was then printed onto the plasma coated compact disc resulting in high purity water printed onto data tracks 1, 2, 3 and BSA printed onto data tracks 4, 5, 6. The compact disc was subsequently incubated in a controlled humidity chamber at 37° for 12 hours then washed in PBS containing 0.1% v/v Tween 20 (3 x 15 min), PBS solution (3 x 15min) and high purity water (3 x 15 min) before finally being dried under a gentle flow of N_2. The data on the compact disc was once again read using the Toshiba DVD-ROM SD-R1002. The cartridges were then re-drained, rinsed three times with high purity water and cartridges 1, 2, 3 filled with BSA and 4, 5, 6 filled with high purity water. The same print image as before was used, however high purity water was printed over tracks 4, 5, 6 and BSA over tracks 1, 2, 3. The compact disc was read using the same Toshiba DVD-ROM drive. At each stage the data was read five times to reduce random error.

4.2.4 Surface Characterization

X-ray photoelectron spectroscopy (XPS) was undertaken using an electron spectrometer (VG ESCALAB MK II) equipped with a non-monochromated Mg $K\alpha_{1,2}$ X-ray source (1253.6 eV) and a concentric hemispherical analyser. Photo-emitted electrons were collected at a take-off angle of 30° from the substrate normal, with electron detection in the constant analyser energy

mode (CAE, pass energy = 20 eV). The XPS spectra were charge referenced to the C(1s) peak at 285.0 eV and fitted with a linear background and equal full-width-at-half-maximum (FWHM) Gaussian components[46] using Marquardt minimization computer software. Instrument sensitivity (multiplication) factors derived from chemical standards were taken as being C(1s): O(1s) equals 1.00: 0.63.

Fourier transform infrared (FTIR) analysis of the films was carried out using a Perkin-Elmer Spectrum One spectrometer equipped with a liquid nitrogen cooled MCT detector operating across the 700 – 4000 cm^{-1} range. Reflection–absorption (RAIRS) measurements were performed using a variable angle accessory (Specac) set at 86° on an Au substrate in conjunction with a KRS-5 polarizer fitted to remove the s–polarized component. All spectra were averaged over 516 scans at a resolution of 4 cm^{-1}.

Contact angle analysis of the plasma-deposited films was carried out with a video capture system (ASE Products, model VCA2500XE) using 2.0 μL droplets of de-ionized water.

Film thickness measurements were obtained using an nkd-6000 spectrophotometer (Aquila Instruments Ltd). Transmittance-reflectance curves (over the 350-1000 nm wavelength range) were fitted to the Cauchy model for dielectric materials using a modified Levenburg-Marquardt method.[47]

4.3 Results

4.3.1 Compact Disc Functionalization

Evidence for the formation of a pulsed plasma poly(glycidyl methacrylate) nanolayer on a compact disc was obtained using FT-IR, XPS and contact angle measurements. The XPS elemental stoichiometry of the nanolayer closely resembles the predicted theoretical composition calculated from the monomer structure. Furthermore there was a decrease in the contact angle of the innate compact disc surface to one resembling the literature value of pulsed plasma poly(glycidyl methacrylate).[48] Table 4.1.

Substrate Surface	Contact Angle / ^{0}	Elemental Composition	
		C %	O %
Compact Disc	95.3 ± 1.5	77.6 ± 0.6	22.3 ± 0.6
Pulsed plasma deposited poly(glycidyl methacrylate) on compact disc.	58.4 ± 1.7	69.3 ± 1.5	30.6 ± 1.5
Theoretical glycidyl methacrylate	-	70	30

Table 4.1 Contact angle and XPS elemental composition of compact disc surface and pulsed plasma poly(glycidyl methacrylate) deposited onto a compact disc surface.

Further confirmation of the high level of retained functionality was evident from peak fitting the C(1s) spectra. The observed environments were found to correspond closely with the five theoretical environments: $\underline{C}_xH_y$ (285.0 eV, α), $\underline{C}$-C=0 (285.7 eV, β), O-$\underline{C}$-C-O (286.7 eV, δ), epoxide carbons (287.2 eV, ε), and O-$\underline{C}$=O (289.1 eV, θ), Figure 4.4.[49]

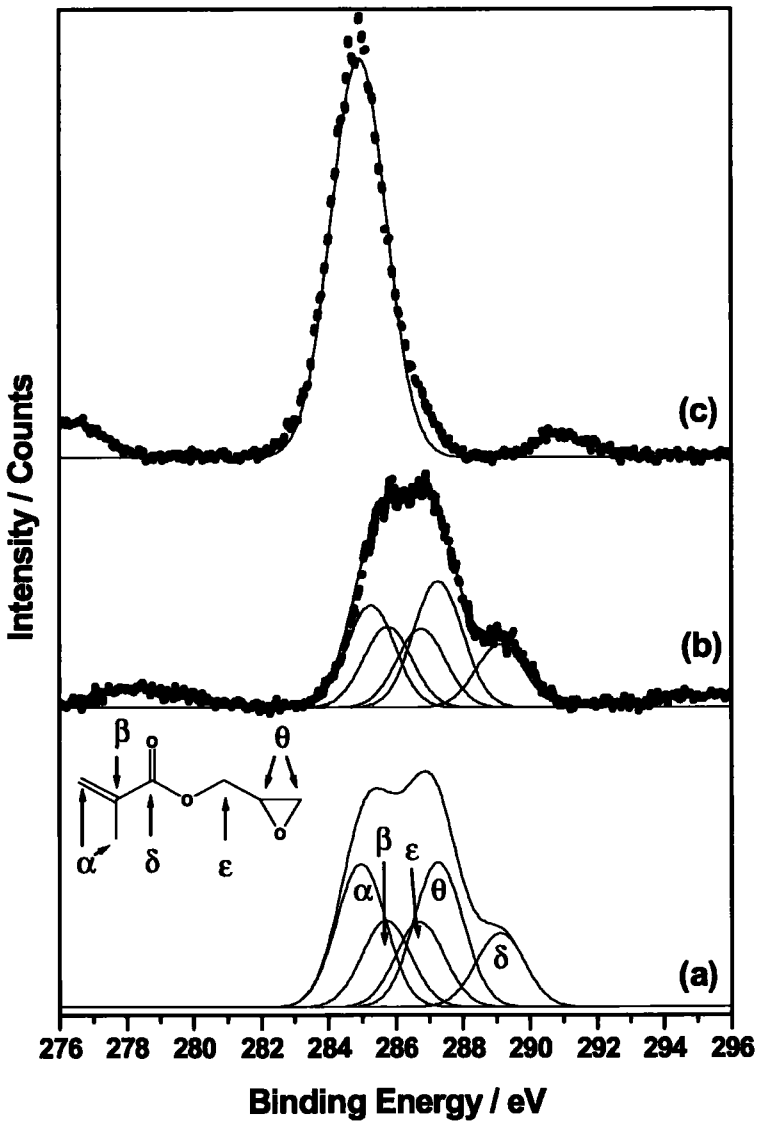

Figure 4.4 C(1s) XPS peak fitting of pulsed plasma deposited: (a) theoretical poly(glycidyl methacrylate); (b) 300 nm poly(glycidyl methacrylate) layer; and (c) compact disc surface.

Infrared studies of the glycidyl methacrylate monomer indicate the presence of epoxide ring C-H stretching (3050 cm^{-1}), C-H stretching (3000-2900 cm^{-1}), acrylate carbonyl stretching (1720 cm^{-1}), acrylate C=C stretching (1637 cm^{-1}), epoxide ring breathing (1253 cm^{-1}), antisymmetric epoxide ring deformation (908 cm^{-1}) and symmetric epoxide ring deformation (842 cm^{-1}), Figure 4.5(a). All of the bands associated with the glycidyl methacrylate monomer were clearly discernible following pulsed plasma polymerization, except for the methacrylate carbon-carbon double-bond features, which disappeared during polymerization, Figure 4.5(b).

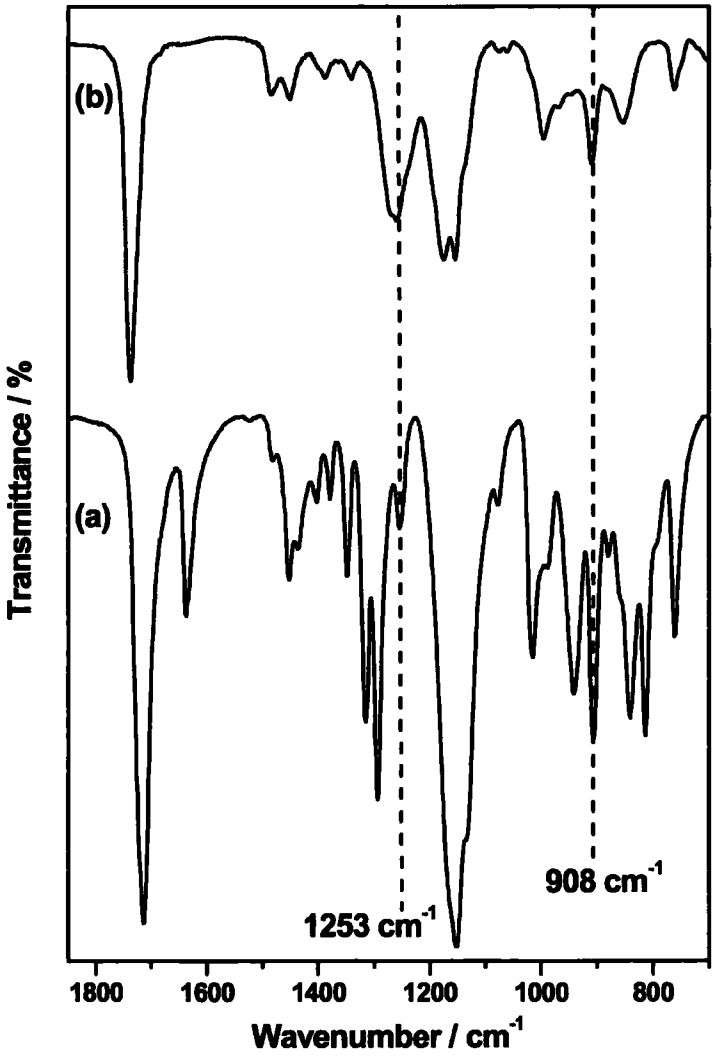

Figure 4.5 Infrared spectra of: (a) glycidyl methacrylate monomer; and (b) pulsed plasma deposited poly(glycidyl methacrylate).

4.3.2 Bio-molecule Functionalization

The CD-Mol software generated a multitude of visualisations to display the change in data throughout the process. The first series of visualisations displays the change in the number of correct bits per set in a data track, after pulsed plasma polymerization or inkjet printing, a set being a string of 4 consecutive bytes, as each byte consists of 8 bits it follows that there are 32 bits in a set. Hence as a track consists of 1, 048, 576 bits it also comprise of 32768 sets. Visualisations on the 32 bit set level are preferred as they provide higher resolution data analysis compared to visualisation on the bit or byte level (this is analogous to a 32 pixel image providing better resolution than one of 8 pixels). While 64 and 128 bit level analysis is possible, they are difficult to visualise due to their size. The visualisations comprise the number of correct bits per set along the x-axis against the percentage of these sets on the y-axis. From this sample it can be determined that 33% of the sets contain 16 correct bits, indicating 16 bits have remained the same and 16 bits have changed, Figure 4.6.

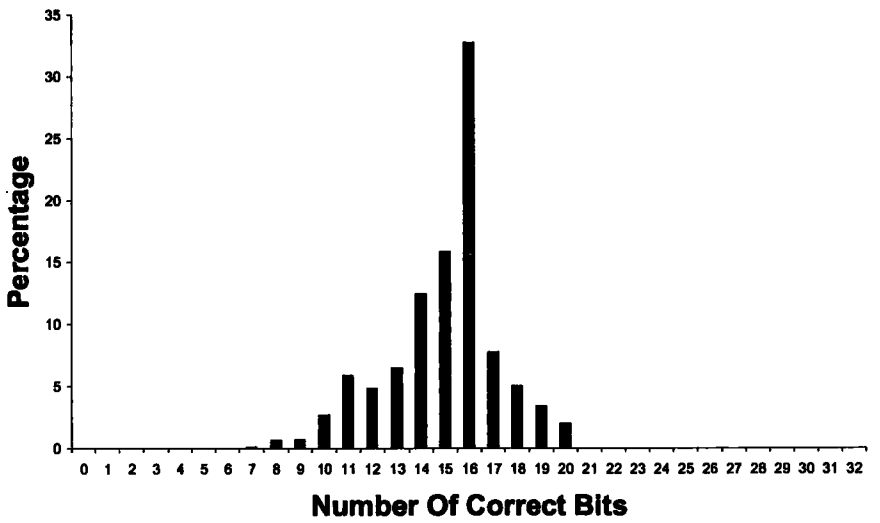

Figure 4.6 Graphical visualisation showing the percentage of sets (y-axis) which contain the same number of correct bits (x-axis).

The first visualisations simultaneously displays the correct number of bits per set obtained following the inkjet printing of high purity water onto tracks 1, 2, 3 and BSA onto tracks 4, 5, 6, and the correct number of bits obtained following the second step of inkjet printing where BSA is printed onto tracks 1, 2, 3 and high purity water onto tracks 4, 5, 6. With the correct bits sequence taken to be the data after pulsed plasma polymerization.

These visualisations indicated no change in the correct number of bits after the first read in tracks 1 and 2, Figures 4.7 and 4.8 respectively. A change was noted in the correct number of bits for tracks 3, 4, 5, and 6 after read 1 which did not vary significantly after read 2, Figures 4.9, 4.10, 4.11 and 4.12 respectively.

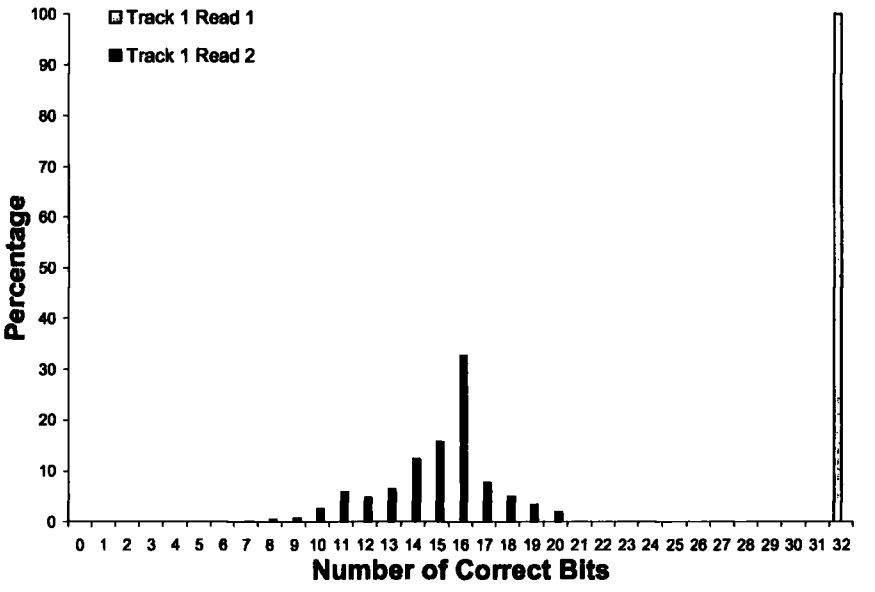

Figure 4.7 Correct bits per set for track 1. Read 1 is performed following inkjet printing of high purity water and read 2 following inkjet printing of BSA.

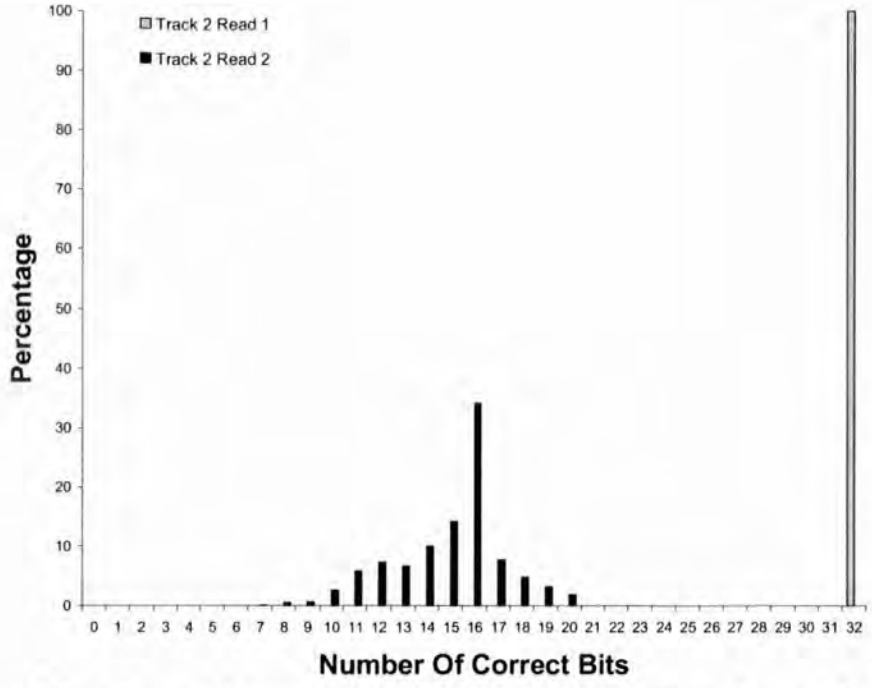

Figure 4.8 Correct bits per set for track 2. Read 1 is performed following inkjet printing of high purity water and read 2 following inkjet printing of BSA.

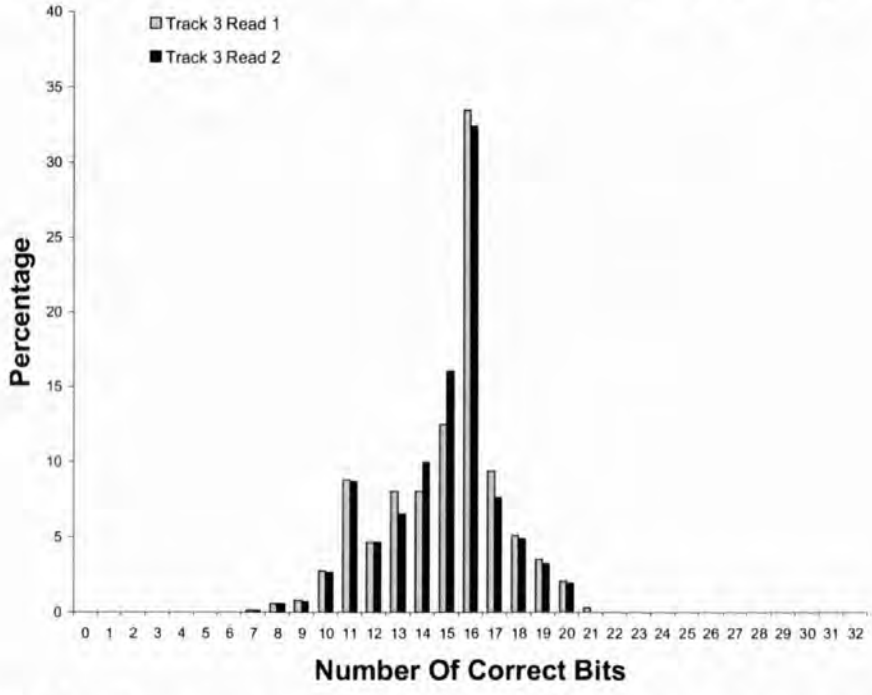

Figure 4.9 Correct bits per set for track 3. Read 1 is performed following inkjet printing of high purity water and read 2 following inkjet printing of BSA.

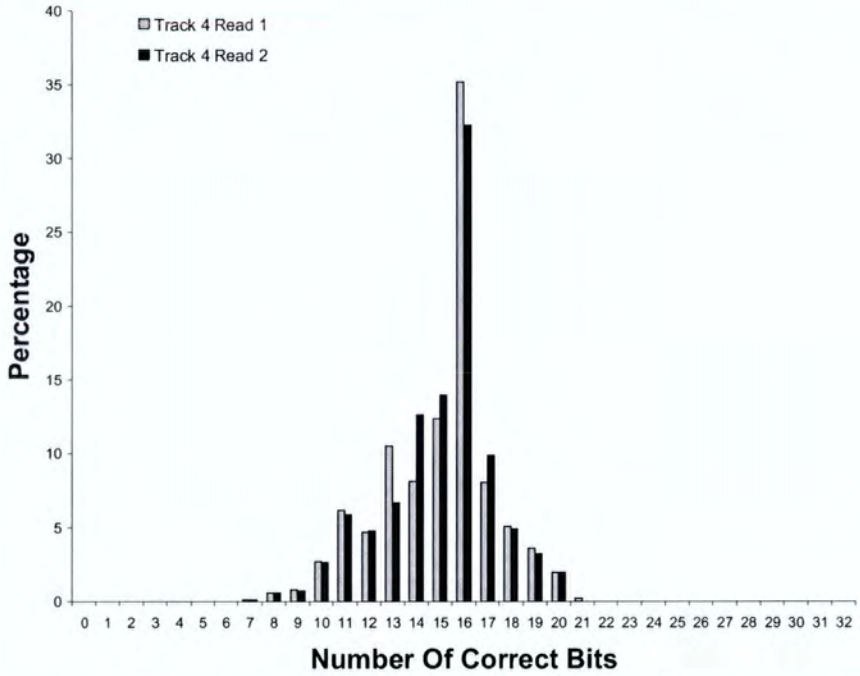

Figure 4.10 Correct bits per set for track 4. Read 1 is performed following inkjet printing of high purity water and read 2 following inkjet printing of BSA.

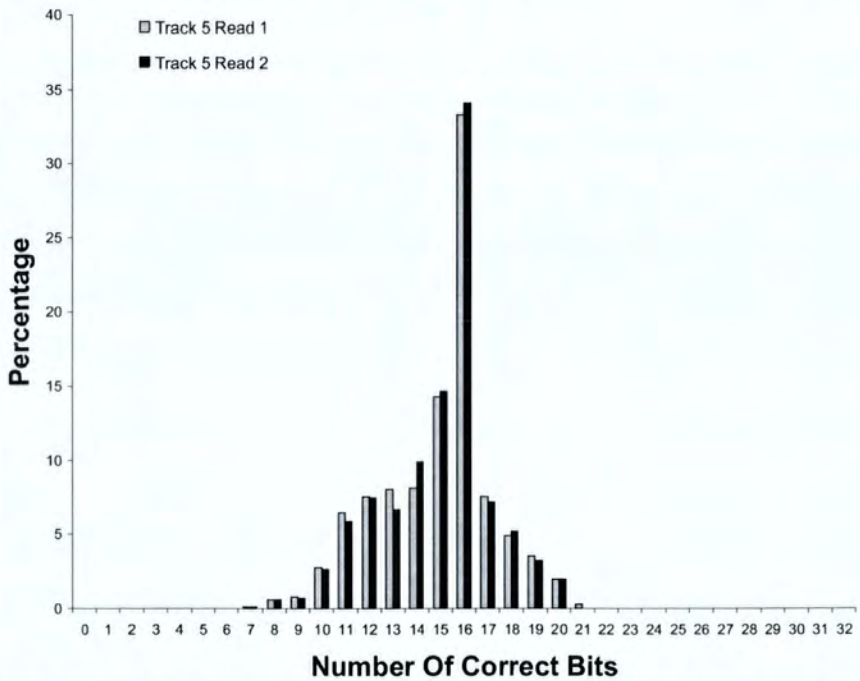

Figure 4.11 Correct bits per set for track 5. Read 1 is performed following inkjet printing of high purity water and read 2 following inkjet printing of BSA .

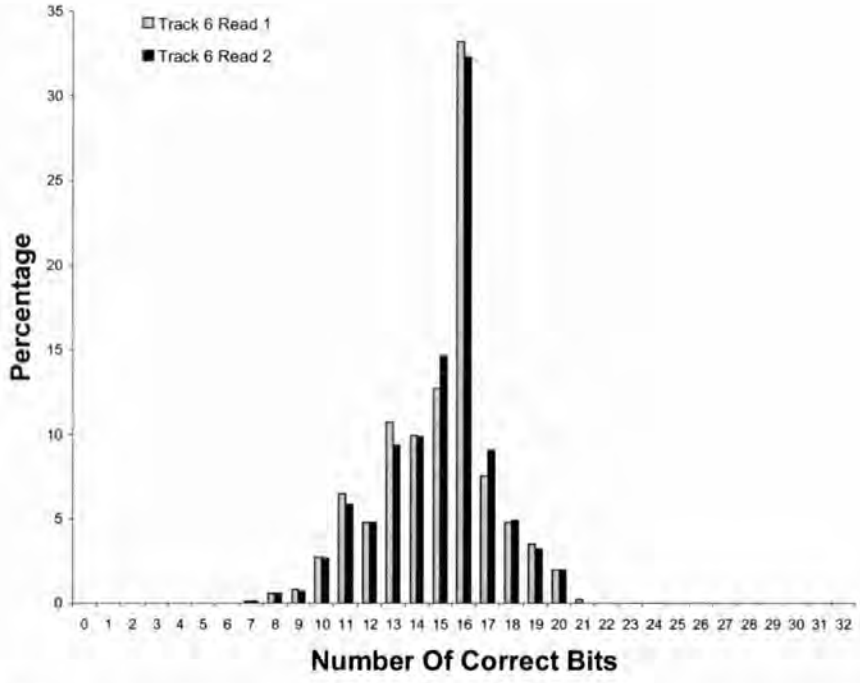

Figure 4.12 Correct bits per set for track 6. Read 1 is performed following inkjet printing of high purity water and read 2 following inkjet printing of BSA.

Two further visualisations, that show a comparison of the correct number of bits for all tracks after the first read and second read, were also produced, Figures 4.13 and Figure 4.14.

This series of visualisations, Figures 4.7 to 4.14, indicate that the inkjet deposition of high purity water does not significantly alter the data, with no change noted in read 1 for tracks 1 and 2, Figure 4.7 and 4.8, and only minor changes in read 2 for tracks 3, 4, 5, 6, Figure 4.9 to 4.12. However a large change in the correct number of bits following BSA immobilization was detected, indicating that BSA has interfered with the optical transmission of the laser. As an extension a 3D visualisation was generated that compared the correct bits per set in read 1 and 2 for all tracks. This visualisation enabled rotation around the x, y and z axis to identify key areas of interest, Figure 4.15.

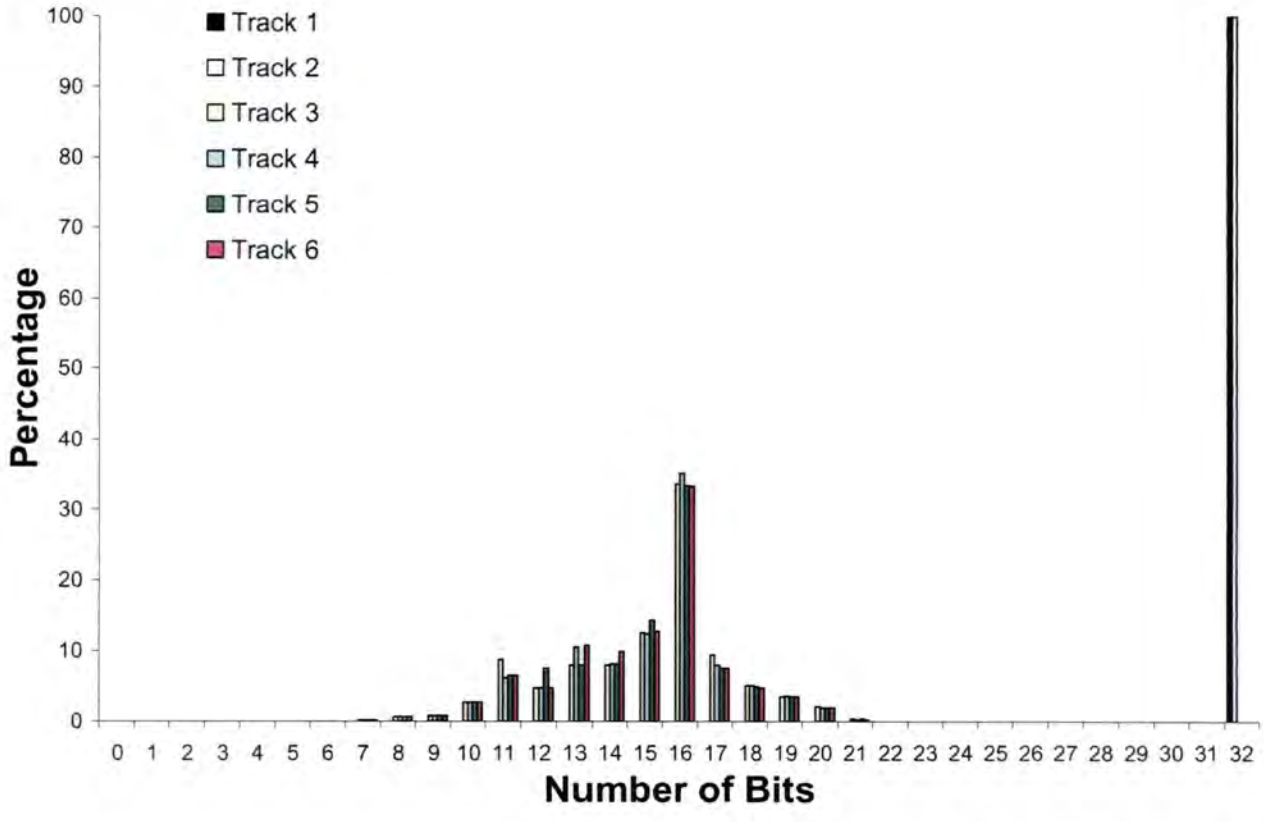

Figure 4.13 Correct bits per set per track after the first read 1.

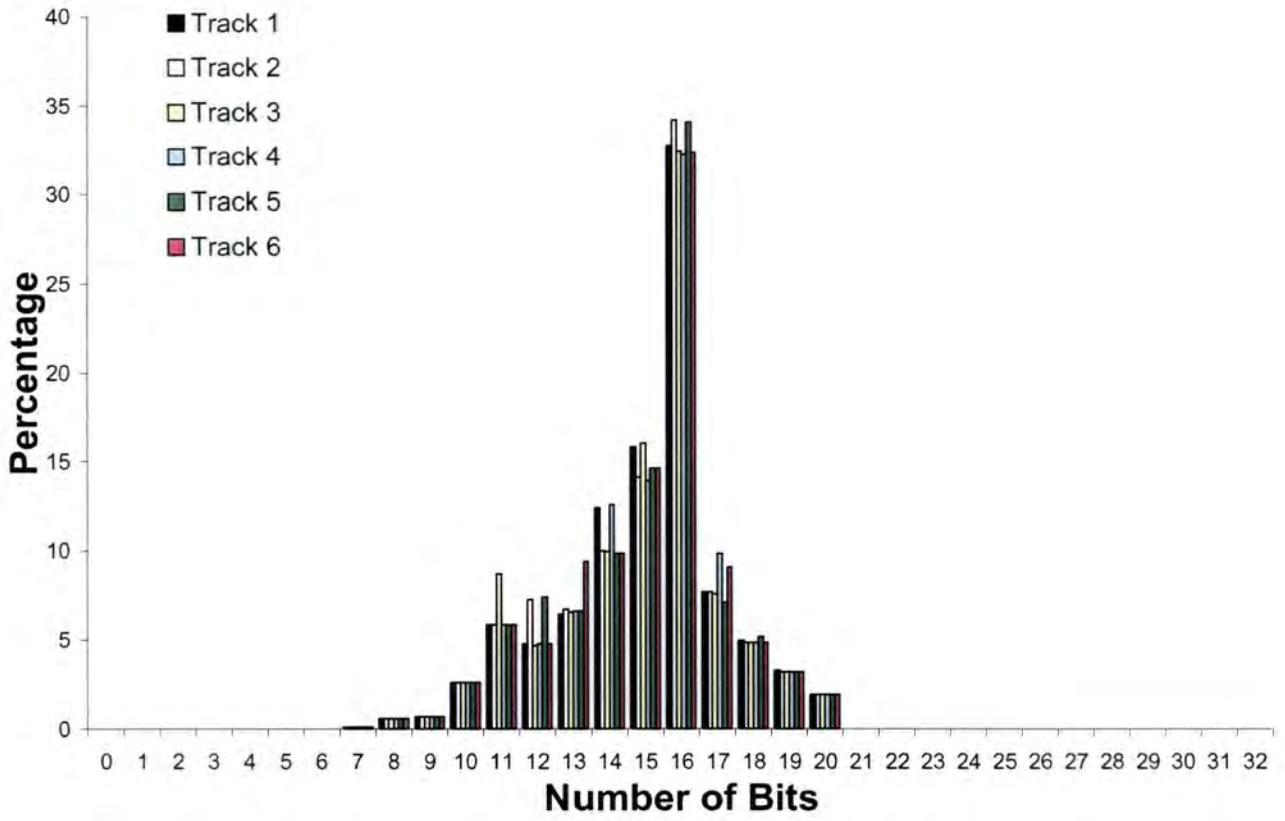

Figure 4.14 Correct bits per set per track after the read 2.

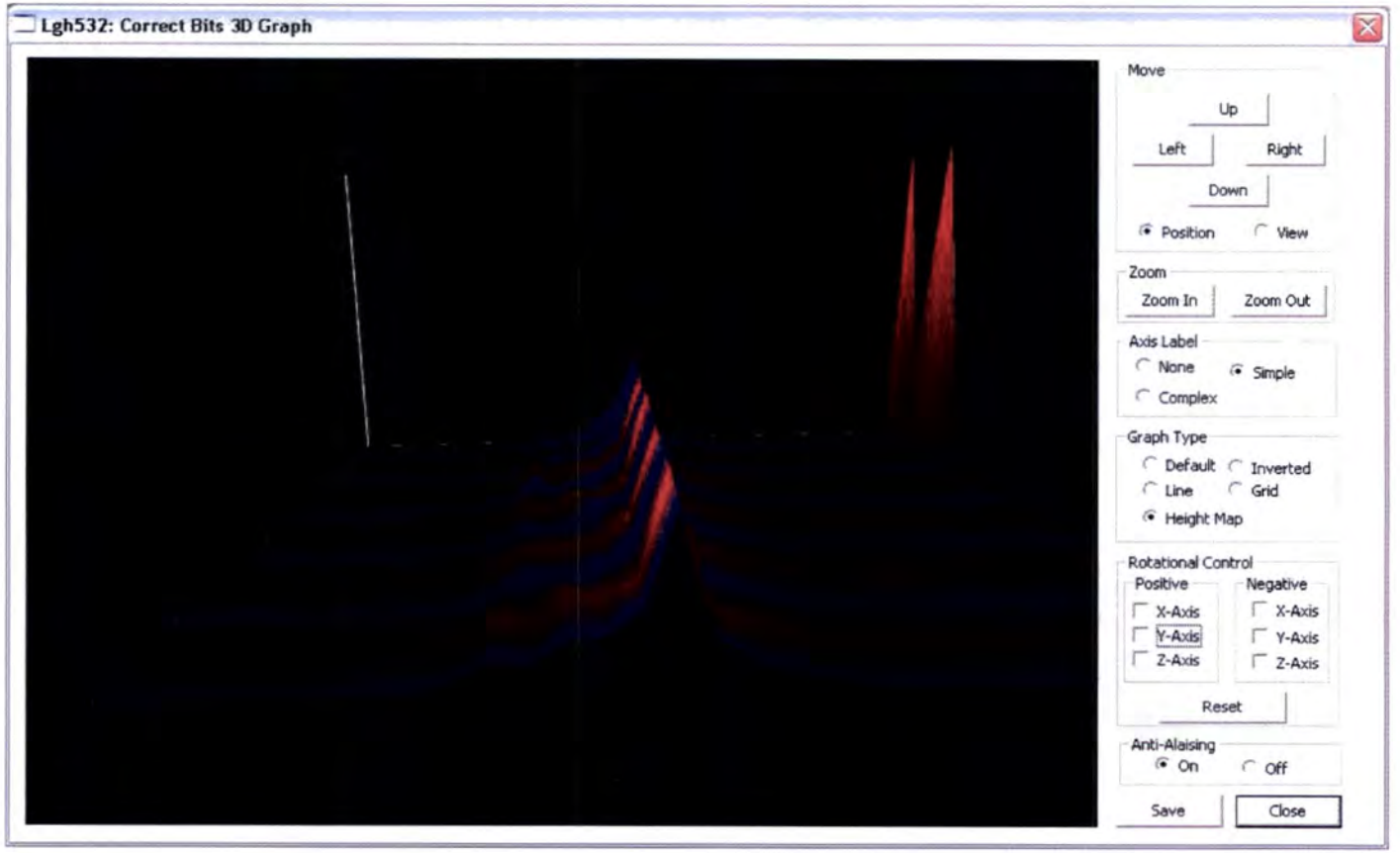

Figure 4.15 Correct bits per set 3D visualisation

The second series of visualisations to utilise the percentage of sets that contain the same number of correct bits, takes the first read after inkjet printing to be the correct bit sequence and compares this to the data obtained in the second read. This enables any changes after the second inkjet printing to be highlighted. For track 1 it can be seen that this visualisation indicates a change has occurred as a result of the second inkjet deposition, Figure 4.16. This is in agreement with the first visualisation where there was no change in track 1 read 1 has but a notable change in track 1 read 2 , Figure 4.7.

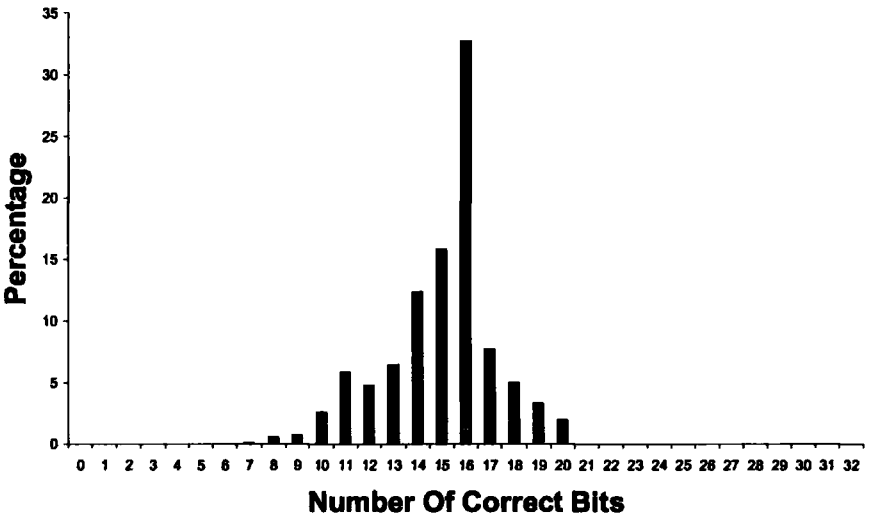

Figure 4.16 Visualisation of the correct number of bits after the second read with the first read data taken as the correct bit sequence. This indicates that the data has changed significantly.

This is further exemplified in the visualisation of track 4. For this track it was previously determined that BSA immobilization created a change in the first read, and that this change did not alter significantly after the inkjet deposition of high purity water, Figure 4.10. This second format of visualisation further clarifies this, indicating little significant change in the correct number of bits between the first and second read, with approximately 90% conserved, Figure 4.17.

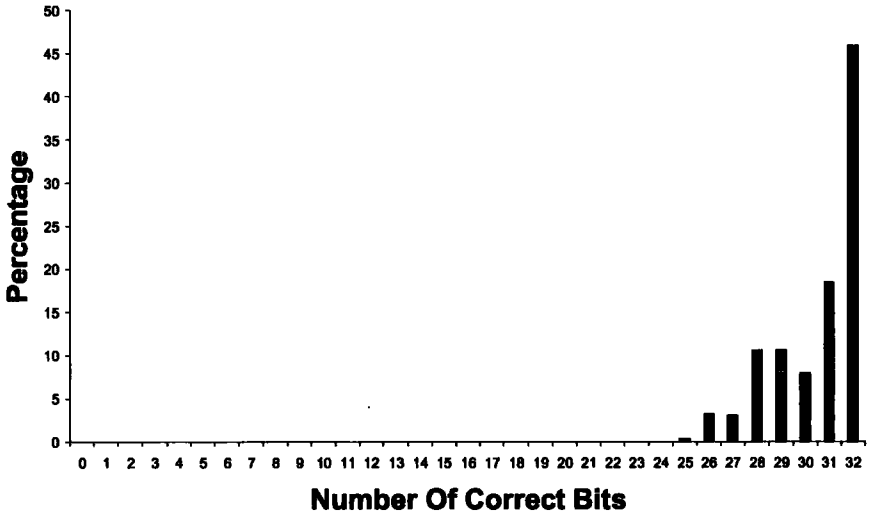

Figure 4.17 Correct bits per set for track 4 after read 2 with the data from read 1 taken as the correct bit sequence.

It can be seen from these visualisations that a significant change in data occurred between the two reads in tracks 1 and 2, Figure 4.16 and 4.18 respectively. However, there was little significant change in tracks 3, 4, 5 and 6, Figure 4.17, 4.19, 4.20 and 4.21 respectively. This further demonstrates that immobilized BSA interferes with the optical transmission of the laser and high purity water does not have any significant effect.

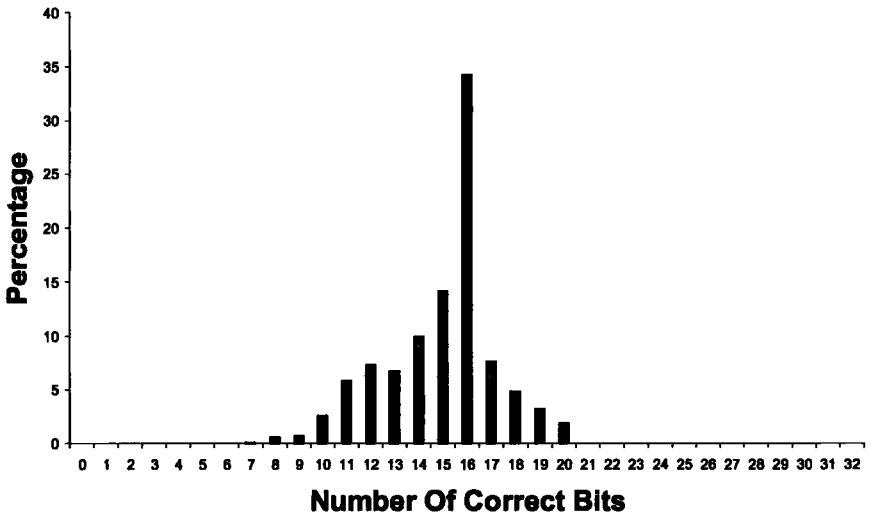

Figure 4.19 Correct bits per set for track 2 after read 2 with the data from read 1 taken as the correct bit sequence.

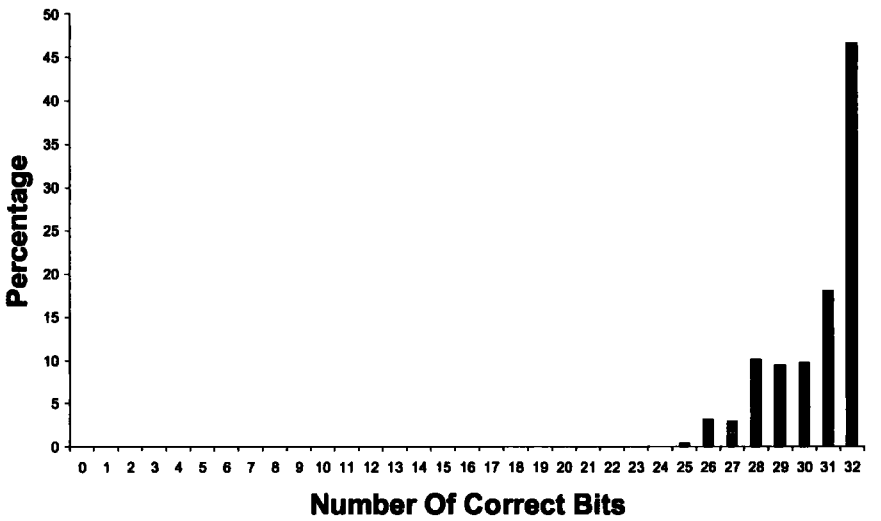

Figure 4.20 Correct bits per set for track 5 after read 2 with the data from read 1 taken as the correct bit sequence.

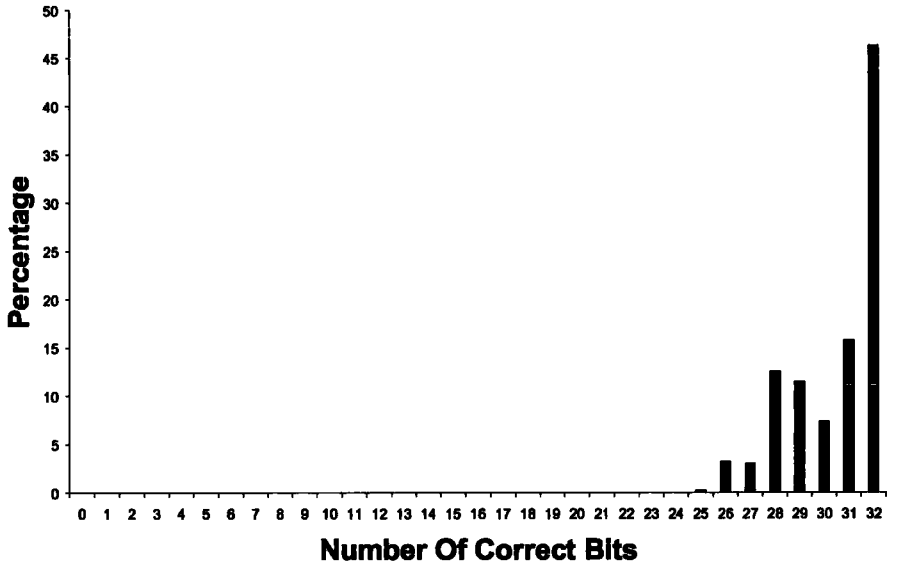

Figure 4.21 Correct bits per set for track 6 after read 2 with the data from read 1 taken as the correct bit sequence.

A further visualisation summarises the change in the correct number of bits for each track, Figure 4.22. This shows a significant change in data in tracks 1 and 2 with little change in tracks 3, 4, 5, and 6. This visualisation enables a rapid assessment of where binding taken place, as shown by tracks 1 and 2, where binding has occurred, showing distinctly different curves to tracks 3, 4, 5, and 6, Figure 4.22.

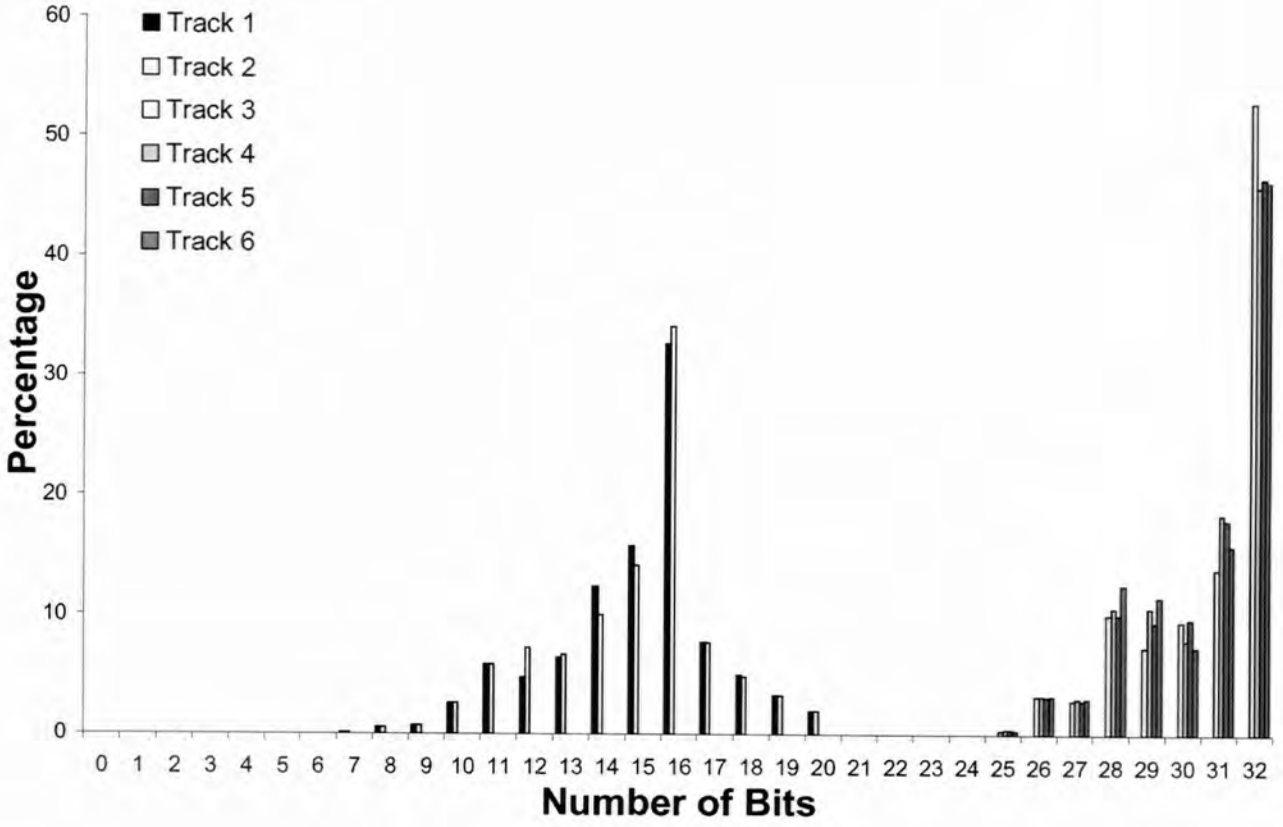

Figure 4.22 Correct bits per set for all tracks after read 2 with the data from read 1 taken as the correct data.

A third visualisation, known as a state change graph, demonstrates how each bit has changed during the process, with four possible state changes available:

0 The bit has not changed in any of the reads.
1 The bit has not changed after the first read.
2 The bit has not changed after the first read, but has change after the second read.
3 The bit has changed in the first and second read.

In track 1 the visualisation indicates 48% in state 0 (the bit has not changed) and 52% in state 2 (the bit has changed after read 2), Figure 4.23. This is comparable to the data presented in the number of correct bits per set visualisations, Figures 4.7 and 4.16, here the only change detected is after the second run, in which BSA has been immobilized. The track 2 state change graph is similar to track 1 with bit change evident after the second read only, Figure 4.24.

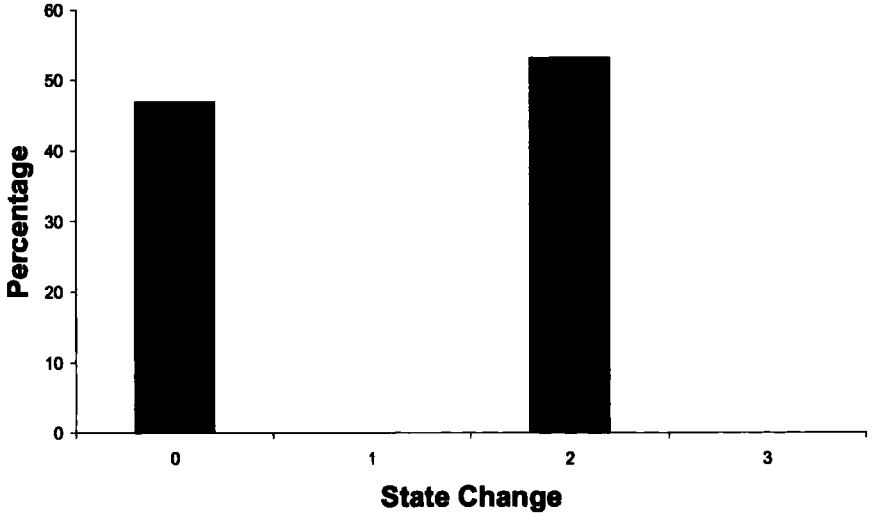

Figure 4.23 State changes for track 1 bits.

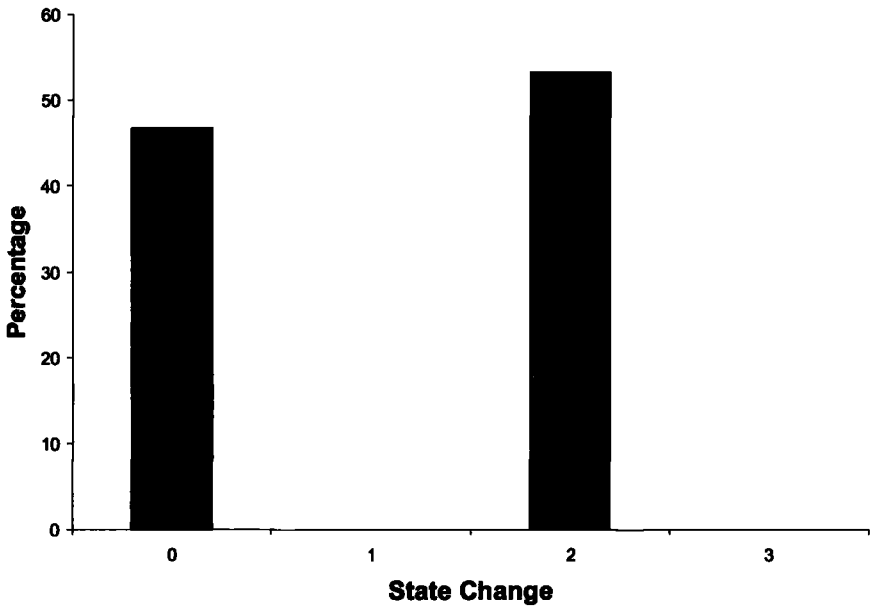

Figure 4.24 State changes for track 2 bits.

The state change graphs for tracks 3, 4, 5 and 6 indicate that the major bit change occurs after the first read, Figures 4.23, 4.24, 4.25 and 4.26 respectively. This is in good agreement with the associated correct bit per set visualisations, with the predominant state change occurring after the first read. The state change in all the tracks is summarised in one final visualisation, Figure 4.27. This shows that some bits have not changed throughout the process, bit change in tracks 1 and 2 occurs exclusively after the second read and the state change in 3, 4, 5, 6, after the first read. This bit change further confirms the ability of BSA to alter the optical path of the laser and demonstrates that a significant change only occurs following after inkjet printing of BSA.

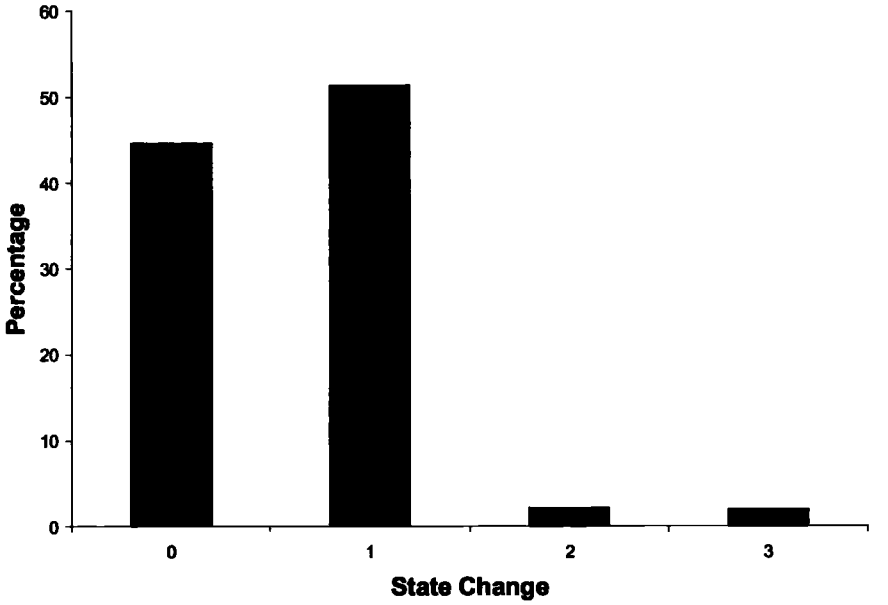

Figure 4.25 State changes for track 3 bits.

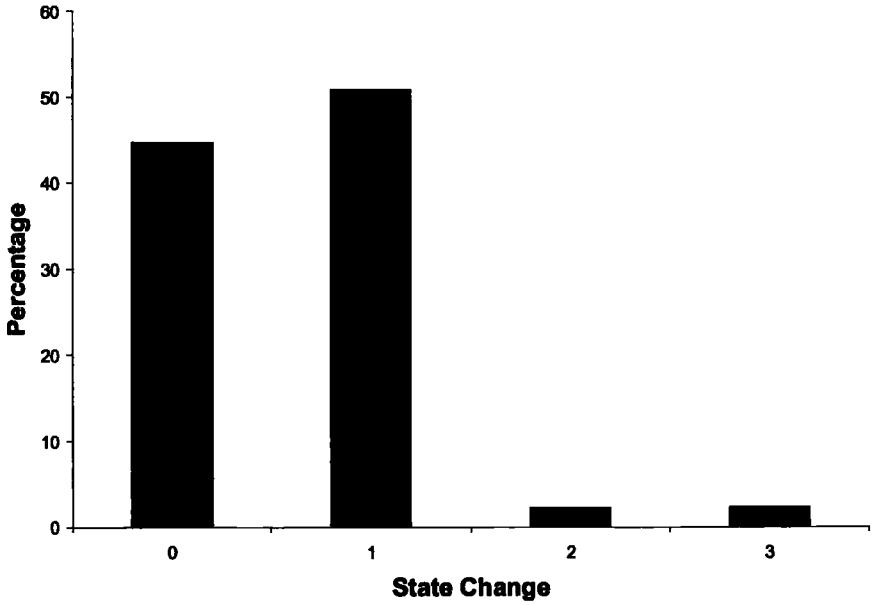

Figure 4.26 State changes for track 4 bits.

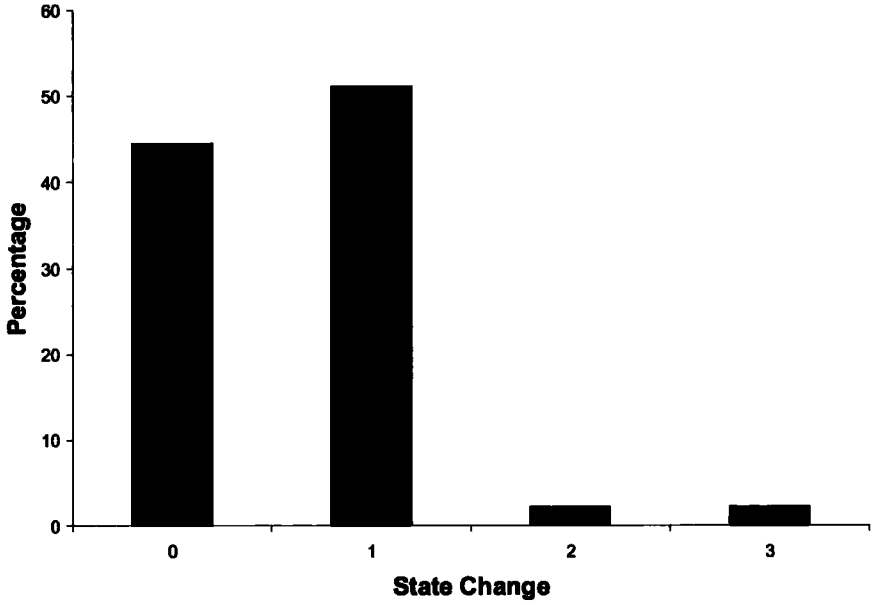

Figure 4.27 State changes for track 5 bits.

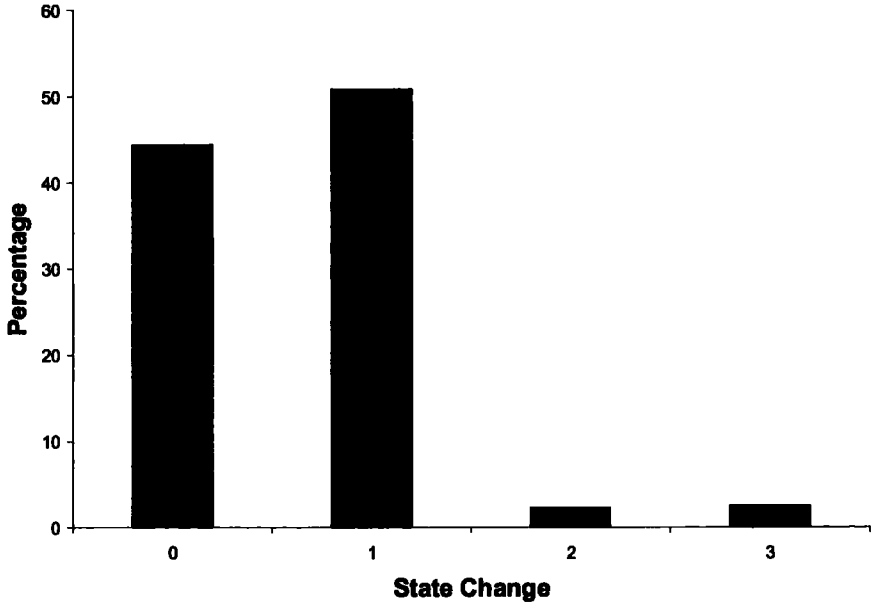

Figure 4.28 State changes for track 6 bits.

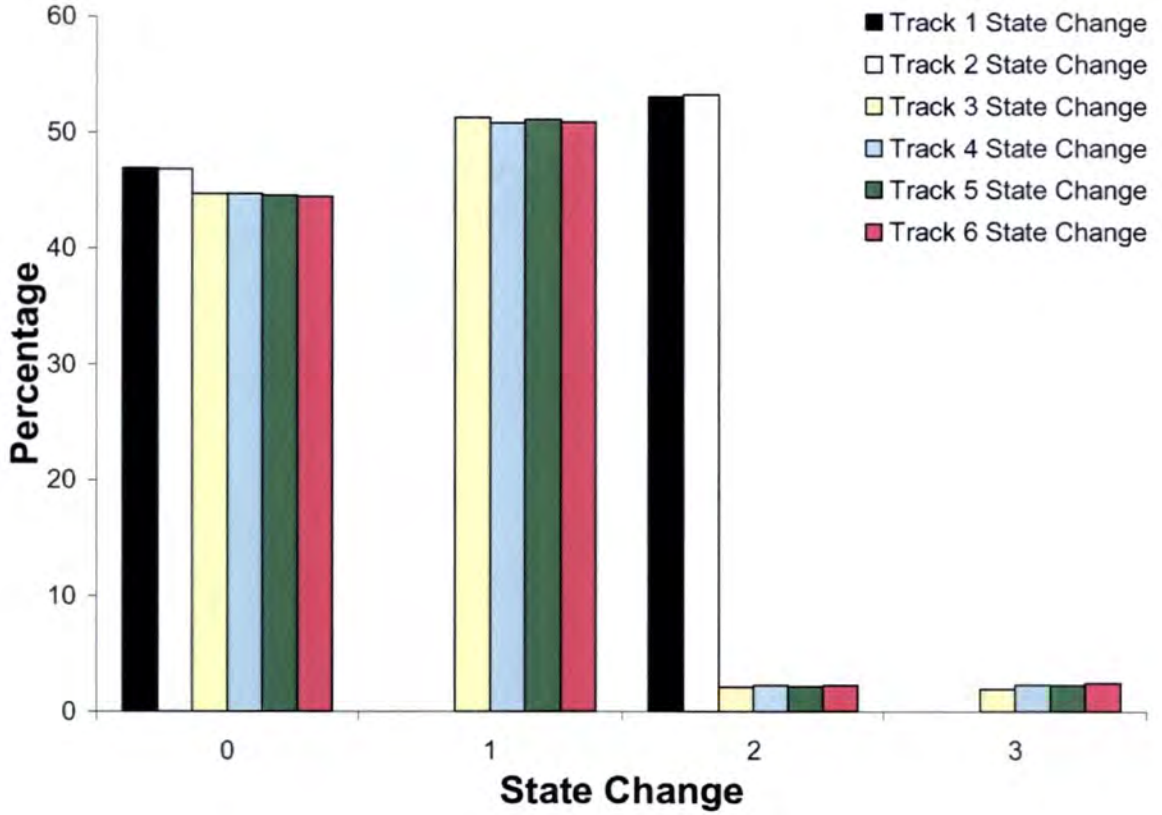

Figure 4.29 State change comparison for all tracks.

4.4 Discussion

The use of diagnostic devices in almost every aspect of science has resulted in the formation of a world wide multi-billion pound industry.[50] Whilst methods have been developed to perform high throughput analysis[51,52] they are often expensive and technically demanding, precluding their application outside the laboratory. The use of affordable compact discs, coupled with commercially available hardware, to perform portable point-of-care diagnostics is therefore an attractive alternative. Previous approaches have relied upon wet chemical modification and masks for functionalization, limiting the range and density of immobilised biomolecules.[30,32,34,35] The approach described in this study avoids these prerequisites by utilising a pulsed plasma deposited glycidyl methacrylate layer to create an epoxy functionalized nanolayer capable of binding the primary amine groups of biomolecules via nucleophilic attack.[38,39] The subsequent functional patterning, data detection and visualisation was performed by user developed software and commercially available hardware. This software burned 6 data tracks into the compact disc, before plasma functionalization, and subsequently directed the inkjet printing so that the contents of each cartridge corresponded to a data track on the compact disc, Figure 4.3.

The extent and position of data change was presented by the software in three different visualisations. The first visualisation displayed the correct number of bits per set for each track after each step, where the correct bit sequence is taken to be the data after pulsed plasma polymerization. These visualisations indicated that upon the inkjet printing of high purity water no significant change in data is created, before or after BSA immobilization. However the inkjet printing of BSA did significantly alter the data, Figures 4.7 to 4.12. This demonstrates that the size of the BSA molecules is sufficient to alter the optical transmission of a laser beam in a standard CD-ROM drive to such an extent that the data interpreted is different from the data burned in the compact disc.

The anomaly generated in track 3, where a change was detected similar to that of tracks 4, 5, 6 despite following the immobilization procedure of tracks 1 and 2, was a result of the colours used in the .jpg file. The four colours of a standard inkjet printer (black, yellow, cyan and magenta) are assigned different colours in the software enabling 100% of ink to print from an individual cartridge. A six inkjet printer contains an additional two colours (light cyan and light magenta) which do not have exact colour matches in the computer software. Therefore the actual colour assigned in the .jpg image to represent these colours result in a mixture of solutions being deposited from a range of cartridges; one of these new colours (light cyan) being used to represent track 3. Further work is required in the formation of the .jpg image to find a colour match which will print 100% from this cartridge.

The second visualisation also utilised the number of correct bits per set. However the correct bit sequence was taken to be the bit sequence after the first read, this highlighted any change in data between read 1 and read 2. These visualisations showed that in tracks 1 and 2, where the correct bit sequence is that after the inkjet deposition of high purity water, that a significant change occurred as a result of BSA immobilization. On tracks 4, 5, 6, where the correct bit sequence is taken following BSA immobilization, there was no significant change after the deposition of high purity water, Figures 4.16 to 4.21. It is envisaged that this visualisation can be used in a manner similar to a molecular array, for example, a screening library can be formed by the inkjet deposition of six different biomolecules onto six different tracks. Subsequent exposure to a solution which contains a biomolecule with a particular affinity for one of the tracks will lead to binding in that particular track. This could be identified with a visualisation showing the correct number of bits for all tracks: where tracks in which binding has occurred are clearly discernable from those were there is no change due to the change in data between read 1 and read 2, Figure 4.27.

A third visualisation enabled the state of each bit to be tracked throughout the process. This produced an output to show whether the bit did

not change at all, changed after the first read only, changed after the second read only, or changed in both reads, Figures 4.23 to 4.28. From the state-change visualisation it can be further verified that high purity water does not change the state of a bit, but BSA can change a bit only detected after BSA immobilization. Once again it can be seen that this visualisation may have viability in molecular screening.

4.5 Conclusions

Pulsed plasma polymerization of glycidyl methacrylate can be used to present reactive epoxy groups at the surface of a compact disc. Furthermore, it is possible to monitor the binding of BSA to this surface by detecting the change in data on the compact disc with the use of the developed surface and commercially available hardware, thus providing a link between the informatic content of a compact disc and molecular binding. The subsequent production of a series of visualisation formats to compare the change in data demonstrates the capability of a compact disc to act as a molecular sensor.

4.6 References

(1) McClesky, S. C.; Griffin, M. J.; Schneider, S. E.; McDevitt, J. T.; Anslyn, E. V. *J. Am. Chem. Soc* **2003**, *125*, 1114.

(2) Nefzi, A.; Ostresh, J. M.; Yu, J.; Houghten, R. A. *J. Org. Chem.* **2004**, *69*, 3603.

(3) Lavine, B. K.; Workman, J. *Anal. Chem.* **2002**, *74*, 2763.

(4) Arlinghaus, H. F.; Kwoka, M. N.; Jacobsen, K. B. *Anal. Chem.* **1997**, *69*, 3747.

(5) Landers, J. P. *Anal. Chem.* **2003**, *75*, 2919.

(6) Epstein, J. R.; Ferguson, J. A.; Lee, K. H.; Walt, D. R. *J. Am. Chem. Soc.*, **2003**, *125*, 13753.

(7) Murrell, A.; Vardhman, K.; Beck, S. *Hum. Molec. Genet.* **2005**, *14*, R3.

(8) Fan, J. B.; Chee, M. S.; Gunderson, K. L. *Nat. Rev. Genet.* **2006**, *7*, 632.

(9) Plass, C. *Hum. Molec. Genet.* **2002**, *11*, 2479.

(10) Cardozo, A. K.; Berthou, L.; Kruhoffer, M.; Orntoft, T.; Nicolls, M. R.; Eizirik, D. L. *J. Proteome. Res.* **2003**, *2*, 553.

(11) Weston, A. D.; Hood, L. *J. Proteome. Res.* **2004**, *3*, 179.

(12) Marko-Varga, G.; Fehniger, T. E. *J. Proteome. Res.* **2004**, *3*, 167.

(13) Wabuyele, M. B.; Farquar, H.; Stryjewski, W.; Hammer, R. P.; Soper, S. A.; Cheng, Y. W.; Barany, F. *J. Am. Chem. Soc.* **2003**, *125*, 6937.

(14) Drukler, A. K.; Ossetrova, N.; Schors, E.; Brown, L. R.; Thomaszewski, J.; Sainsbury, R.; Zimmerman, J. *J. Proteome. Res.* **2005**, *4*, 2375.

(15) Zhao, X.; Dytioco, R.; Tan, W. *J. Am. Chem. Soc.* **2003**, *125*, 11474.

(16) Sokoll, L. J.; Chan, D. W. *Anal. Chem.* **1999**, *71*, 356R.

(17) Lawruk, T. S.; Lachman, C. E.; Jourdan S. W.; Fleeker, J, R.; Hayes, M. C.; Herzog, D. P.; Rubio, F. M. *Eviron. Sci. Technol.* **1996,** *30,* 695.

(18) Johnson, J. C.; Emon, J. M. *Anal. Chem.* **1996,** *68,* 162.

(19) Dubois, J. *Anal. Chem.* **2004,** *76,* 361A.

(20) Schmitt, J.; Beekes, M.; Brauer, A.; Udelhoven, T.; Lasch, P.; Naumann, D. *Anal. Chem.* **2002,** *74,* 3865.

(21) Ng, L. M.; Simmons, R. *Anal. Chem.* **1999,** *71,* 343R.

(22) Thomas, C. E.; Kelleher, N. L.; Mizzen, C. A. *J. Proteome. Res.* **2006,** *5,* 240.

(23) Zimmerman, L. J.; Wernke, G. R.; Caprioll, R. M.; Liebler, D. C. *J. Proteome. Res.* **2005,** *4,* 1672.

(24) Issaq, H. J.; Conrads, T. P.; Prieto, D. A.; Tirumali, R.; Veenstra, T. D. *Anal. Chem.* **2003,** *75,* 149A.

(25) Dyson, H. J.; Wright, P. E. *Chem. Rev.* **2004,** *104,* 1.

(26) Lacey, M. E.; Subramanian, R.; Olsen, D. L.; Webb, A. G.; Sweedler, J. V. *Chem. Rev.* **1999,** *99,* 3133.

(27) Chow, C. S.; Bogdan, F. M. *Chem. Rev.* **1997,** *97,* 1489.

(28) Lange, S. A.; Roth, G.; Wittemann, S.; Lacoste, T.; Vetter, A.; Grassle, J.; Kopta, S.; Kolleck, M.; Breitinger, B.; Wick, M.; Horber, J. K. H.; Dubel, S.; Bernard, A. *Angew. Chem. Int. Ed.* **2006,** *45,* 270.

(29) Kumaresan, P. R.; Lam, K. S. *Mol. BioSyst.* **2006,** *2,* 259.

(30) Yu, H. Z.; *Chem. Commun.* **2004,** *23,* 2633.

(31) Ivanov, Y. D.; Govorun, V. M.; Bykov, V. A.; Archakov, A. I. *Proteomics* **2006,** *6,* 1399.

(32) Kido, H.; Maquieira, A.; Hammock, B. D. *Anal. Chim. Acta.* **2000,** *411,* 1.

(33) Morais, S.; Moles, R. M.; Puchades, R.; Maquieira, A. *Chem. Commun.* **2006,** *22,* 2368.

(34) Felton, M. J. *Anal. Chem.* **2003,** *75,* 303A.

(35) Clair, J. J., Burkat, M. D. *Org. Biomol. Chem.* **2003,** *1,* 3244.

(36) Pohlmann, K. C. *The Compact Disc Handbook;* A-R editions, Inc., Madison, 1992.

(37) How Stuff Works http://computer.howstuffworks.com/cd-burner.htm/printable (accessed Sept 2006).

(38) Deng, Y.; Zhu, W. Y.; Kienlen, T.; Guo, Q. *J. Am. Chem. Soc.* **2006,** *128,* 2768.

(39) Mateo, C.; Torres, R.; Fernandez-Lorente, G.; Ortiz, C.; Fuentes, M.; Hidalgo, A.; Lopez-Gallego, F.; Abian, O.; Palomo, J. M.; Guisan, J. M.; Betancor, L.; Pessela, B. C. C.; Fernandez-Lafuente, R. *Biomacromolecules* **2003,** *4,* 772.

(40) Theriault, T.; Winder, S. C.; Gamble, R. C.; *Application of ink-jet printing technology to the manufacture of molecular arrays.* In Schena M (ed): DNA Microarrays: A Practical Approach. Oxford, UK: Oxford University Press, 1999.

(41) Allain, L. R.; Askari, M.; Stokes, D. L.; Dinh, T. V. *Fresenius J. Anal. Chem.* **2001,** *371,* 146.

(42) Clavert, P.; *Chem. Mater.* **2001,** *13,* 3299.

(43) Stevens, P. W.; Wang, C. H. J.; Kelso, D. M. *Anal. Chem.* **2003,** *75,* 1141.

(44) Xu, L. C.; Logan, B. E. *Eviron. Sci. Technol.* **2005,** *39,* 3592.

(45) Charters, S. D.; Munor, M. Dept of Computer Science, Durham University. **2005**

(46) Evans, J. F.; Gibson, J. H.; Moulder, J. F.; Hammond, J. S.; Goretzki, H. *Fresenius J. Anal. Chem.* **1984,** *319,* 841.

(47) Tabet, M. F.; McGahan, W. A. *Thin Solid Film* **2000,** *370,* 122

(48) Tarducci, C.; Kinmond, E.; Brewer, S.; Willis, C.; Badyal J. P. S. *Chem. Mater.* **2000,** *12,* 1884.

(49) Beamson, G.; Briggs, D. *High Resolution XPS of Organic Polymers*; Wiley: Chichester, 1992.

(50) Schena, M. *Microarray Analysis*; Wiley: New Jersey, 2003.

(51) Wang, J. *Biosens. Bioelectron.* **2006**, 21, 1887.

(52) Walter, G.; Bussow, K.; Lueking, A.; Gloker, J. *Trends in Molecular Medicine.* **2002**, *8*, 250.

CHAPTER 5

PROTEIN IMMOBILIZATION TO PROTEIN RESISTANT SURFACES

5.1 Introduction

Electrostatic interactions between charged particles are amongst the strongest bonds known, being comparable in strength to covalent bonds,[1,2,3] and are utilised in aerosol and membrane filtration to remove particulate matter.[4,5,6] Electrets, materials that contain quasi-permanent regions of charge, within an insulating surface, further apply the electrostatic interaction for a range of applications, including the attachment of charged pigments to a surface in xerography,[7,8] microphones[9,10] and radiation dosimeters.[11,12] Furthermore, the development of techniques such atomic force microscopy,[13,14] microcontact printing[15,16] and photolithography,[17,18,19] with the capability to form small scale charge regions within the electret, have been utilised in the development of molecular sensors,[20,21] and scaffolds for self assembly.[22,23]

Proteins comprise of a series of amino acids, containing both amino and carboxyl groups, which regulate a variety of biologically important events.[24] It is known that at defined pH (the isoelectric point) the protein exists as a neutral zwitterion. Below the isoelectric point the protein exists primarily as a cation, and above exists primarily as a deprotonated anion.[25] It follows that charged proteins can be electrostatically immobilize to an appropriately charged substrate.[26,27,28,29] In one particular embodiment arrays of anionic protein were formed via immobilization to positive charge stored within an electret[30] (molecular arrays are of particular importance in the field of proteomics as they provide high throughput diagnostics of protein-protein interactions). The drawback to this method is the requirement of blocking proteins to prevent protein fouling to the electret background. This use of blocking proteins is particularly undesirable due to the necessity of an additional step in the array fabrication and the Vroman effect (where adsorbed blocking proteins are vulnerable to replacement by more active proteins).[31]

Previously, it has been demonstrated, that pulsed plasma deposited poly(*N*-acrylolysarcosine methyl ester) is resistant to protein adsorption,[32] furthermore, in separate studies, it has also been demonstrated that pulsed plasma deposited films can act as electrets upon exposure to a corona discharge emanating from a metallized AFM tip,[33] forming regions of localised charge, of both polarities, that may be used to immobilize particulate matter.[34,35]

This study investigates the application of voltages to a metallized AFM tip to form regions of localised charge within a protein resistant pulsed plasma deposited poly(*N*-acrylolysarcosine methyl ester) nano-layer, and to utilise the strong electrostatic interaction to immobilize proteins. Furthermore, by tailoring the pH of the protein to form cationic and anionic variants, it is envisaged that the protein may be selectively immobilized onto regions of negative and positive charge respectively, Figure 5.1.

The major attribute of this method utilises the electret nature of pulsed plasma polymers and the protein resistive properties of pulsed plasma deposited poly(*N*-acrylolysarcosine methyl ester) to fabricate protein arrays with low background fluorescence, capable of determining protein-protein interactions.

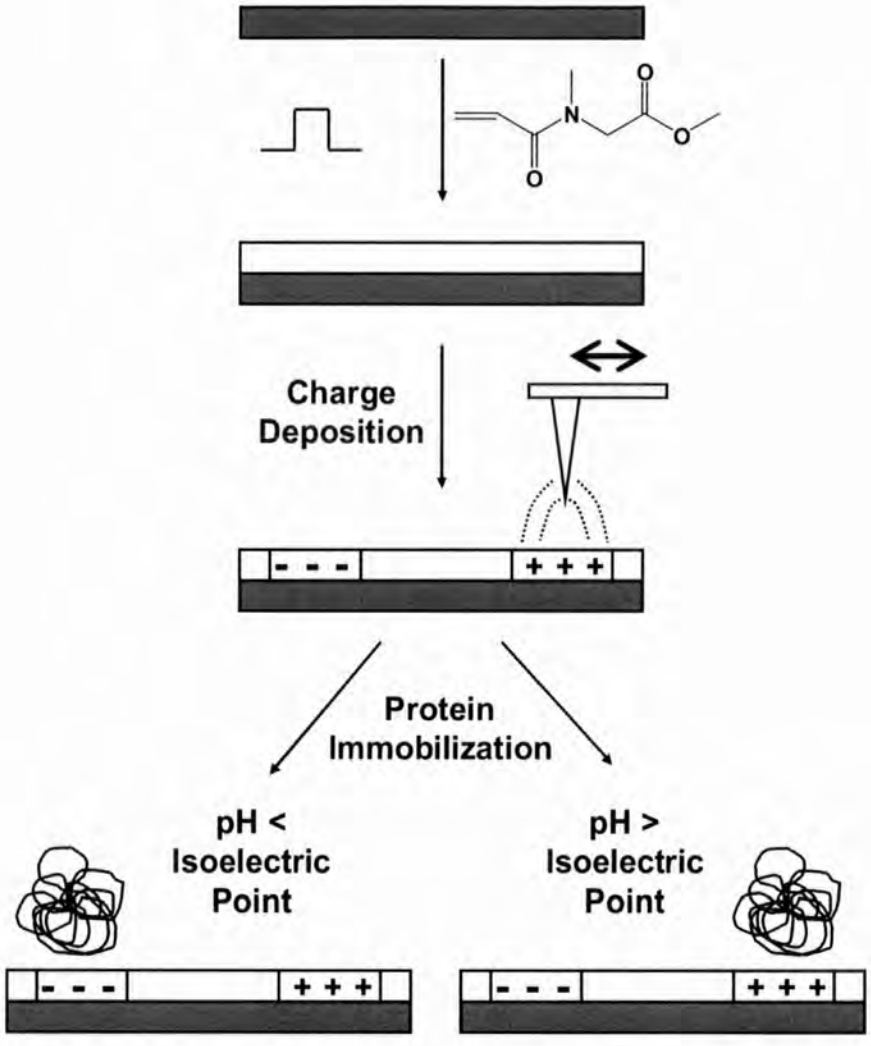

Figure 5.1 Formation of localised negative and positive charge in poly(*N*-acrylolysarcosine methyl ester) via a corona discharge emanating from a scanning probe tip, followed by protein immobilization at varying pH.

5.2 Experimental

5.2.1 Plasmachemical Nanolayering

N-acryloylsarcosine methyl ester monomer (97%, Lancaster) was loaded into a sealable glass tube, followed by degassing using multiple freeze-pump-thaw cycles. Pulsed plasma polymerization was carried out in a cylindrical glass reactor (4.5 cm diameter, 460 cm^3 volume, 2×10^{-3} mbar base pressure, and 1.6×10^{-9} mol s^{-1} leak rate) surrounded by a copper coil (4 mm diameter, 10 turns, located 15 cm away from the precursor inlet) connected to a 13.56 MHz radio frequency (RF) power supply and an L-C matching network. The plasma chamber was located inside a temperature-controlled oven and a Faraday cage. A 30 L min^{-1} rotary pump attached to a liquid nitrogen cold trap was used to evacuate the reactor, while the system pressure was monitored with a Pirani gauge. All fittings were grease-free. During pulsed plasma deposition, the RF power source was triggered by a signal generator, and the pulse shape monitored with an oscilloscope. Prior to each deposition, the apparatus was scrubbed with detergent, rinsed in 2-propanol, and oven dried. Further cleaning entailed running a 40 W continuous wave air plasma at 0.2 mbar pressure and lasting 20 min. The substrate of interest was inserted into the reactor and the reactor pumped down to base pressure. At this stage, a continuous flow of *N*-Acryloylsarcosine methyl ester vapour was introduced into the chamber at a pressure of 0.1 mbar and 50 ℃ temperature for 5 min prior to plasma ignition . The optimum pulsed plasma duty cycle corresponded to 30 W peak power continuous wave bursts lasting 20 μs and 5 ms off. Upon completion of deposition, the RF power source was switched off and the monomer allowed to continue to purge though the system for a further 5 min prior to evacuation to base pressure and venting to atmosphere.

5.2.2 Localised Charge Deposition

Localised charge deposition was performed by applying +/-150 V, from an external power supply in conjunction with a signal access module, to a Cr sputter coated AFM probe (125 μm long silicon tip, force constant ≈ 40 nN, resonance frequency ≈ 270 kHz after metallization, MikroMasch NSC15/Cr) coupled to a Nanoscope III atomic force microscope (Digital Instruments). Localise charge deposition was carried out during lift mode scanning at a height of 30 nm above the sample surface, with a set point of 1.1 V and a scan rate of 1.0 Hz. Localised regions of charge within in the pulsed plasma polymer were monitored via the topography and phase lag of the surface after charge deposition.

The phase lag of an oscillating cantilever (Φ) is defined as the difference between the actual frequency of oscillation and the driving source, with phase lags normally expressed as angles. The phase shift images acquired in tapping mode AFM represent the difference between the phase lag of the freely vibrating cantilever and the cantilever interacting with the underlying substrate, Equation 5.1.

$$\Delta\phi = \phi_{free} - \phi_{interacting} \qquad \textbf{Equation 5.1}$$

$\Delta\ \Phi$ = Displayed AFM phase shift.

Φ_{free} = Phase lag of a freely vibrating cantilever.

$\Phi_{interacting}$ = Phase lag of the interacting cantilever.

The driving frequency of the freely vibrating cantilever is normally chosen to be close to its resonance frequency. According to the theory of freely driven oscillators, the phase lag of a freely vibrating cantilever at its maximum amplitude is equal to 90°.[36] Hence the phase lag of the freely vibrating cantilever (Φ_{free}) is 90°. However when tip-substrate interactions are present the resonant frequency of the cantilevered is altered from the driving frequency resulting in a new phase lag ($\Phi_{interacting}$).[37] If the cantilever experiences a repulsive field gradient then the resonant

frequency is increased, and the corresponding phase lag of the interacting cantilever ($\Phi_{interacting}$) at the driving frequency drops below 90°. This results in the phase shift ($\Delta\Phi$) becoming positive, with its magnitude corresponding to the degree of repulsion (contrast in phase images brightens), Table, 5.1. Conversely an attractive force gradient reduces the resonant frequency, with the interacting phase lag at the driving frequency being raised above 90° producing a negative phase[38] (contrast in phase images darkens), Table 5.1.

Force Gradient	**Resonance Frequency of Cantilever**	**Phase Shift $\Delta\Phi$**	**AFM Phase Image**
Repulsive	Increases	Positive	Brighter
Attractive	Decreases	Negative	Darker

Table 5.1 Effect of force gradients on the phase shift of a freely oscillating cantilever.

As the phase image produced in tapping mode AFM is dominated by the short range forces above the sample (including elasticity[39], adhesion[40] and energy dissipation),[41] electric field studies via the AFM are carried out during a lift-mode, where a topographical map of the surface is determined by a preliminary scan followed by a scan where the tip is held at a fixed distance above the surface. Any further changes in phase are therefore due to additional long range forces such as Van der Waals and electrostatic interactions, with the latter dominant for charged surfaces, Figure 5.2

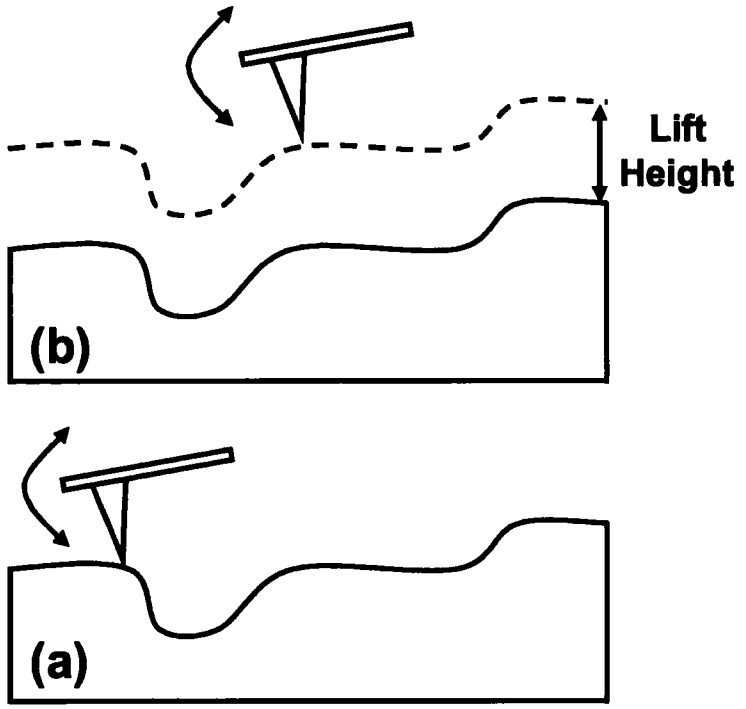

Figure 5.2 Atomic force microscope scanning by: (a) intermittent contact mode AFM: and (b) using lift mode scanning of the same area.

In addition to electrostatic interactions the lift mode phase shift also has a dependence on the voltages from the surface ($V_{surface}$) and tip (V_{tip}), with the voltage on the surface inducing a mirror charge on the tip. In addition to this an external power supply may be utilised to apply a voltage to the tip ($V_{applied}$) resulting in a new tip voltage, Equation 5.2.

$$V_{tip} = V_{applied} - V_{Surface} \qquad \textbf{Equation 5.2}$$

V_{tip} = *total voltage at the tip.*

$V_{applied}$ = *external voltage applied to the tip.*

$V_{surface}$ = *voltage at the substrate surface.*

It follows that the phase shift experienced in lift mode will depend on the sign and magnitude of V_{tip} and $V_{surface}$. When V_{tip} and $V_{surface}$ have the same polarity there will be a repulsive force, resulting in a bright phase

shift, however when they are of opposite polarity the force is attractive and a dark phase shift occurs. Furthermore the magnitude of the phase shift will depend on the product of V_{tip} and $V_{surface}$, from this it is possible to monitor the extent that the corona discharge has altered the surface.

5.2.3 Protein Immobilization

Protein immobilization above the isoelectric point (pH 4.19[42]) entailed exposing charged pulsed plasma deposited poly(N-acryloylsarcosine methyl ester) to Protein G from streptococcus sp (200 μg mL^{-1} in PBS, pH 7.2, Sigma-Aldrich) for 30 minutes, followed by immersion in Alexa-fluor 633 goat anti-mouse immunoglobulin (2 mg mL^{-1} in phosphate-buffered saline, pH 7.2, Molecular Probes) further diluted to a concentration of 200 μg mL^{-1} in phosphate-buffered for a further 30 minutes. Finally the samples were washed in high purity water for 10 minutes before being allowed to dry in air. Protein immobilization below the isoelectric point utilised was carried out as above, however Protein G was adjusted to pH 3 upon addition of 200 μM HCl.

5.2.4 Surface Characterization

X-ray photoelectron spectroscopy (XPS) was undertaken using an electron spectrometer (VG ESCALAB MK II) equipped with a non-monochromated Mg $K\alpha_{1,2}$ X-ray source (1253.6 eV) and a concentric hemispherical analyser. Photo-emitted electrons were collected at a take-off angle of 30° from the substrate normal, with electron detection in the constant analyser energy mode (CAE, pass energy = 20 eV). The XPS spectra were charge referenced to the C(1s) peak at 285.0 eV and fitted with a linear background and equal full-width-at-half-maximum (FWHM) Gaussian components[43] using Marquardt minimization computer software. Instrument sensitivity (multiplication) factors derived from chemical standards were taken as being C(1s): O(1s): N(1s): equals 1.00: 0.63: 0.45.

Fourier transform infrared (FTIR) analysis of the films was carried out using a Perkin-Elmer Spectrum One spectrometer equipped with a liquid nitrogen cooled MCT detector operating across the 700 – 4000 cm^{-1} range. Reflection–absorption (RAIRS) measurements were performed using a variable angle accessory (Specac) set at 86° on an Au substrate in conjunction with a KRS-5 polarizer fitted to remove the s–polarized component. All spectra were averaged over 4,000 scans at resolution of 4 cm^{-1}.

Contact angle analysis of the plasma-deposited films was carried out with a video capture system (ASE Products, model VCA2500XE) using 2.0 µL droplets of de-ionized water.

Film thickness measurements were carried out using an nkd-6000 spectrophotometer (Aquila Instruments Ltd). Transmittance-reflectance curves (over the 350-1000 nm wavelength range) were fitted to the Cauchy model for dielectric materials using a modified Levenburg-Marquardt method.[44]

Fluorescence microscopy was performed using an Olympus IX–70 system (DeltaVision RT, Applied Precision, WA). Image data was collected using an excitation wavelength of 633 nm.

5.3 Results

5.3.1 Poly(*N*-acryloylsarcosine methyl ester)

The contact angle, infra-red spectra, XPS elementary stoichiometry and XPS C(1s) spectra values of the pulsed plasma deposited poly(*N*–acryloylsarcosine methyl ester) protein-resistant film were identical to section 2.3.1.

5.3.2 Protein Immobilization above the Isoelectric Point

Evidence for positive charge deposition within poly(*N*- acryloylsarcosine methyl ester) following the scanning of an AFM tip over a 20 μm x 20 μm square, whilst being subjected to an applied voltage of +150 V, 30 nm above the surface, was obtained using atomic force microscope topographical and phase images.

AFM topography showed no change in the surface topography following positive charge deposition, Figure 5.3(a). The phase image upon application of +35 V revealed a bright square in the area of deposited charge approximately 20 μm x 20 μm, Figure 5.3(b). The bright square indicated that a repulsive force was present between the tip and the sample. Lowering the magnitude of the applied voltage reduced the intensity of the phase shift until it is no longer present at an applied voltage of +12 V at the tip, Figure 5.3(c). Further reduction in the applied voltage of -35 V yielded a dark square in the phase image, indicating an attractive field gradient between the tip and the surface was present, Figure 5.3(d). Fluorescence images obtained prior to protein exposure showed no change in the fluorescent properties of the surface as a result of charge deposition, Figure 5.3(e). However after protein immobilization of protein G and subsequent exposure to complementary Alexa Fluor 633 labelled IgG, a fluorescent square of approximately the same dimension of the charged area was revealed.

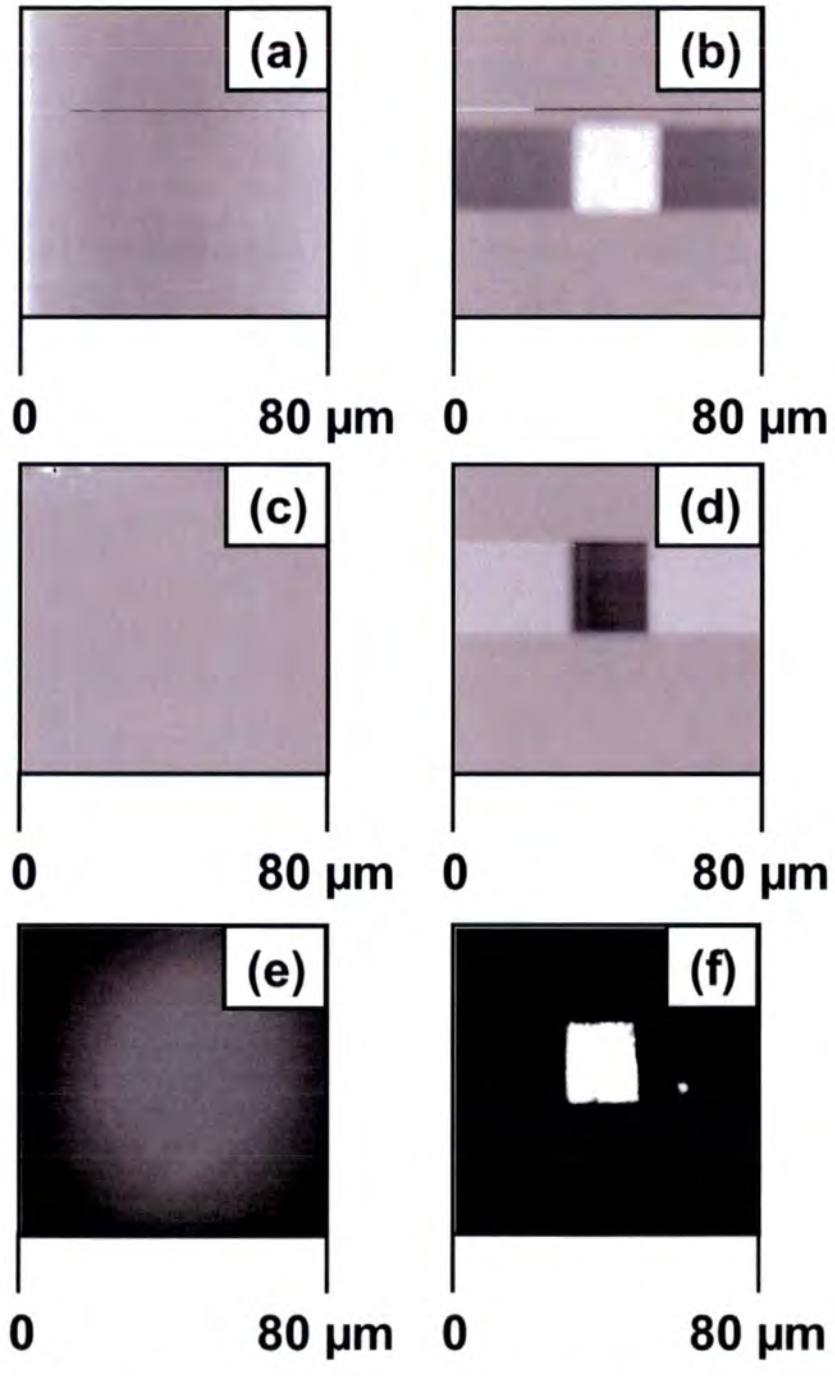

Figure 5.3 Atomic force micrograph images of poly(*N*-Acryloylsarcosine methyl ester) after exposure to a metallized AFM tip biased at +150 V: (a) Tapping mode topography; and (b-d) Lift mode phase images recorded at +35 V, +12 V and -12 V respectively. Corresponding fluorescence images of the surface: (e) Prior to protein exposure; and (f) Subsequent to protein exposure.

Negative charge deposition comprised the scanning a 20 μm x 20 μm square while the tip subjected to an applied voltage of -150 V, 30 nm above the surface. AFM topography showed no change in the surface topography following negative charge deposition, Figure 5.4(a). The phase image upon application of +35 V revealed a dark square of similar to dimensions to the area subjected to the negative charge, Figure 5.4(b). This dark square indicated that an attractive force gradient was present between the tip and the sample. Lowering the magnitude of the applied voltage reduced the intensity of the phase shift until it is no longer present at an applied voltage of -13 V, Figure 5.4(c). Further reduction in the applied voltage to negative voltage of -35 V yields a bright square in the phase image, indicating a repulsive field gradient between the tip and the surface, Figure 5.4(d). Fluorescence images obtained prior to protein exposure, once again, revealed no change in the fluorescent properties of the surface as a result of charge deposition, Figure 5.4(e). After protein immobilization of protein G and subsequent exposure to complementary Alexa Fluor 633 labelled IgG no significant fluorescence at the surface was noted.

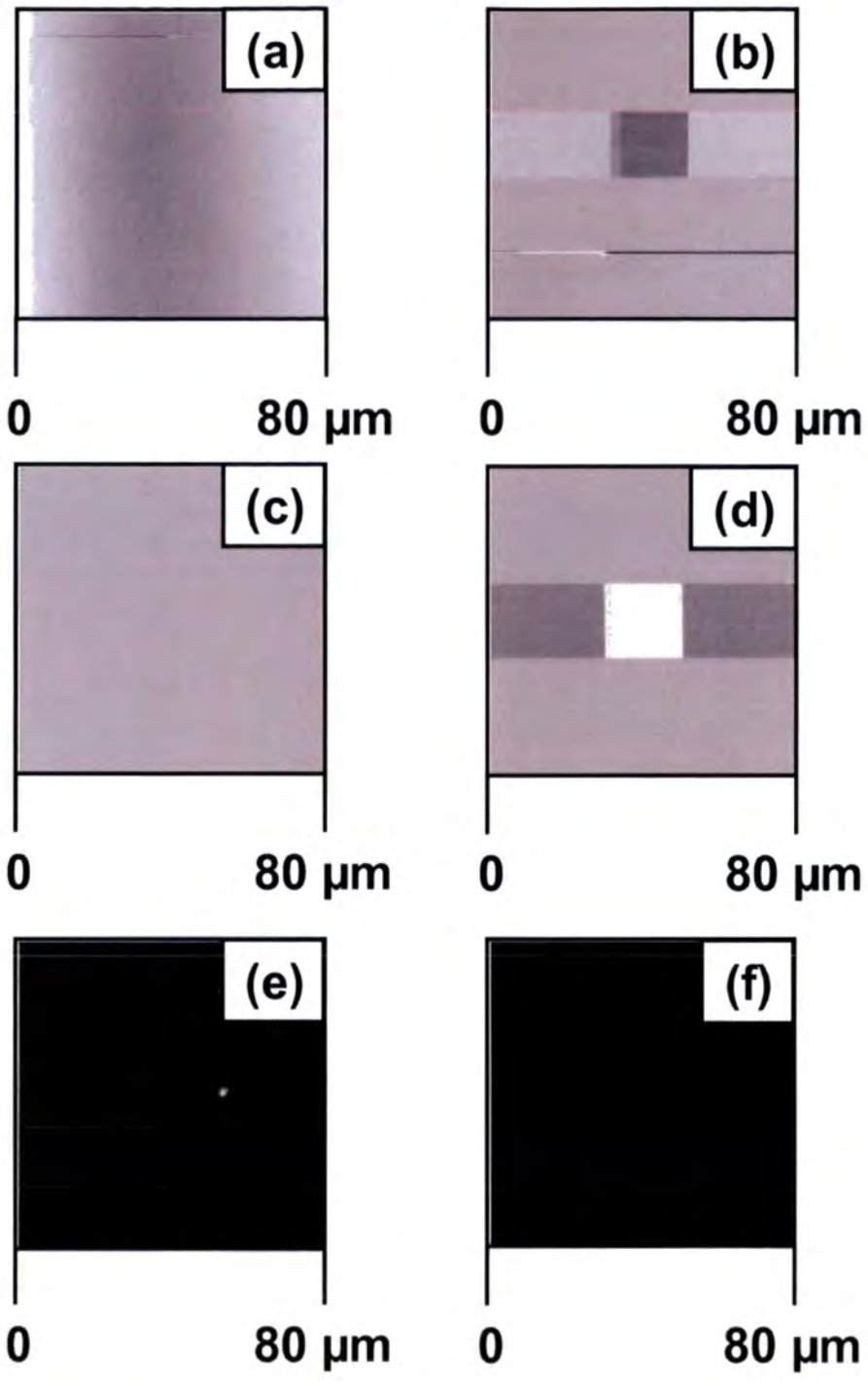

Figure 5.4 Atomic force micrograph images poly(*N*-Acryloylsarcosine methyl ester) after exposure to an EFM tip biased at -150 V: (a) Tapping mode topography; and (b-d) Lift mode phase images recorded at +35 V, -13 V and -35 V respectively. Corresponding fluorescence images of the surface: (e) Prior to protein exposure; and (f) Subsequent to protein exposure.

5.3.3 Protein Immobilization below the Isoelectric Point

The topographical and phase images obtained for the positive and negative charge deposition were as section 5.3.2. Fluorescence images of the sample after charge deposition but prior to protein immobilization showed an approximately uniform fluorescence across the surface with no feature present, Figure 5.5(a) and (c). After exposure to Protein G, modified to pH 3, and subsequent exposure to Alexa Fluor 633 IgG revealed fluorescence only is samples which contain an area of positive charge, Figure 5.3(b) and (d).

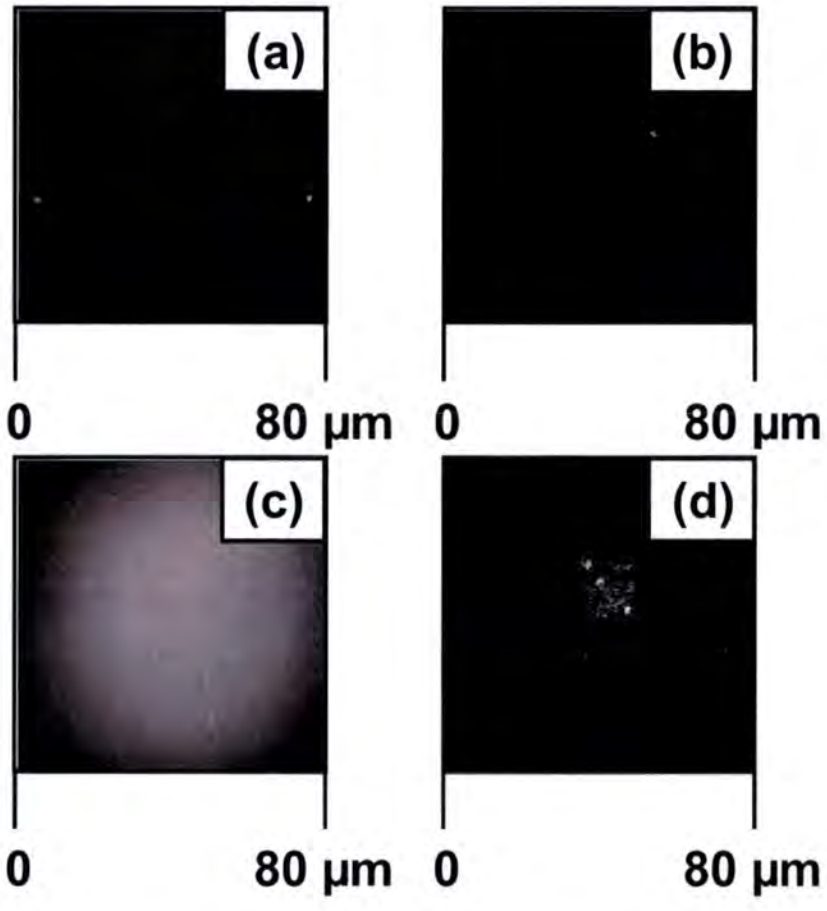

Figure 5.5 Fluorescence images obtained from poly(*N*-Acryloylsarcosine methyl ester): (a) and (c) after -150 V charge deposition; and (b) positive charge after washing in Protein G and subsequent exposure to Alexa Fluor 633 IgG; and (d) negative charge subjected to the same procedure.

5.4 Discussion

The development of protein micro-arrays as an analogue to DNA microarrays,[45,46] provided the capability to perform high throughput diagnostics of protein-protein interactions[47]. To facilitate the fabrication of protein arrays a plethora of techniques were developed for immobilization, including attachment via reactive linker groups,[48,49] immobilization onto gel-coated slides,[50] affinity capture of proteins via biomolecular interactions,[51] and the electrostatic interaction between proteins and charged substrates.[30,52,53] Of major concern in preparing protein arrays is the non-specific adsorption of proteins to the background, this may occur via the aforementioned electrostatic interactions or irreversible unfolding of the protein on the surface to maximise hydrophobic interactions.[54] Previous attempts to prevent this involved either the application of protein resistant surfaces[55,56,57] , which are know to limit the application to a wide range of substrate, or the use of blocking proteins,[58,59] with the use of blocking proteins known to suffer from the Vroman effect.[31] Pulsed plasma deposited poly(*N*-acryloylsarcosine methyl ester)[32] is an example of a non-fouling, substrate independent, protein resistant surface, with the surface rendered protein resistant as a results of terminal ester groups presenting a hydrophilic surface that may be easily hydrated, which can not disrupt the ordering of water molecules in the domain local to the protein, as a result the protein can not unfold.

It is known that pulsed plasma polymers may act as electrets, by storing charge within in a localised area of the polymer. Following positive discharge modification of the poly(*N*-acryloylsarcosine methyl ester) surface, the systematic varying of the phase imaging indicated that at high positive voltages the tip experienced a repulsive field gradient and produced a light square and upon the application of large negative voltages this is replaced by a dark square indicating that tip is now subjected to an attractive field gradient. The point at where no phase change is present occurs when the tip is not subjected to a field gradient.

This occurs when the applied voltage to the tip is the same as the voltage on the surface, this is a result of the applied voltage on the tip being of sufficient magnitude to overcome the mirror charge induced in the tip by the surface, but not enough to create a charge on the tip that will electrostatically interact with the surface, from this is can be deduced that the surface contains approximately +12 V charge, Figure 5.3. Following the same principles it can be determined that the surface contains approximately -13 V of surface charge, Figure 5.4. This potential has a similar magnitude to that resulting from positive discharge.

At pH 4.19 protein G exists primarily as a neutral zwitterion, above this point it exists primarily in the cationic state. Upon exposure of the protein in its cationic state to a poly(*N*-acryloylsarcosine methyl ester) nano-layer, containing both positive and negative charges, followed by washing in fluorescently tagged complementary protein IgG[60] only fluorescence to areas of positive charge was noted, Figure 5.3 and 5.4. However when protein G is below the isoelectric point, at pH 3, only immobilization to the negative charge is noted, Figure 5.5. This demonstrates that the electrostatic interactions between the protein and the localised charged poly(*N*-acryloylsarcosine methyl ester) are sufficient to overcome the protein resistant properties of the polymer. Furthermore it demonstrates that by controlling the pH of the protein, it is possible to selectively immobilize the protein onto positive and negative charges respectively.

It was noted that the fluorescence intensity of the positive charge was twice that of the negative charge, suggesting greater protein adsorption to positive charge. This discrepancy is related to the difference between the isoelectric point and protein pH. With a larger difference between the isoelectric point pH and experimental protein pH above the isoelectric point, a greater magnitude of charge is inferred to the protein as a function of distance from the isoelectric point.[26] As the strength of electrostatic interactions are proportional to the magnitude of charge[61] it follows that the immobilization above the positive pH is subjected to a greater electrostatic force than that below the isoelectric point. This

further demonstrates that the degree of protein immobilization can be controlled via pH modification.

5.5 Conclusions

Localised corona discharge from a metallized AFM tip can be used to store charge in pulsed plasma poly(*N*-acryloylsarcosine methyl ester), that can be utilised to selectively immobilize proteins, with retention of biological selectivity. Furthermore the protein resistant nature of poly(*N*-acryloylsarcosine methyl ester) negates the necessity of blocking solutions required to prevent protein fouling.

5.6 References

(1) Maboudian, R.; Howe, R. T. *J. Vac. Sci. Technol., B* **1997,** *15,* 1.

(2) Israelachvili, J. N. *Intermolecular and Surface Forces,* 2nd ed; Academic Press, New York, 1992.

(3) Bowen, W. R.; Sharif, A. O. *Nature* **1998,** *393,* 663.

(4) Hilczer, B.; Malecki, J. *Electrets*; Elsevier, New York, 1986.

(5) Chang, S, Waite, T. D.; Schafer, A. I.; Fane, A. G. *Environ. Sci. Technol.* **2003,** *37,* 3518.

(6) Makhaeva, E. E.; Tenhu, H.; Khokhlov, A. R. *Macromolecules* **2002,** *35,* 1870.

(7) Pai, D.; Springett, B. E.; *Rev. Mod. Phys.* **1993,** *65,* 163.

(8) Williams, E. M.; *The Physics and Technology of Xerographic Processes;* Wiley, New York, 1984.

(9) Schenk, M.; Reichelt, M. A. *Ultramicroscopy* **1996,** *65,* 109.

(10) Sprenkles, A. J.; Groothenge, R. A.; Verloop, A. J.; Bergveld, P. *Sens. Actuators, A* **1989,** *17,* 509

(11) MacDonald, B. A.; Fallone, B. G.; Ryner, L. N. *Phys. Med. Biol.* **1992,** *37,* 1825.

(12) Miki, T.; Ikeya, M.; Matsuyama, M.; Watanabe, K. *Jpn. J. Appl. Phys., Part 1* **1984,** *12,* L931.

(13) Stern, J. E.; Terris, B. D.; Mamin, H. J.; Rugar, D. *Appl. Phys. Lett.* **1998,** *53,* 2717.

(14) Schonenberger, C. *Phys. Rev. B: Condens. Matter Mater. Phys.* **1992,** *45,* 3861.

(15) Jacobs, H. O.; Whitesides, G. M. *Science* **2001,** *291,* 1763

(16) Jacobs, H. O.; Whitesides, G. M. Electric Microcontact Printing Method and Apparatus. WO 02/003142 A3, 2002.

(17) Tien, J.; Terfort, A.; Whitesides, G. M. *Langmuir* **1997,** *13,* 5349.

(18) Yang, S. U.; Rubner, M. F. *J. Am. Chem. Soc.* **2002.** *124,* 2100.

(19) Xu, H.; Hong, R.; Lu, T.; Uzun, O. ; Rotello, M. *J. Am. Chem. Soc.* **2006,** *128,* 3162.

(20) Zhou, Y.; Yu, B.; Levon, K. *Chem. Mater.* **2003,** *15,* 2774.

(21) Liu, S.; Volkmer, D.; Kurth, D. G. *Anal. Chem.* **2004,** *76,* 4579.

(22) Decher, G. *Science* **1997,** *277,* 1232.

(23) Grzybowski, B. A.; Winkleman, A.; Wiles, J. A.; Brumer, Y.; Whitesides, G. M. *Nat. Mater.* **2003,** *2,* 241.

(24) Pennington, S. R.; Dunn, M. J. *Proteomics*; BIOS, Oxford, 2001.

(25) McMurry, J. *Organic Chemistry,* 3rd ed.; Brookes/Cole, California, 1992.

(26) Chun, K. Y.; Mafe, S.; Ramirez, P.; Stroeve, P. *Chem. Phys. Lett.* **2006,** *418,* 561.

(27) Suci, P. A.; Klem, M. T.; Douglas, T.; Young, M. *Langmuir* **2005,** *21,* 8686.

(28) Du, Y. Z.; Saavedra, S. S. *Langmuir* **2003,** *19,* 6443.

(29) Yamada, K.; Yoshii, S.; Kumagai, S.; Fujiwara, I.; Nishio, K.; Okuda, M.; Matsukawa, N.; Yamashit, I. *Jpn. J. Appl. Phys.* **2006,** *45,* 4259.

(30) Naujoks, N.; Stemmer, A. *Colloids Surf., A* **2004,** *249,* 69.

(31) Vroman, L.; Adams, A. L.; Fischer, G. C.; Munoz, P. C. *Blood* **1980,** *55,* 156.

(32) Teare, D. O. H.; Schofield, W. C. E., Garrod, R. P. E.; Badyal, J. P. S. *J. Phys. Chem. B.* **2005,** *109,* 20923.

(33) Giacometti, J. A.; Olivera, O. O. *IEEE Transactions on Electrical Insulation* **1992,** *27,* 924

(34) Ebbens, S. J. Ph.D. thesis, University of Durham, 2001.

(35) Bradley, T. J. Ph. D. thesis, University of Durham, 2006.

(36) Kreyszig, E. *Advanced Engineering Materials,* 7th Ed; John Wiley & Sons: New York, 1993

(37) Martin, Y.; Williams, C. C.; Wickramasinghe, H. K. *J. Appl. Phys.* **1987,** *61,* 4723

(38) Garcia, R.; Paulo, A. S. *Phys. Rev. B.* **1999,** *60,* 4961

(39) Tamayo, J.; Garcia, R. *Appl. Phys. Rev.* **1999,** *71,* 2394

(40) Noy, A.; Sanders, C. H.; Vezenov, D. V.; Wong, S. S.; Liber, C. M. *Langmuir* **1998,** *14,* 1508

(41) Tamayo, J.; Garcia, R. *Appl. Phys. Lett.* **1998,** *73,* 2926

(42) Goward, C. R.; Murphy, J. P.; Atkinson, T.; Barstow, D. A. *Biochem. J.* **1990,** *267,* 171.

(43) Evans, J. F.; Gibson, J. H.; Moulder, J. F.; Hammond, J. S.; Goretzki, H. *Fresenius J. Anal. Chem.* **1984,** *319,* 841.

(44) Tabet, M. F.; McGahan, W. A. *Thin Solid Film* **2000,** *370,* 122

(45) Kozarova, A.; Petrinac, S.; Ali, A.; Hudson, J. W. *J. Proteome Res.* **2006,** *5,* 1051.

(46) MacBeath, G.; Schreiber, S. L.; *Science* **2000,** *289,* 1760.

(47) Stites, W. E. *Chem. Rev.* **1997,** *97,* 1233.

(48) Zhu, H.; Klemic, J. F.; Chang, S.; Bertone, P.; Casamayor, A.; Klemic, K. G.; Smith, D.; Gerstein, M.; Reed, M. A.; Snyder, M. *Nat. Genet.* **2000,** *26,* 283.

(49) Wilson, D. S.; Nock, S. *Curr. Opin. Chem. Biol.* **2001,** *6,* 81.

(50) Arenkhov, P.; Kukhtin, A.; Gemmell, A.; Voloschuck, S.; Chupeeva, V.; Mirzabekov, A. *Anal. Biochem.* **2000,** *278,* 123.

(51) Zhu, H.; Bilgin, M.; Bangham, R.; Hall, D.; Casamayor, A.; Bertone, P.; Lan, N.; Jansen, R.; Bidlingmaier, S.; Houfek, T.; Mitchell, T.; Miller, P.; Dean, R. A.; Gerstein, M.; Snyder, M. *Science,* **2001,** *293,* 2101.

(52) Mesthrige, K. W.; Xu, S.; Liu, G. *Langmuir* **1999,** *15,* 8580.

(53) Xu, W.; Zhou, H.; Regnier, F. E. *Anal. Chem.* **2003,** *75,* 1931.

(54) Nakanishi, K.; Sakiyama, T.; Imamura, K. *J. Biosci. Bioeng.* **2001,** *91,* 233.

(55) Prime, K. L.; Whitesides, G. *Science* **1991,** *252,* 1164.

(56) Cinliffe, J. M.; Baryla, N. E.; Lucy, C. A. *Anal. Chem.* **2002,** *74,* 776.

(57) Ostuni, E.; Chapman, R. G.; Holmlin, R. E.; Takayama, S.; Whitesides, G. *Langmuir* **2001,** *17,* 6336.

(58) Krawiec, S. B.; Devaraj, H.; Jacob, G.; Hickman, J. J. *Langmuir* **2004,** *20,* 2054.

(59) Malmsten, M.; Muller, D.; Lassen, B. *J. Colloid Interface Sci.* **1977,** *193,* 88.

(60) Lindmark, R.; Thoren-Tolling, K.; Sjoquist, J. J. *Immunol. Methods* **1983,** *62,* 1.

(61) Atkins, P. W. *Physical Chemistry*, 5th ed; Oxford University Press, Oxford, 1994.

CHAPTER 6

CONCLUSIONS

6.0 CONCLUSIONS

The fabrication of molecular devices, capable of providing insights into biological interactions, require suitably functionalized substrates. Existing methods include Langmuir-Blodgett films, self assembled monolayers and spin coated layers coupled with patterning techniques such as atomic force lithography, e-beam lithography, microcontact printing, microarraying and exposure through a mask to a reactive medium. However there exist drawbacks, such as the substrate dependence of self assembled monolayers on the Au-S and Si-O bond affinity, or the inability to coat complex 3D- geometries. Pulsed plasma polymerization can overcome these limitations. It ensures covalent bonding to the substrate via free radical sites created at the substrate surface during the onset of electrical discharge. Appropriate choice of functional gaseous precursors (containing polymerizable carbon-carbon double bonds) in combination with electric discharge modulation on millisecond-microsecond time scales makes it possible to easily build up functional nanolayers.

In this thesis genomic arrays have been created via di-sulfide bridge formation between thiol terminated DNA and thiols groups presented by pulsed plasma deposited poly(allylmercaptan) with retention of biological activity shown via the binding of a fluorescently tagged complementary DNA strands. Proteomic arrays have been formed by the immobilization of proteins to reactive epoxide functionalities formed from pulsed plasma deposited poly(glycidyl methacrylate). These are shown to be amenable to binding primary amine groups, belonging to the protein, via nucleophilic attack. The preservation of the protein configuration is revealed via the binding of complementary proteins only. Similarly, glycomic arrays have been produced by a further exploitation of poly(allylmercaptan) presented thiol groups, in this case β-D-galacto-methanethiosulfonate has been covalently attached via a di-sulfide bridge. An alternate method for sugar immobilisation has been demonstrated via Schiff base imine formation with the aldehyde terminus

of D-maltose. Retention of biological activity has been exemplified by the binding of the fluorescently labelled galactose binding lectin PNA and maltose binding lectin concanavalin A.

A major limitation in array analysis is non-specific adsorption to the background leading to unwanted fluorescence. Plasmachemical nano-layering catered to create a bi-functional stacks comprising pulsed plasma deposited poly(*N*–acryloylsarcosine methyl ester) protein-resistant top coating with a suitably tailored reactive underlayers has been shown to overcome this due to the elimination of non-specific protein adsorption. The marrying of these molecular scratchcards with traditional robotic microarraying has been show to produce arrays with low background fluorescence due to the elimination of non-specific protein adsorption as a consequence of the protein-resistant top layer. In a similar fashion, the utilisation of an SPM probe tip to mechanically remove the tip has been shown to provide reactive pixels on the micro and nano-scales to produce arrays capable of high-throughput diagnostics for genomics, glycomics and proteomics. Furthermore, it is possible utilise the protein resistant nature poly(*N*–acryloylsarcosine methyl ester) to immobilize proteins, through electrostatic interactions. This is possible due to the electret nature of plasma polymers, whereby regions of charge, if both polarities can formed via a corona discharge emanating from a metallized AFM tip. In addition, modification of the protein pH can be utilised to selectively immobilize the cationic and anionic protein variants to areas of positive and negative charge respectively, whilst maintaining the protein resistant properties of the background.

Finally, the expense and technical expertise demanded by many diagnostic methods often precludes their application in most laboratories. Reactive epoxide nanolayers have been formed through pulsed plasma polymerization onto a compact disc surface. These have been functionalized through inkjet printing of proteins, to create spatially addressed arrays. Linking of these arrays to tracks stored in the compact disc with subsequent visualisations of the any data within these tracks

has been shown to provide a link between the informatic process of the compact disc and molecular binding. This shows promise as a potential cheap point-of-care diagnostic sensor.

To summarize, in this thesis, for the first time, it has been shown that pulsed plasma deposited films can be utilised to fabricate high throughput molecular arrays for genomics, glycomics and proteomics on the micron and nano-scales, with elimination of background fluorescence.